Glycoprotein hormone receptor signaling in the endosomal compartment

Glykoproteinhormon-Rezeptor Signaltransduktion im endosomalen Kompartiment

Dissertation for a doctoral degree
at the Graduate School of Life Sciences,
Julius-Maximilians-Universität Würzburg
(Section Biomedicine)

submitted by

Sandra Lyga

from Gießen

Würzburg, April 2016

Submitted on: …………………………………………………………

Members of the *Promotionskomitee*:

Chairperson: Prof. Dr. Jörg Schultz

Primary Supervisor: PD Dr. Davide Calebiro

Supervisor (Second):   Prof. Dr. Martin J. Lohse

Supervisor (Third):   Prof. Dr. Alexander Buchberger

Supervisor (Fourth):   Prof. Dr. Frank Runkel

Date of Public Defence: …………………………………………

Date of Receipt of Certificates: ………………………………….

Table of contents

Figure index

Abbreviations

7TM	seven transmembrane
AC	adenylyl cyclase
AKAPs	A-kinase anchoring proteins
AKAR	A-kinase activity reporter
Akt	Rac-alpha serine/threonine-protein kinase
AP-2	adaptor protein 2
Approx.	approximately
APS	ammoniumpersulfat
ATP	adenosintriphosphat
β_2-AR	β_2 adrenergic receptor
BFP	blue fluorescent protein
BSA	bovine serum albumin
cAMP	3´,5´-cyclic adenosine monophosphate
cGMP	3´,5´-cyclic guanosine monophosphate
CBX	carbenoxolone
CNG	cycle nucleotide-gate
COC	cumulus oocyte complex
COX2	cyclooxygenase
Ct	cycle threshold
CREB	cAMP response element-binding protein
CFP	cyan fluorescent protein
CNBD	cyclic nucleotide-binding domain
DAG	diacylglycerol
DEPC	diethylpyrocarbonat
DMSO	dimethylsulfoxide
DNA	Desoxyribonucleic acid
dNTP	desoxyribonucleotide triphosphate
DTT	dithiothreitol
EtBr	ethidium bromide

EGF	epidermal growth factor
EPAC	exchange proteins directly activated by cAMP
ERK1/2	extracellular regulated kinase
FHA1	forkhead associated domain 1
FSH	follicle stimulating hormone
FRET	Förster/fluorescence resonance energy transfer
FRTL-5	Fischer rat thyroid cell line 5
GDP	guanosine diphosphate
GFP	green fluorescent protein
GnRH	gonadotropin-releasing hormone
GPCR	G protein-coupled receptor
GPH	glycoprotein hormone
GPR3	G protein-coupled receptor 3
GPR12	G protein-coupled receptor 12
GRK	G protein-coupled receptor kinases
GTP	guanosine triphosphate
GVBD	germinal vesicle breakdown
hCG	human chorionic gonadotropin
HEK	human embryonic kidney
IP3	inositol trisphosphate
IGF-1	insulin-like growth factor 1
LB	Luria-Bertani
LH	luteinizing hormone
MAPK	mitogen-activated protein kinase
NES	nuclear export signal
NLS	nuclear localization signal
NIS	sodium-iodide symporter
NPPC	C-type natriuretic peptide
NPR2	guanylyl cyclase natriuretic peptide receptor
O/N	overnight

PCK1	phosphoenolpyruvate carboxykinase 1
PDE	phosphodiesterase
PI3K	phosphatidylinositol 3-kinase
PFA	paraformaldehyde
PKA	protein kinase A
PKC	protein kinase C
PLC	phospholipase C
PMSF	phenylmethylsulfonylfluorid
PTH	parathyroid hormone
PTHrP	PTH related peptide
Rap1	ras-related protein 1
RhoA	ras homolog gene family member A
RT	room temperature
S1P1	sphingosine-1-phosphate
SDS	sodium dodecyl sulphate
TRITC	tetramethylrhodamine isothiocyante
T3	triiodothyronine
T4	thyroxine
TEMED	tetramethylethylenediamine
Tg	thyroglobulin
TPO	thyroid peroxidase
TRH	thyrotropin releasing hormone
TSH	thyroid stimulating hormone
VASP	vasodilator-stimulated phosphoprotein
YFP	yellow fluorescent protein

1. Introduction

1.1. GPCR SIGNALING AND ITS PHYSIOLOGICAL RELEVANCE

G protein-coupled receptors (GPCRs) represent the largest group of cell-surface receptors that transmit extracellular signals into the cell. They comprise receptors for light, taste and smell as well as calcium ions, small neurotransmitters, peptides and hormones. Given their important role in a variety of physiological processes, together with evidence for dysfunctional and/or disordered GPCR signaling in diverse pathological conditions, GPCRs are the most common targets of drugs including beta-blockers, antihistamines and opiates (Pierce et al., 2002;Lagerström and Schioth, 2008).

The first crystal structure of a GPCR was solved in 2000 for rhodopsin by Palczewski (Palczewski et al., 2000) and became the most famous and investigated representative of this receptor family. According to the sequence similarity GPCRs can be subdivided into six distinct families: A, B, C, D, E, and F. A characteristic feature of these receptors is the seven-helical transmembrane domain (7TM) and coupling to heterotrimeric G proteins consisting of α-, β- and γ-subunits. All 7TM receptors which are not coupled to G proteins, are assigned to O "other" family (Pierce et al., 2002).

Family A represents the largest group with ca. 670 full-length human receptor proteins containing rhodopsin, adrenergic receptors and the olfactory receptors (Pierce et al., 2002;Lagerström and Schioth, 2008).

In the classical signaling pathway, GPCRs mediate signals via the activation of heterotrimeric G proteins, also known as G protein-cycle. As a result of ligand binding, the receptor undergoes a conformational change followed by G protein activation. The activation of the G protein induces a conformation change of the heterotrimeric subunits (α, β, γ), resulting in an exchange of the guanosine diphosphate (GDP) bound to the α-subunit with guanosine triphosphate (GTP) (Gilman, 1987;Pierce et al., 2002). Subsequently, the active G_α protein dissociates from the $\beta\gamma$-complex and activates various signaling cascades depending on the G_α protein coupled to the receptor (**Figure 1**). Such effectors include enzymes such as adenylyl cyclase (AC), which is responsible for cAMP accumulation, phospholipase C (PLC) and potassium or calcium channels. Not only the active G_α protein, but also the $\beta\gamma$-complex is involved in mediating signals from the ligand-activated GPCR to effectors. The intrinsic GTPase activity of the G_α protein hydrolyses GTP to GDP. As a result, the inactive G_α protein reassociates with the $\beta\gamma$-complex and the initial state is restored (Patel, 2004).
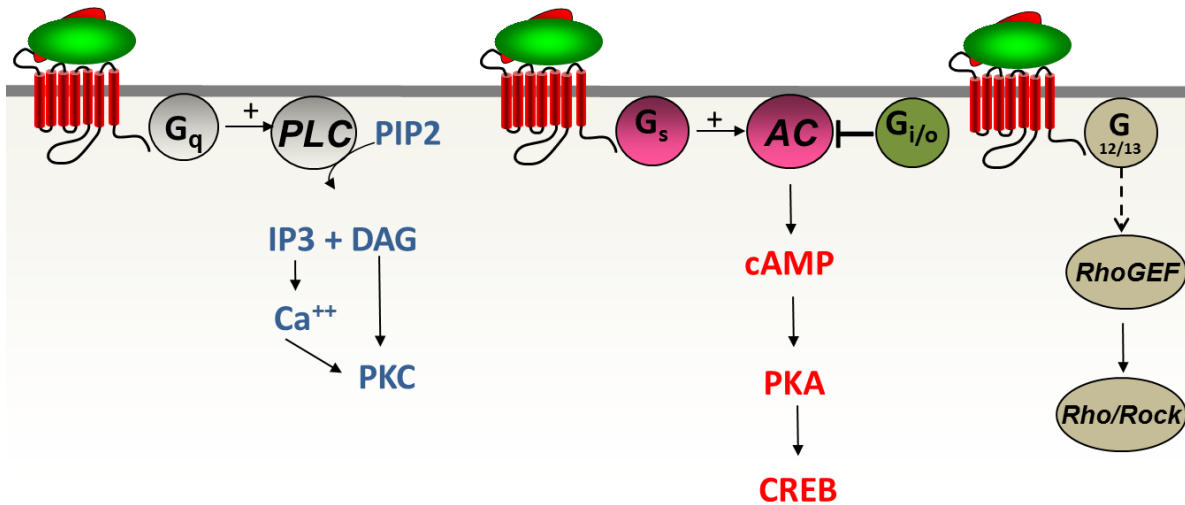
Figure 1: G protein-dependent signaling.
GPCRs are able to signaling via different G proteins: G_q, G_s, $G_{i/o}$ and $G_{12/13}$. G_q activation results in the stimulation of the PLC/PKC pathway. G_s activation leads to stimulation of cAMP/PKA pathway via AC activation, whereas $G_{i/o}$ activation leads to inhibition of this pathway. $G_{12/13}$ activation results in a stimulation of the RhoA pathway.

1.1.1. Receptor desensitization and internalization

Upon stimulation, GPCRs become phosphorylated by second messenger kinases such as protein kinase A (PKA) or protein kinase C (PKC). They uncouple the G proteins from their receptors and thereby serve as classical negative feedback mechanism. Not only PKA and PKC can be responsible for fast GPCR desensitization, but also a distinct family of G protein-coupled receptor kinases (GRK) regulates receptor activity upon agonist stimulation by phosphorylation of GPCRs. Subsequently, β-arrestin recruitment takes place (Lohse, 1993;Pierce et al., 2002), which leads to receptor uncoupling and internalization via clathrin-mediated endocytosis (Koenig and Edwardson, 1997;Krupnick and Benovic, 1998;Lefkowitz, 1998).

Clathrin-mediated endocytosis can be divided into three stages: assembly, curvature and fission. The clathrin-coated pit formation begins with assembly of a range of proteins at the plasma membrane, such as clathrin itself and the adapter protein 2 (AP-2) (Goodman et al., 1997;Laporte et al., 1999). Because clathrin is not able to bind to the membrane itself, AP-2, a key adaptor, acts as a linker between plasma membrane and clathrin and recruits clathrin to stabilize its interaction with the membrane. Clathrin assembly initially leads to the formation of a lattice that recruits a variety of clathrin-associated proteins that drive membrane curvature and receptor recruitment for subsequent vesicle transport (Traub, 2003). The generated clathrin-coated pits are finally released into the cytoplasm via a dynamin-mediated membrane fission reaction. Dynamin is a GTPase

implicated in membrane budding and transition from a fully formed pit to a pinched-off vesicle called endosome (Doherty and McMahon, 2009) (**Figure 2**).
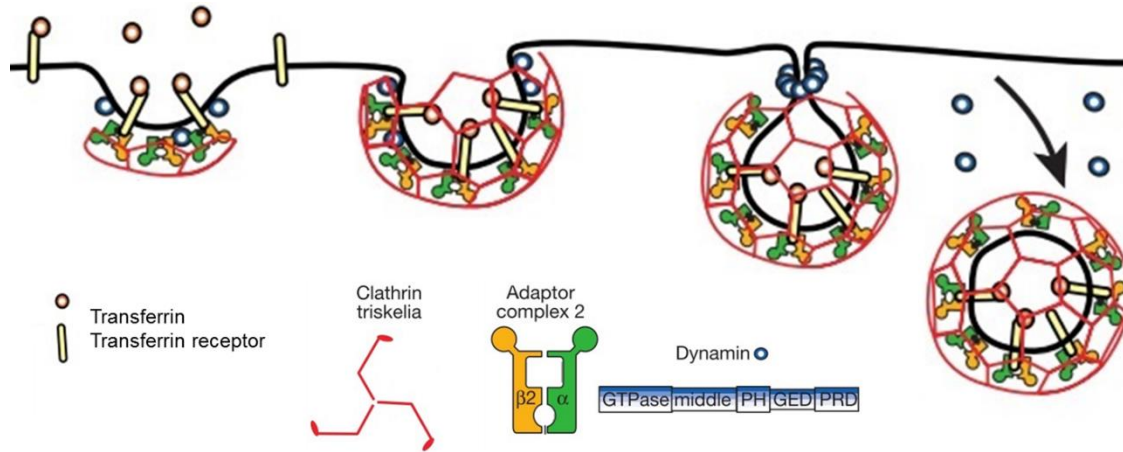
Figure 2: Mechanism of clathrin-dependent receptor endocytosis.
Upon transferrin binding to its receptor, adaptor protein 2 (AP-2) is recruited to the cytoplasmic surface of the receptor. AP-2 interacts with clathrin triskelia, followed by formation of a polyhedral clathrin lattice, which surrounds the pit. Dynamin, a GTPase, is recruited to the necks of coated pits where they invaginate inwards and pinch off from the plasma membrane to allow formation of clathrin-coated vesicles. Figure modified from Conner and Schmid, 2003 .

Once internalized, the ligand is mostly degraded and the receptor is either recycled back to the cell-surface or degraded along with the ligand in lysosomes (Lohse, 1993;Yu et al., 1993;Krueger et al., 1997;Tsao et al., 2001).

Originally, it was believed that receptor internalization plays a major role in signal desensitization, but it has been shown that desensitization takes place already at the cell-surface and is much faster than receptor internalization (Lohse, 1993). At the same time, receptor endocytosis seems to be involved in other important functional mechanism, such as receptor resensitization. This could be explained by the internalization of GPCRs via endosomes, which are known to be rich in phosphatases. Therefore, trafficking through this compartment back to the cell-surface is apparently necessary for receptor resensitization (Yu et al., 1993;Krueger et al., 1997).
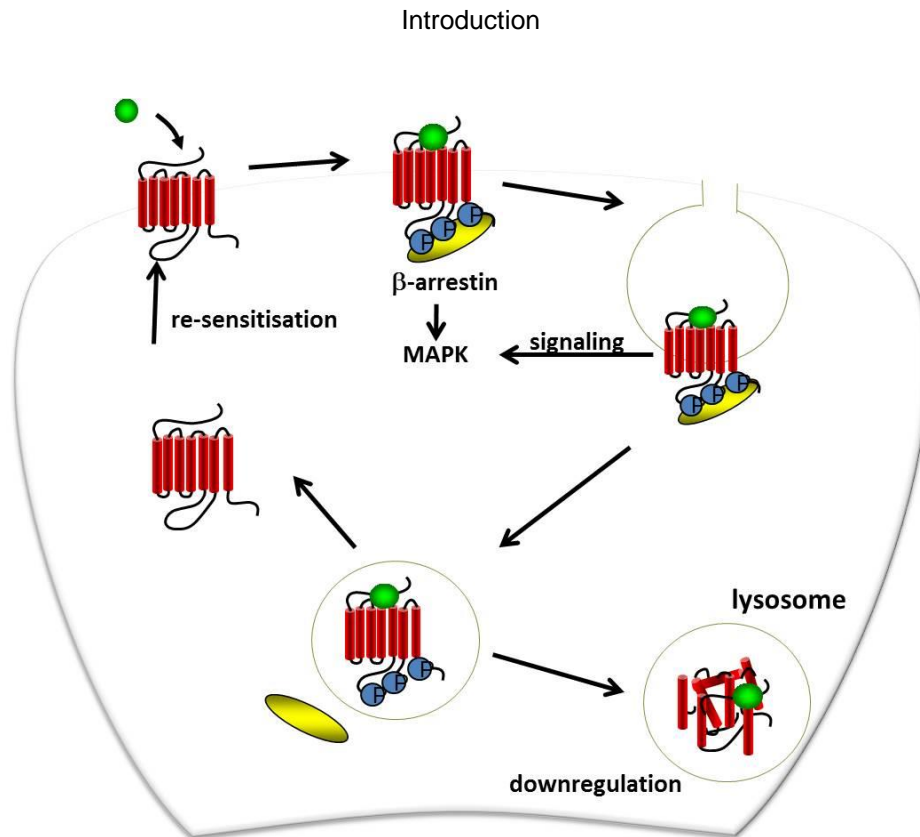
Figure 3: Functional role of GPCR internalization.
Prolonged receptor stimulation lead to receptor phosphorylation and subsequently to β-arrestin recruitment. Receptor/β-arrestin complex can activate the MAPK kinase pathway from the cell-surface and from endosomal membranes. Internalized receptor is either targeted to lysosomes for degradation or dephosphorylated followed by recycling back to the plasma membrane.

In addition, internalized receptors can signal from endosomes via a G protein-independent pathway via β-arrestin. In particular, the internalized receptor/β-arrestin complex activates the mitogen-activated protein kinase (MAPK) cascade (activation of ERK1/2 enzyme, which regulate cell growth and survival) not only from the cell-surface, but also from endosomal membranes after receptor internalization (Vieira et al., 1996;Daaka et al., 1998;Pierce et al., 2002;Sorkin and von Zastrow, 2009) (**Figure 3**).

1.1.2. New functional role of GPCR internalization

Although GPCRs were long assumed to signal via G proteins exclusively from the cell membrane, in the last years a new paradigm of GPCR signaling has been brought to light i.e. receptor signaling from intracellular compartments. It could be shown that ligand-induced receptor internalization leads to a persistent G protein-dependent signaling. The TSH receptor was one of the first GPCRs in which GPCR signaling from the endosomal compartment was shown. In particular, it could be demonstrated that TSH receptor internalization induces a second cAMP signal. Indeed, TSH receptor internalization was related to TSH, G_s and AC localization in a perinuclear compartment (Calebiro et al., 2009) (**Figure 4**).
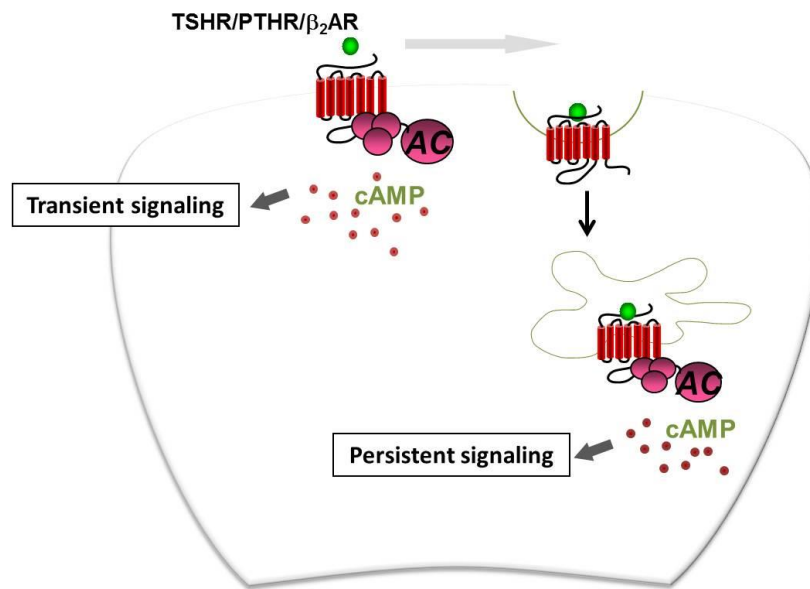
Figure 4: New role of GPCR internalization.
Ligand binds to the receptor (TSHR/PTHR/β_2AR) and activates the G_s pathway via cAMP signaling from the cell-surface. Upon prolong stimulation, the ligand/receptor complexes undergo endocytosis into the intracellular site. Internalized ligand/receptor complex continues to stimulate cAMP production from the intracellular site.

At the same time, a similar phenomenon was revealed for the parathyroid hormone (PTH) receptor (Ferrandon et al., 2009) and the sphingosine-1-phosphate (S1P1) receptor (Müllershausen et al., 2009). The study of S1P1 receptor shows that GPCR signaling from endosomes can also be G_i protein-dependent. Binding of FTY720 phosphate, a functional antagonist involved in the treatment of multiple sclerosis (Pinschewer et al., 2000;Kappos et al., 2006), to the S1P1 receptor, a G_q- and G_i-coupled receptor (Pyne and Pyne, 2000;Yoon et al., 2008;Müllershausen et al., 2009), on the cell-surface leads to a rise in intracellular Ca^{++} levels and simultaneously to a decrease in cAMP concentration. Upon internalization, the S1P1 receptor continues signaling via

G_i protein, resulting in a reduction of cAMP. Remarkably, the internalized ligand/receptor complex traffics to the Golgi/trans-Golgi compartment and could not be visualized in early and late endosomes and lysosomes (Müllershausen et al., 2009).

In the case of the PTH receptor signaling, two different physiological ligands mediate cAMP accumulation via G_s protein activation within different duration. PTH, a circulating hormone, induces PTH receptor internalization and thus persistent cAMP signaling. PTH related peptide (PTHrP), a paracrine factor, does not undergo endocytosis in a complex with the PTH receptor. Its effects are completely reversible and limited to the plasma membrane (Ferrandon et al., 2009). Besides the persistent signaling initially discovered for the TSH and PTH receptor, other peptide hormone receptors such as the glucagon-like peptide 1 receptor , the pituitary adenylate cyclase activating polypeptide type 1 receptor and vasopressin type 2 receptor have been reported to persistently signal via cAMP upon internalization into endosomes (Feinstein et al., 2013;Kuna et al., 2013;Merriam et al., 2013). The D_1 dopamine receptor was the first monoamine neurotransmitter receptor, which was known to elicit cAMP signaling upon endocytosis in primary neuronal cultures (Kotowski et al., 2011).

A key step to identifying the mechanisms of endosomal GPCR signaling was achieved for the β_2-adrengeric receptor (β_2-AR) by the group of Mark von Zastrow, who showed two separate phases of cAMP signaling. In particular, they were able to selectively monitor the active state of either the β_2-AR or G_s protein by using GFP-tagged nanobodies (Irannejad et al., 2013;Vilardaga et al., 2014;Tsvetanova et al., 2015). Besides the direct detection of active β_2-AR and G_s protein on the plasma membrane and on early endosomes upon isoproterenol stimulation, differences in cAMP accumulation with and without blocking β_2-AR internalization were detected. Above all, the lack of activated β_2-AR and activated G_s protein, detected by nanobodies during clathrin-coated pit formation until uncoating, provides strong evidence that isoproterenol/β_2-AR complex stimulate cAMP production via two spatially and temporally distinct events: the first occurring at the plasma membrane and the second happening in early endosomes.

In the same study, it was shown that endosomal signaling by internalized GPCRs not only affects cAMP signaling, but is also responsible for downstream signaling. Indeed, the internalization of β_2-AR has shown to be involved in gene transcription, in particular in the induction of cAMP-dependent genes, including, for example PCK1, a cAMP response element-binding protein (CREB) target (Tsvetanova and von Zastrow, 2014).

GLYCOPROTEIN HORMONE RECEPTOR SIGNALING

Glycoprotein hormone (GPH) receptors belong to the family A of GPCRs, the rhodopsin receptor like subfamily, and consist of three members including the thyroid stimulating hormone (TSH), follicle stimulating hormone (FSH) and luteinizing hormone (LH) receptors. FSH, LH and human chorionic gonadotropin (hCG) are classified as gonadotropins and all GPHs, including TSH, belong to the superfamily of cysteine-knot growth factors. GPHs are dimeric glycoproteins of ~30 kDa and are composed of a conserved α-subunit and a ligand-specific β-subunit, which are non-covalently associated (Vassart et al., 2004;Jiang et al., 2014). β-LH and β-hCG have a similarity of 80% and bind the same receptor, i.e. the LH receptor (Vassart et al., 2004). Consistently to the hormones, also their receptors have high structural similarities. The hallmark of the subfamily of GPH receptors is a large extracellular N-terminal domain. This domain contains several leucine-rich-repeats, which are responsible for the high affinity and selective binding of their respective hormone (Ascoli et al., 2002;Dias et al., 2002;Szkudlinski et al., 2002;Fan and Hendrickson, 2005;Kleinau et al., 2013) (**Figure 5**).
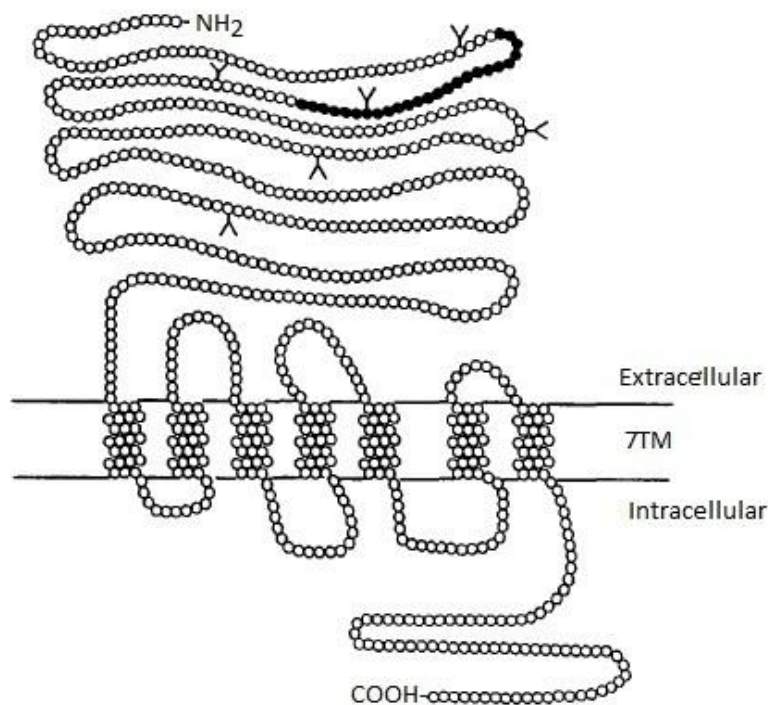
Figure 5: Schema of the primary structure of the human TSH receptor.
The extracellular part of the TSH receptor consists of 398 residues with a repetition of 25-residue long leucine-rich motifs. One leucine repeat is indicated in black. Y represents the potential N glycosylation. 7 transmembrane (7TM) domains and the intracellular part of the TSH receptor consist of 346 residues. Figure modified from Vassart and Dumont, 1992.

1.2. LH RECEPTOR SIGNALING IN OVARIAN FOLLICLES AND ITS PHYSIOLOGICAL RELEVANCE

The hypothalamus secretes the gonadotropin-releasing hormone (GnRH) in pulses, which in turn stimulates the anterior pituitary gland to secrete the gonadotropic hormones, FSH and LH in females, which control reproductive cycles. FSH and LH promote ovarian synthesis of estrogen and progesterone, which in turn, influence the pattern of GnRH release from the hypothalamus through a negative feedback mechanism. These three basic components, hypothalamus, anterior pituitary gland and ovaries constitute the hypothalamic-pituitary-ovarian axis (Mauras, 1996;Veldhuis, 1996;Apter, 1997;Ludwig et al., 2002;Lunenfeld, 2002;2004) (**Figure 6**).
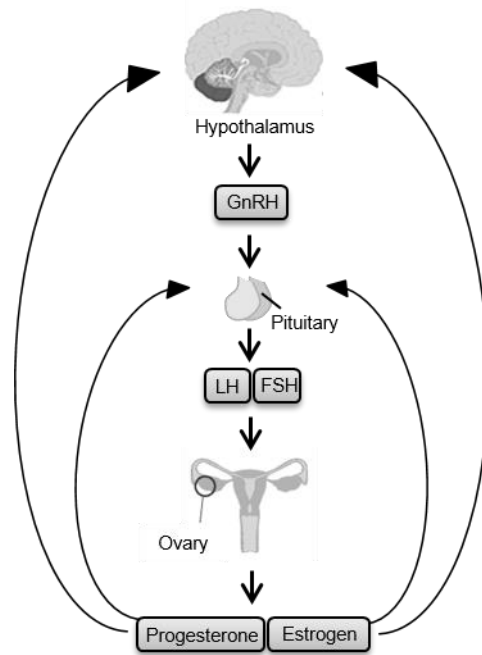
Figure 6: Hypothalamic-pituitary-ovarian axis.
Gonadotropin-releasing hormone (GnRH) expressed by the hypothalamus stimulates the synthesis of luteinizing hormone (LH) and follicle stimulating hormone (FSH) in the anterior pituitary. In the ovary LH and FSH trigger the secretion of progesterone and estrogen. Hypothalamic and pituitary activities are controlled by ovarian hormone feedback loops. Figure modified from Du Plessis et al., 2010 .

Antral, i.e. mature, ovarian follicles are multicellular complexes that consist of several layers of cells (theca, mural granulosa, cumulus oophorus cells) surrounding the oocyte, which remains arrested at the prophase of the first meiotic division (Pincus and Enzmann, 1935;Edwards, 1965). These cells are tightly interconnected, e.g. via gap junctions (Anderson and Albertini, 1976;Sela-Abramovich et al., 2006;Norris et al., 2008;Su et al., 2009;Norris et al., 2010), and communicate via a network of well-orchestrated paracrine factors (Albertini et al., 2001;Park et al., 2004;Su et

al., 2009). In particular, LH regulates ovarian function at several levels (Hsueh et al., 1984;Hillier et al., 1994;Richards et al., 2002). First, it stimulates the production of androgens in theca cells, the outer ovarian follicle cell layer, and their subsequent conversion to estrogens in the adjacent layer of mural granulosa cells. Second, it is responsible for the final maturation of ovarian follicles, which culminates in meiosis resumption in the oocyte and ovulation (Hsueh et al., 1984;Hillier et al., 1994;Conti, 2002).

The effects on ovarian follicles are mediated by activation of the LH receptor, which is expressed on the surface of theca and mural granulosa cells and is virtually lacking in cumulus oophorus cells that directly surround the oocyte or on the oocyte itself (Amsterdam et al., 1975;Eppig, 1979;Lawrence et al., 1980;Peng et al., 1991;Eppig et al., 1997;Russell and Robker, 2007) (**Figure 7**).
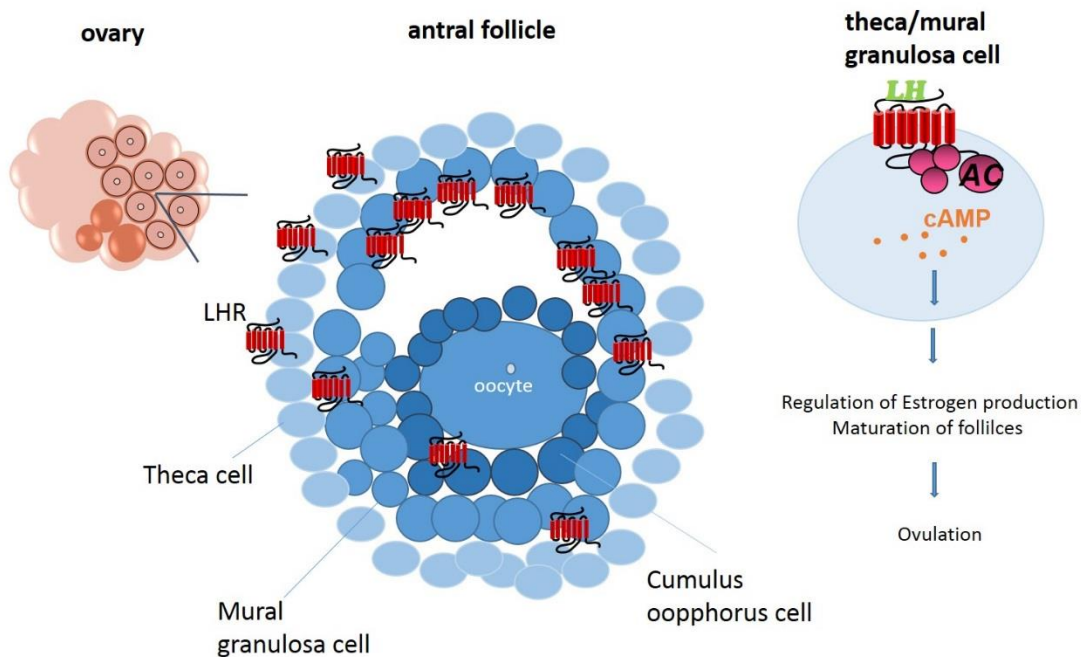
Figure 7: LH receptor signaling in ovarian follicles.
A schema of an ovary containing follicles. Shown is the zoom-in of an antral follicle consisting of three different cell layers corresponding to theca (light blue), mural granulosa (middle blue) and cumulus oophorus (dark blue) cells expressing the LH receptor (LHR) surrounding the oocyte. G_s signaling pathway of an activated LH receptor in a theca/mural granulosa cell leading to adenylyl cyclase (AC) stimulation of cAMP production, which promotes ovulation.

Hence, paracrine signaling and intracellular communication are essential for the cumulus oocyte complex (COC) response to LH. Mural granulosa cells, cumulus oophorus cells and oocytes are interconnected via gap junctions that enable the diffusion of intracellular mediators form the periphery to the core of the follicle to transduce ovulatory signals in oocytes (Tsafriri and Reich, 1999). Gap junctions consist of homo- or hetero-hexamers of connexin proteins. More specifically,

gap junctions between theca and mural granulosa cells are predominantly containing Connexin-43, whereas the major connexin present in junction between cumulus oophorus cells and oocyte is connexin-37 (Simoni et al., 1997;Conti et al., 2012).

Although the LH receptor has also been demonstrated to be able to couple to G_q (Breen and Knox, 2012), most of its effects are mediated by activation of the G_s protein and the downstream generation of cAMP in mural granulosa cells (Rajagopalan-Gupta et al., 1998;Richards, 2001;Conti, 2002).

In general, stimulation of the LH receptor by LH leads to a large intracellular increase of cAMP in mural granulosa cells. The elevated cAMP activates PKA (Marsh, 1976;Richards, 1994), which in turn is responsible for ERK1/2 activation (Seger et al., 2001;Salvador et al., 2002) and phosphorylation of the cAMP response element-binding protein (CREB), a transcription factor (Russell and Robker, 2007). ERK1/2 activation induces downregulation of genes related to follicular development together with upregulation of the ovulation-related genes (Richards, 1994;Russell and Robker, 2007). Furthermore, ERK1/2 is responsible for the immediate effect of LH on gap junctional closure in mural granulosa cells (Sela-Abramovich et al., 2005), which blocks cAMP diffusion into the oocyte from somatic cells, resulting in a decrease of intracellular cAMP levels in the oocyte, which in turn allows meiosis resumption (Anderson and Albertini, 1976;Sela-Abramovich et al., 2006;Norris et al., 2008). Resumption of oocyte meiosis upon LH-induced cAMP decrease in the oocyte has been observed in previous studies (Vivarelli et al., 1983;Törnell et al., 1991;Conti, 2002), but the underlying mechanism as to how this is brought about, especially considering that LH receptor is not expressed in oocytes (Amsterdam et al., 1975), is a topic of discussion.

Prior studies claimed that the intracellular cAMP is generated in the oocyte itself due to LH independent G_s signaling via a constitutively active G protein-coupled receptor 3 (GPR3; mouse) or (GPR 12; rat), which is expressed in the oocyte (Mehlmann et al., 2004;Ledent et al., 2005). Contrary to this study, Sela-Abramovich et al. (2006) showed that intraoocyte cAMP is provided by mural granulosa cells via gap junctions without PDE3A activity increase after a LH surge (Sela-Abramovich et al., 2006).

However, the diffusion of cyclic nucleotides is limited by local pools of phosphodiesterases (PDEs). It has been demonstrated that inhibition of PDE4, which is expressed exclusively in mural granulosa cells, leads to meiosis resumption, while inhibition of PDE3, which is expressed exclusively in the oocyte, leads to meiotic arrest (Tsafriri et al., 1996). PDE3 is a dual substrate enzyme and shows high affinity for both cAMP and cGMP but hydrolyzes cAMP with a 10-fold higher catalytic activity compared to cGMP. Thus, cGMP acts as an endogenous cAMP/PDE

inhibitor and thus prevents the degradation of cAMP in the oocyte (Solc et al., 2010;Conti et al., 2012). Under resting conditions, cGMP, originating in mural granulosa cells, is synthesized through C-type natriuretic peptide (NPPC) binding to its receptor guanylyl cyclase natriuretic peptide receptor (NPR2). Dephosphorylation and inactivation of NPR2 guanylyl cyclase and the decrease of its ligand NPPC due to LH/LH receptor signaling (Robinson et al., 2012;Egbert et al., 2014) contribute to the decrease of cGMP in cumulus oophorus cells and oocytes and therefore also to meiosis resumption (Egbert et al., 2014;Shuhaibar et al., 2015). According to these data, LH/LH receptor signaling prevents the diffusion of cGMP by activating the MAPK pathway and thus meiosis resumption (Robinson et al., 2012;Egbert et al., 2014).

It is well established that not only direct cAMP/LH receptor signaling transduces ovulatory signals from mural granulosa cells to the COC, but also indirect mediators of the epidermal growth factor (EGF)-like family are involved (Park et al., 2004). LH stimulation induces transcription of epiregulin, amphiregulin and betacellulin and EGF-like molecules specifically in mural granulosa cells (Park et al., 2004;Hsieh et al., 2009), which then promote oocyte maturation, cumulus expansion, COX2 expression and luteinization in mouse ovarian follicles by binding to the EGF receptor (Park et al., 2004;Norris et al., 2008). Recently, it was demonstrated that LH/EGF receptor signaling is involved not only in gap junction closure (Norris et al., 2010), but also in the inhibition of the expression of NPPC in mural granulosa cells (Egbert et al., 2014).

1.2.1.   LH receptor internalization

In the late seventies, a study from Ascoli showed for the first time the internalization of hCG/LH receptors in ovaries (Ascoli and Puett, 1978). Since then, a wealth of information has been obtained regarding the mechanism of LH receptor endocytosis, for instance it could be demonstrated that the agonist/LH receptor complex undergoes internalization via clathrin-coated pits into endosomes followed by trafficking to lysosomes. As soon as they reach the lysosome, the hormone dissociates and both the ligand and receptor are degraded (Ascoli, 1984;Ghinea et al., 1992). However, a small fraction of the internalized receptors is also recycled back to the cell-surface (Ghinea et al., 1992). Moreover, it could be shown that two distinct structural motifs present in the C-terminal tail of the LH receptor are responsible for entering the degradation pathway (Kishi et al., 2001;Galet et al., 2003). LH receptor occupation with hCG causes a 50-time slower LH receptor internalization than occupation with ovine LH (Mock and Niswender, 1983). This phenomenon has been associated with differences in the structure of the β-subunit of ovine LH and hCG (Mock et al., 1983).

1.3. TSH RECEPTOR SIGNALING IN THYROID CELLS AND ITS PHYSIOLOGICAL RELEVANCE

The hypothalamus secretes the TSH releasing hormone (TRH) in pulses and is consequently responsible for the synthesis and secretion of TSH from the anterior pituitary gland (Brabant et al., 1990;Magner, 1990). TSH promotes synthesis and release of two main hormones, triiodothyronine (T3) and thyroxine (T4), from the thyroid gland into the blood stream. Circulating T3 and T4 levels in the bloodstream, in turn influence the release of TSH from the anterior pituitary gland through a negative feedback mechanism and hence the release of TRH from the hypothalamus. A normal functional thyroid gland produces in average ca. 20% T3 and about 80% T4. However, T4 is converted in the periphery to T3, which is the active metabolite with a four times higher potency than T4. The main function of T3 and T4 is metabolism, development and differentiation of all cells of the human body (Köhrle, 2000) as well as the regulation of bone growth (Klaushofer et al., 1995).

The structural and functional unit of the thyroid gland is the thyroid follicle, which is comprised of a single layer of epithelial cells enclosing a lumen containing the thyroid hormone precursor, thyroglobulin (Tg). Tg is stored in an iodinated state upon iodine uptake. (Rousset and Mornex, 1991;Dunn, 1996). The major physiological regulator for thyroid functions is TSH, which binds to a GPCR, the TSH receptor, located on the basolateral membrane of thyroid cells (Vassart and Dumont, 1992), and activates predominantly the G_s protein pathway, resulting in thyroid cell differentiation, proliferation as well as stimulation of thyroid function and gene expression (Vassart and Dumont, 1992;Dremier et al., 2002) (**Figure 8**).
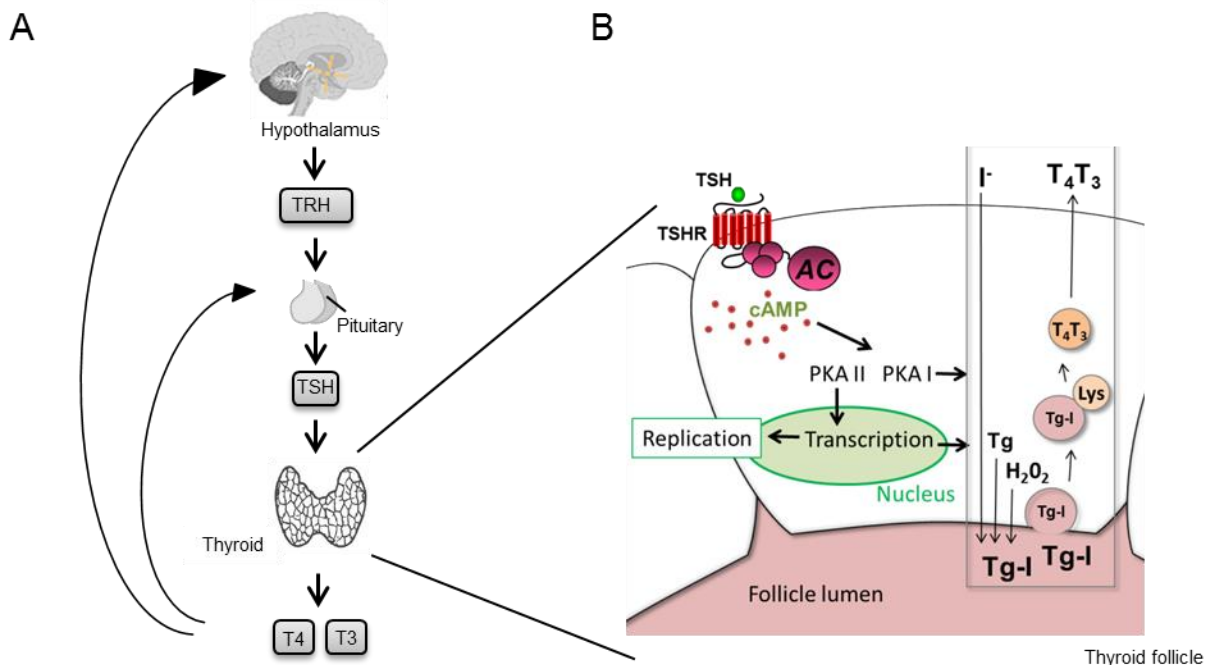
Figure 8: The thyroid model.
(**A**) Hypothalamus-pituitary-thyroid axis. Thyrotropin releasing hormone (TRH) expressed by the hypothalamus stimulates the synthesis of thyroid stimulating hormone (TSH) by the pituitary. In the thyroid TSH triggers the secretion of thyroid hormones (T3, T4). Hypothalamic and pituitary activities are controlled by T3 and T4 feedback loops.
(**B**) TSH receptor signaling pathway and its functional consequences in a thyroid follicle. Upon TSH binding to its receptor the G_s signaling cascade is activated, leading to stimulation of adenylyl cyclase (AC) producing cAMP. The cAMP level is increased and provides the phosphorylation of a number of targets by PKA, which in turn are linked to the effects of TSH i.a. Tg synthesis and the storage of iodinated Tg (Tg-I) in the follicle lumen. Upon Tg-I reuptake, thyroid hormones (T4, T3) are released by an enzymatic digestions in lysosomes (Lys). Figure modified from Du Plessis et al., 2010 .

Dysfunction of this pathway can cause an abundance of diverse thyroid disorders, including goiter, Graves' disease, Hashimoto's thyroiditis, thyroid cancer, thyroid nodules, which indeed can result in profound effects on the cardiovascular and musculoskeletal system (Weetman, 2000).

In the classical TSH/TSH receptor pathway, G_s proteins activate ACs, resulting in an intracellular increase of cAMP. The elevated cAMP activates PKA (Feliciello et al., 2000;Calebiro et al., 2006), the exchange proteins directly activated by cAMP (EPAC) (Bos, 2003) and the cyclic nucleotide-gate ion (CNG) channels (Zagotta et al., 2003). The catalytic subunit of PKA is responsible for phosphorylation of the transcription factor CREB (Porcellini et al., 2003) followed by transcription of cAMP-induced genes that promote cell growth and differentiation. Well-known genes involved in thyroid differentiated function are *Tg*, thyroid peroxidase *(Tpo)* and the sodium-iodide symporter *(Nis)* (Santisteban et al., 1987;Gerard et al., 1989;Zarrilli et al., 1990;Levy et al., 1997). These three genes express proteins that are involved in the synthesis of thyroid hormones. In particular,

NIS regulates the transport of iodine into the cell, which consequently is responsible for the iodination of Tg. The iodination reaction is catalyzed by TPO in the presence of its essential substrate H_2O_2. In contrast, cAMP-induced stimulation of EPAC results in Rap1 activation (Pannekoek et al., 2009), but has no effect on gene expression, which is promoted only by the cAMP/PKA signaling cascade (van Staveren et al., 2012).

Although most effects of the TSH receptor are mediated by coupling to G_s, it has been shown that upon stimulation by higher concentration of TSH, the TSH receptor is able to signal also through $G_{q/11}$ (Kero et al., 2007). The activation of $G_{q/11}$ leads to downstream generation of second messengers diacylglycerol (DAG) and inositol trisphosphate (IP3) via PLC activation (Allgeier et al., 1994;Laugwitz et al., 1996), followed by a subsequent rise in the intracellular calcium concentration in thyroid cells (Allgeier et al., 1997;Dremier et al., 2002). As a result, protein kinase C (PKC) activation occurs, which indeed is required for TSH-induced thyroid hormone synthesis and release. A lack of $G_{q/11}$ protein expression leads to a reduced iodine uptake resulting in hypothyroidism (Kero et al., 2007). In 2008, the group of Büch demonstrated for the first time that the TSH receptor is able to activate MAPK via a cAMP-independent pathway through the G_{13} protein (Büch et al., 2008). Besides conventional signaling via G_α proteins, the dissociated $G_{\beta\gamma}$ subunits can also cause direct activation of the PI3K/Akt pathway (Zaballos et al., 2008), leading to *NIS* gene expression and consequently thyroid hormone synthesis in a cAMP-independent manner (Riedel et al., 2001).

While TSH is believed to be the major regulator of thyroid function, insulin-like growth factor 1 (IGF-1) receptor signaling plays an essential role in the regulation of thyroid hormone biosynthesis and thyroid growth (Kimura et al., 2001;Ock et al., 2013). It has been shown that cAMP induces the production of autocrine growth factors in thyroid cells (Brown et al., 1986), like IGF-1, insulin or EGF, which in turn together with the initial G_s signaling allows full expression of the cell cycle progression and proliferative response in Fischer rat thyroid cell line 5 (FRTL-5) (Tramontano et al., 1986;Takahashi et al., 1990;Kimura et al., 2001). In various thyroid cell culture systems, it is controversially discussed whether TSH and IGF-1 act synergistically or are signaling through distinct cascades (Kimura et al., 2001).

1.3.1. Protein kinase A signaling in thyroid cells

The cAMP-dependent protein kinase A (PKA) is a heterotetramer composed of two regulatory (R) and two catalytic (C) subunits. Upon cAMP production each regulatory subunit is occupied by two cAMP molecules and the regulatory subunits dissociate from the catalytic subunits. The catalytic subunits are now capable to freely diffuse inside the cells either in the cytosol or into the nucleus and phosphorylate specific serine and/or threonine residues of target proteins (Adams et al., 1991) (**Figure 8**).
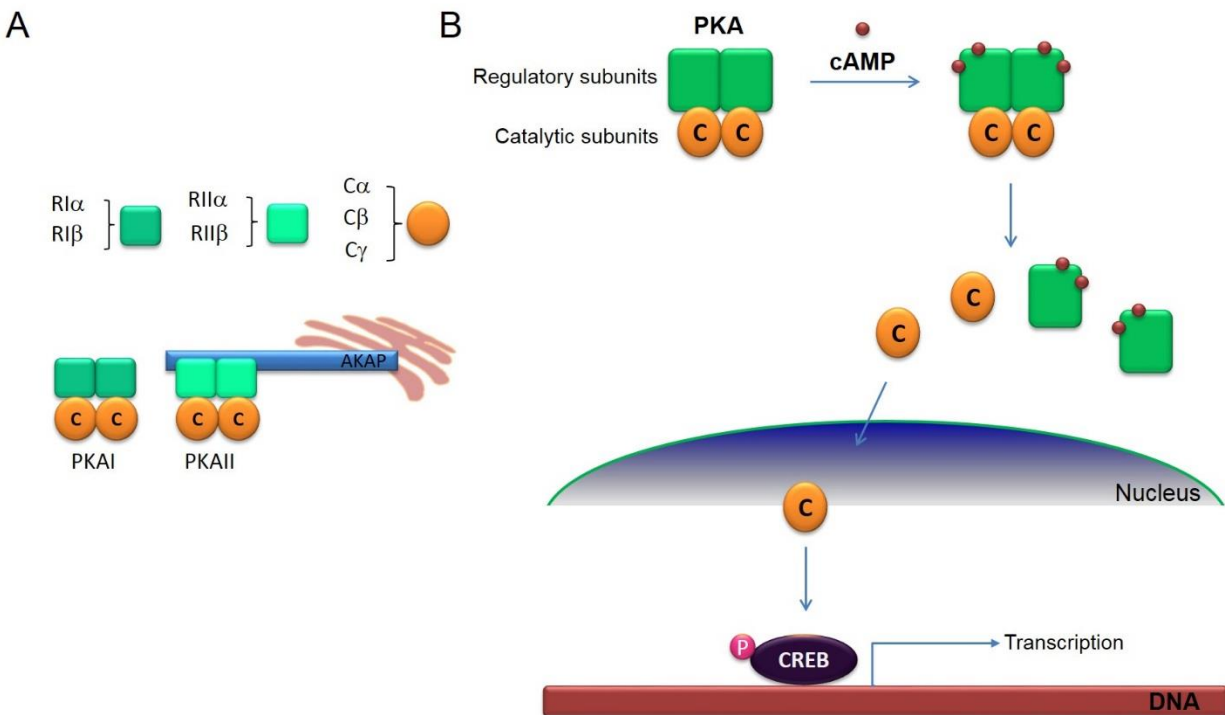
Figure 9: PKA signaling.
(A) Multiple isoforms of PKA subunits with different subcellular localization. PKA I diffuses freely in the cytosol, whereas PKA II is anchored to cellular membranes.
(B) Upon cAMP binding to the regulatory subunit of PKA, the regulatory subunit dissociates from the catalytic subunits. The catalytic subunit enters the nucleus and phosphorylates the transcription factor CREB.

Depending on the differences in regulatory subunits, two main isoforms of PKA were identified (PKA I and II) (Corbin et al., 1975), which was followed by discovery of multiple isoforms for the subunits: mainly four R subunit isoforms (RIα, RIβ; RIIα and RIIβ) and three C subunit isoforms (Cα, Cβ, Cγ) (McKnight et al., 1988;Beebe, 1994). Moreover, it was also shown that the subunits differ in their subcellular localization and tissue distribution (Skalhegg and Tasken, 2000) with PKA I being mostly cytosolic and PKA II being prevalently targeted via A-kinase anchoring proteins

(AKAPs) to cell structures like the plasma membrane, the cytoskeleton and the Golgi (Rios et al., 1992;Rubin, 1994;Li et al., 1996).

In thyroid cells, signaling by PKA isoforms (PKA I and PKA II) plays an important role in mediating the effects on thyroid function. It was long believed that PKA I is more effective on mediating TSH proliferation than PKA II, based on experiments performed in dog primary thyroid cells as well as in FRTL-5 cells (Vansande et al., 1989;Tortora et al., 1993). However, the study of Feliciello et al. (1996) demonstrated that the lack of PKA RIIβ expression and its delocalization result in a reduced nuclear targeting/translocation of the catalytic subunit and lack of induction of cAMP-dependent genes in FRTL-5 cells (Feliciello et al., 1996). This is supported by another study in mouse fibroblasts stably expressing the TSH receptor, which indicated that PKA RIIβ is necessary for TSH-dependent growth (Porcellini et al., 2003). This is confirmed by the fact that AKAP disruption prevents CREB phosphorylation induced by PKA II signaling (Calebiro et al., 2006).

Additionally, it has been shown that PKA I and PKA II promote different biological effects of TSH in FRTL-5 cells. PKA I is involved in post-transcriptional regulations like iodine uptake and has inhibitory effects on ERK phosphorylation, thus affecting the MAPK pathway. Whereas, PKA II, especially RIIβ, promotes gene transcription of early genes (*Nr4a1, Nr4a3*) as well as of late genes (*Nis, Tpo*) and cell growth (Feliciello et al., 2000;Calebiro et al., 2006). These findings indicated that PKA II has a major role in TSH signaling.

1.3.2. TSH receptor internalization

In 1982, internalization of fluorescently labeled TSH into endosomes was demonstrated in FRTL-5 cells (Avivi et al., 1982), but the involved mechanisms and the functional role of TSH receptor endocytosis was still unclear. Since then, a series of studies have investigated TSH receptor endocytosis (Haraguchi et al., 1994;Shi et al., 1995;Baratti-Elbaz et al., 1999;Lahuna et al., 2005). Perhaps the most conclusive one was by Baratti-Elbaz et al. (1999), who showed the localization of the TSH receptor on the cell-surface and in clathrin-coated vesicles in L-cells stable expressing the TSH receptor. Interestingly, 90% of the internalized TSH receptor was recycled back to the cell-surface, whereas the majority of the internalized TSH was degraded in lysosomes. These findings could be confirmed by similar experiments in primary human thyroid cells (Baratti-Elbaz et al., 1999). In contrast, it was shown for the LH receptor expressed in L-cells that almost no LH receptors are recycled back to the cell-surface and instead are degraded in lysosomes (Ghinea et al., 1992).

Recent studies in primary thyroid follicles challenged the original view of the functional role of receptor internalization by showing TSH-induced internalization of TSH/TSH receptor complexes in the intracellular site causes persistent cAMP elevations. In particular, it could be shown that cAMP is continuing to signal after TSH removal. In addition, after TSH receptor internalization TSH was seen in a pre-Golgi compartment that contained also G_s proteins and AC III (Calebiro 2009). Similar to the study of Frenzel et al. (2006), showing TSH receptors do not co-localize with β-arrestin in endosomes (Frenzel et al., 2006).

Another study of stably expressed TSH receptors in HEK 293 cells demonstrated no persistent cAMP signaling induced by TSH. This indicates that TSH/TSH receptor co-internalized into a compartment, which is just present in primary thyroid cells to elicited persistent cAMP signaling (Werthmann et al., 2012).

Blocking TSH receptor internalization with an endocytosis inhibitor dynasore prevents the irreversibility of the cAMP signal. In addition, TSH receptor internalization is responsible for signaling effects downstream of PKA in thyroid cells. In particular, the TSH-induced phosphorylation of vasodilator-stimulated phosphoprotein (VASP), a PKA substrate, and the TSH-induced rearrangement of actin cytoskeleton were impaired by blocking TSH receptor internalization (Calebiro et al., 2009).

1.4. METHODS FOR VISUALIZATION OF cAMP AND PKA DYNAMICS

1.4.1. Principle of fluorescence resonance energy transfer

Förster/Fluorescence Resonance Energy Transfer (FRET) has become one of the most important tools to study protein-protein interactions inside living cells (**Figure 10**). FRET describes an energy transfer process between two fluorophores. By excitation of a donor the energy of the excited state is transmitted through dipole-dipole interactions to a near acceptor fluorophore, which results in emission from the acceptor (Förster, 1948).
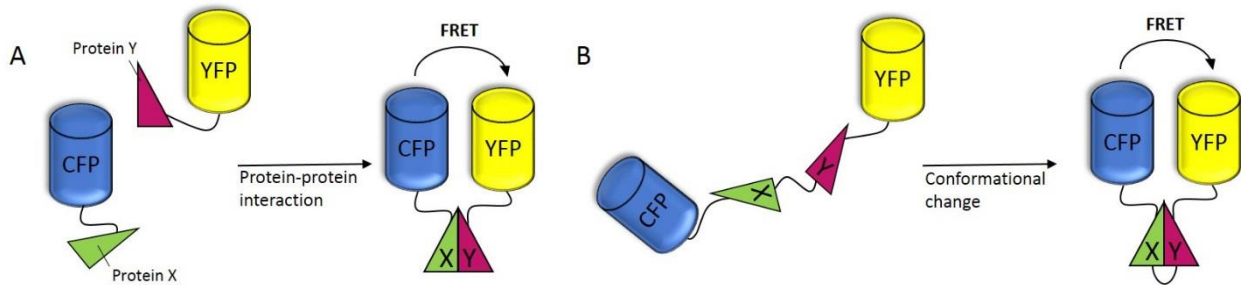
Figure 10: FRET technique.
Close proximity of donor (CFP) and acceptor fluorescent protein (YFP) results in increase of FRET. This technique allows visualization of dynamic protein-protein interactions (**A**) and conformational changes within a single protein (**B**); cyan fluorescent protein (CFP), yellow fluorescent protein (YFP). Figure modified from Zhang et al., 2002 .

The efficiency of FRET depends on 1st the spectral overlap between the donor emission and the acceptor excitation, 2nd the distance between donor and acceptor, 3rd the quantum yield of the donor and 4th the relative orientation of the donor and acceptor (Day and Davidson, 2012).
More in detail, the energy transfer efficiency largely depends on the space/proximity between the donor and acceptor molecules and varies as the inverse of the sixth power of the distance (Förster, 1948;Piston and Kremers, 2007), as described by the Förster equation:

$$E_{FRET} = \frac{1}{\left[1 + \left(\frac{r}{R_0}\right)^6\right]}$$

where r is the distance between donor and acceptor fluorophore and R_0 (Förster radius) is the distance between donor and acceptor fluorophore that gives 50% FRET efficiency. Due to the fact that the FRET efficiency falls off with the sixth power, the distance r is the critical parameter for measurable FRET to occur and thus FRET can be used as a molecular ruler, i.e. to monitor distances (Stryer, 1978).

R_0 is specific for each FRET pair of fluorescent proteins and can be calculated for aqueous solutions as follows:

$$R_0 = [2.8 \times 10^{17} * \kappa^2 * Q_D * \varepsilon_A * J(\lambda)]^{\frac{1}{6}} \, nm,$$

where κ^2 is the orientation angle variable which describes the angle between the two dipoles of the fluorophores. The alignment of the two fluorophores to each other is also contributing to the FRET efficiency. Parallel orientated dipoles of the fluorophores show higher FRET efficiencies compared to a perpendicular orientation. Theoretically, values can range from 0 to 4, but in general, the value is implicit to be approximately 2/3 assuming random orientation of the two fluorophores. Q_D is the donor quantum yield and ε_A the maximal acceptor extinction coefficient, both values are constant. $J(\lambda)$ is the spectral overlap integral, which describes the region between the normalized donor emission spectrum $F_D(\lambda)$ and the acceptor excitation spectrum $E_A(\lambda)$:

$$J(\lambda) = \int F_D(\lambda) * E_A(\lambda) * \lambda^4 d\lambda$$

In theory, for an optimal FRET pair, one has to choose a donor with high quantum yield, an acceptor with a strong extinction coefficient, and the donor emission and acceptor excitation spectra must overlap to a sufficient degree (Piston and Kremers, 2007) (**Figure 11**).
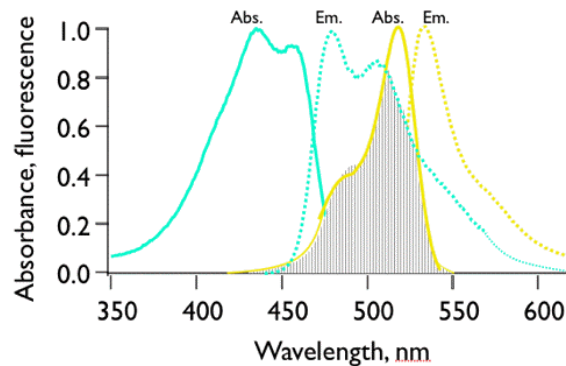
Figure 11: Excitation and emission spectra of CFP and YFP.
Shown are the absorption (Abs.) and emission (Em.) spectrum of CFP and YFP. The overlap of CFP emission spectrum (turquoise broken line) with YFP excitation spectrum (yellow line) is indicated in grey. Figure modified from Visser and Rolinski (http://photobiology.info/Visser-Rolinski.html).

1.4.2.   Biosensors for visualization of cAMP dynamics

In the past 20 years, a large number of genetically encoded biosensors have been developed to allow monitoring GPCR signaling directly in living cells, ranging from ligand binding and receptor activation to the downstream signaling by cAMP (Zaccolo et al., 2000;Janetopoulos et al., 2001;Castro et al., 2002;Bünemann et al., 2003;Vilardaga et al., 2003;DiPilato et al., 2004;Nikolaev et al., 2004;Ponsioen et al., 2004;Lohse et al., 2008;Calebiro et al., 2009). Most of these sensors are FRET-based and allow not only to observe protein-protein interaction but also conformational change in real time. This allows capturing fast signaling events and at the same time defining their subcellular location. Thus, FRET-based sensors are a great tool to measure the second messenger cAMP dynamics in high spatial and temporal resolution (Zaccolo et al., 2000;Nikolaev and Lohse, 2006).

The first FRET sensor for cAMP was developed by Adams et al., 1991 and was based on dissociation of the catalytic and regulatory subunit of PKA upon cAMP binding. Purified catalytic and regulated subunits had to be chemically labeled with two different fluorophores (rhodamine and fluorescein, respectively) before microinjecting them into cells to monitor FRET changes in the intracellular cAMP level (Adams et al., 1991). This sensor was modified 19 years later by Zaccolo et al. (2000) via replacing rhodamine and fluorescein with two mutants of the green fluorescent protein (GFP); blue GFP mutant (BFP) and GFP-S65T mutant. The most useful advantage of this modification was the new sensor DNA, which easily allows transfection into cells without purification, labeling and microinjection processes (Zaccolo et al., 2000).

A third generation of cAMP sensors was developed because of the slow on and off kinetics of the PKA-based sensors and the circumstance of expressing two different proteins of equal concentration in a single cell. In principle, the new biosensor generation for cAMP used the exchange proteins directly activated by cAMP, either full-length, partially truncated or just a single-chain cAMP binding domain (Epac1-camps) flanked on either side with two fluorophore to allow FRET. Cyan and yellow fluorescent proteins (CFP and YFP respectively) function as a common FRET pair (DiPilato et al., 2004;Nikolaev et al., 2004;Ponsioen et al., 2004;Dunn et al., 2006). Upon cAMP accumulation, the sensor undergoes a conformational change leading to loss of the proximity of the two fluorophore, which results in a decrease of the FRET ratio (**Figure 12**). A decrease of FRET is proportional to an increase of cAMP level.
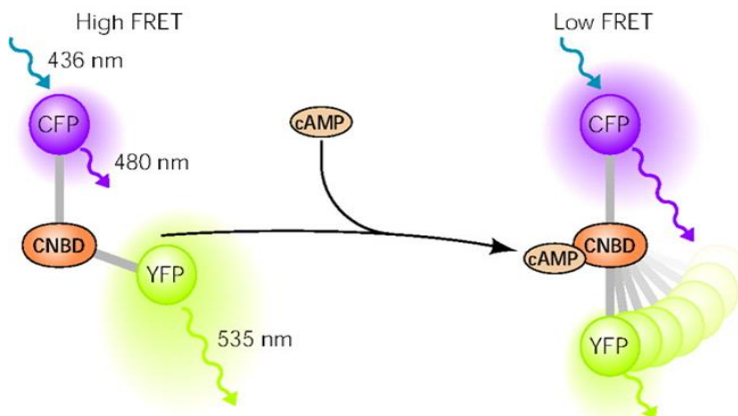
Figure 12: Principle of the Epac1-camps sensor.
The Epac1-camps sensor is based on a single cAMP binding domain from Epac1 sandwiched by cyan and yellow fluorescent proteins. At low cAMP levels, donor (CFP) and acceptor (YFP) are in close proximity and FRET occurs. Upon cAMP binding to the cyclic nucleotide-binding domain (CNBD) a conformational change and a concomitant decrease in FRET occurs. Excitation of CFP is at 436 nm, CFP and YFP emission are collected at 480 and 535 nm, respectively. Figure modified from Nikolaev and Lohse, 2006 .

A remarkable improvement was the creation of a transgenic mouse model with ubiquitous expression of the cytosolic cAMP indicator Epac1-camps allowing detection of GPCR/cAMP signaling in different living primary cell systems and tissues (Calebiro et al., 2009).

1.4.3. Biosensors for visualization of PKA dynamics

In contrast to extensive studies on cAMP signaling using FRET sensors, less attention was given to the development of fluorescent sensors/FRET-based sensors for PKA dynamics. Over the last 10 years, a new requirement of investigation was born to detect protein kinase dynamics in a spatial and temporal manner. Methods, like immunocytochemistry (Verveer et al., 2000) or fluorescently labeled peptide substrates for kinases (Lee et al., 1999), were not successful in visualizing compartmentalized activities of kinase and phosphatases.

One of the first pioneers, who were able to monitor spatial and temporal PKA signaling in live cells, was the group of Roger Tsien. In 2001, this group succeeded in creating a genetically encoded fluorescent reporter for PKA termed AKAR (A-kinase activity reporter), which gained great attention (Zhang et al., 2001). The first generation of biosensor, AKAR1, consists of a phosphoamino acid binding domain derived from 14-3-3 protein (Muslin et al., 1996) and a consensus substrate for PKA, sandwiched between a fluorophore pair (enhanced CFP and Citrine). Enhanced CFP and Citrine function as FRET donor and acceptor, respectively. For PKA substrate a modified version of the kemptide (LRRASLP) was used. Two flexible linkers were inserted into the sensor: one was fused between the substrate and citrine and another was used as a replacement of the C-terminal of 14-3-3 protein. Upon serine phosphorylation induced by PKA, the derived domain of 14-3-3 protein binds to phosphoserine resulting in a conformational change of the sensor and causes an increase in fluorescence intensity (**Figure 13A**). Although AKAR1 shows uniform distribution/ubiquitous expression in living cells, there was a need of optimization regarding improvement in the specificity, dynamic range, reversibility and integrity. Initially, AKAR1 showed an almost irreversible FRET response in living cells leading to the assumption that the phosphoamino binding domain derived from 14-3-3 protein, had a high binding affinity to the PKA substrate and prevents the phosphorylated substrate from being dephosphorylated by phosphatases (Zhang et al., 2001). Therefore, the design of a new version of the original sensor was created termed, AKAR2, to achieve a better reversibility. The 14-3-3 protein was replaced by a forkhead associated domain 1 (FHA1), classified as a phosphotheorine binding domain with submicromolar binding affinity to its substrate (LRRATLVD) (Zhang et al., 2005;Allen and Zhang, 2006) (**Figure 13B**).
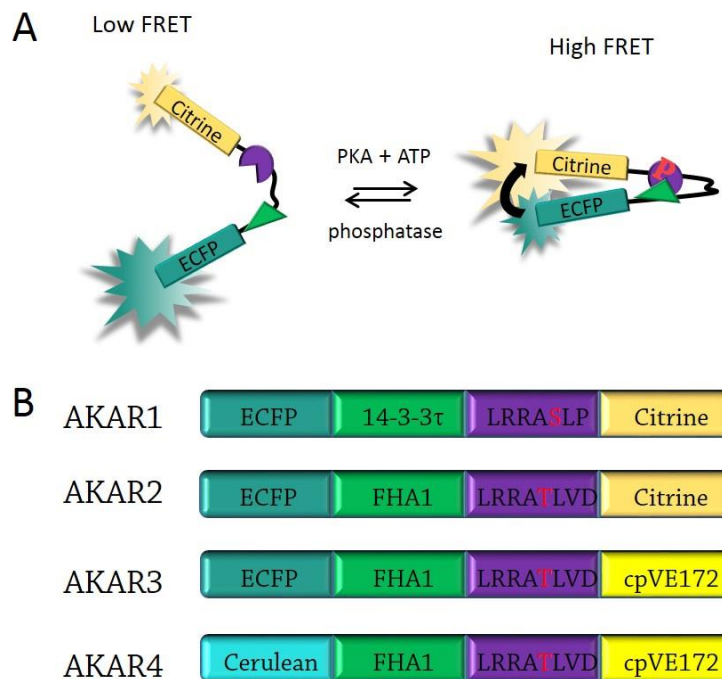
Figure 13: Principle of the AKAR sensor.
(A) The AKAR sensor is based on a phosphoserine/threonine binding site and a PKA-specific peptide sequence sandwiched by two fluorophores (cyan and yellow fluorescent proteins). At low PKA levels, donor (ECFP) and acceptor (Citrine) are in distant proximity and no FRET occurs. Upon PKA activation the PKA substrate gets phosphorylated and a conformational change and an associated increase in FRET occurs.
(B) AKAR sensor development. Figure modified from Zhou et al., 2012.

Due to the fact that the FRET efficiency strongly depends on the distance and orientation of the FRET pair, the linker length between different domains of a FRET reporter is critical. In the case of the AKAR2 sensor the modification of the linker length between FHA1 allowed an increased FRET signal and faster kinetics (Zhang et al., 2005;Allen and Zhang, 2006). A further possibility to improve FRET efficiency is direct manipulation of FRET pairs: either to replace them or use circularly permutated FRET pair, which has also been tried by Jin Zhang. While a replacement of a fluorescent protein itself did not improve the emission ratio changes, a circular permutation of the replaced fluorescence protein enhanced the dynamic range by 2-fold. This new version was termed AKAR3 (Allen and Zhang, 2006;Zhou et al., 2012). The latest version, designated AKAR4, took advantage of the fluorescent protein cerulean, a brighter version of the previously used enhanced CFP. The Cerulean containing reporter showed a further increase in the dynamic range of 67 % over AKAR3 (Depry et al., 2011).

2. Aim of the study

GPCR signaling has been long believed to occur only at the cell-surface, but findings of the last seven years have demonstrated that GPCR signaling persists after agonist-induced internalization of ligand/receptor complex. This is associated with persistent cAMP signaling and is required for functional outcomes. Our laboratory has revealed that the TSH receptor, a glycoprotein hormone receptor, continues signaling via cAMP from the intracellular site and this persistent signaling is required for depolymerization of actin. However, a key biological effect of GPCR signaling at intracellular sites, which would demonstrate its physiological relevance, still remained to be shown.

The aim of the present study was to provide insights into intracellular GPCR signaling downstream of cAMP and the physiological relevance of GPCR signaling after internalization.

Three main questions were addressed:

1. Do other glycoprotein hormone receptors continue signaling via cAMP after internalization?
2. Does internalized and cell-surface GPCR signaling differ in the type and spatiotemporal course of PKA activation?
3. What are the specific signaling outcomes and biological consequence of intracellular signaling?

The results provide important insights into the recently published paradigm of GPCR signaling after internalization.

3. Materials und Methods

3.1. MATERIALS

All solutions were prepared using ultrapure water from Milli-Q Reference Water Purification System (EMD Millipore, Billerica, USA) if not stated otherwise.

3.1.1. Cell lines and mouse strains

Human embryonic kidney (HEK) 293AD cell line   (ATCC)

Epac1-camps transgenic mice   (Calebiro et al.,(2009) Plos Biol.)

FVB mice   (Janvier Lab, France)

3.1.2. Plasmid vectors

AKAR2   (Dr. Jin Zhang, Baltimore, MD)

AKAR2-CAAX   (this work)

AKAR2-NES   (this work)

AKAR2-NLS   (this work)

AKAR4-CAAX   (Dr. Jin Zhang, Baltimore, MD)

AKAR4-NES   (Dr. Jin Zhang, Baltimore, MD)

AKAR4-NLS   (Dr. Jin Zhang, Baltimore, MD)

YFP-hLH receptor   (Ulrike Zabel)

3.1.3. Enzymes

Benzonase   (Sigma Aldrich)

Collagenase I   (Life Technologies)

Collagenase II   (Life Technologies)

Dispase I   (Roche diagnostic)

Pfu DNA polymerase   (Promega)

RNase H   (Life Technologies)

RNaseOUT   (Life Technologies)

Restriction enzymes for molecular cloning   (New England Biolabs)

SuperScript® II Reverse Transcriptase   (Life Technologies)

T4-DNA ligase 400,000 U/ml   (New England Biolabs)

Trypsin   (PAN biotech)

3.1.4. Antibodies

Primary antibodies:

anti-GOLPH4 rabbit polyclonal	(Abcam)
anti-PKA Cα mouse monoclonal	(BD Transduction)
anti-PKA RIα mouse monoclonal	(BD Transduction)
anti-PKA RIIα mouse monoclonal	(BD Transduction)
anti-PKA RIIβ mouse monoclonal	(BD Transduction)
anti-α-tubulin mouse monoclonal	(Sigma Aldrich)
anti-Phospho-CREB rabbit monoclonal	(Cell Signaling)

Secondary antibodies:

goat anti-mouse HRP-conjugated	(BioRad)
goat anti-rabbit HRP-conjugated	(BioRad)
goat anti-rabbit AlexaFluor594-conjugated	(Life Technologies)
goat anti-mouse Cy3-conjugated polyclonal	(Jackson ImmunoResearch dianova)

3.1.5. Chemicals

Acrylamide (Rotiphoreses Gel 30)	(ROTH)
Agarose	(peqlab)
AlexaFluor488-conjugated transferrin	(Life Technologies)
Ammonium persulfate (APS)	(Sigma Aldrich)
Ampicillin	(AppliChem)
Aprotinin	(AppliChem)
8-Br-cAMP	(BioLog Life Science Inst.)
BNa_3O_3	(AppliChem)
Bovine serum albumin V (BSA)	(AppliChem)
Bovine thyroid stimulating hormone (bTSH)	(Sigma Aldrich)
Bromophenol blue	(AppliChem)
$CaCl_2$	(Merck Millipore)
Carbenoxolone (CBX)	(Sigma Aldrich)
Chloroform	(Roth)
Complete protease inhibitor cocktail mini tablet	(Roche diagnostic)
Diethylpyrocarbonate (DEPC)	(AppliChem)
Dimethylsulfoxide (DMSO)	(AppliChem)

Dithiothreitol (DTT)	(AppliChem)
Dynasore	(Sigma Aldrich)
Ethylenediaminetetraacetic acid (EDTA)	(AppliChem)
Ethidium bromide solution	(ROTH)
Forskolin	(Tocris)
Glycerol	(Sigma)
Glycine	(Sigma)
Goat serum	(Thermo Scientific)
H-89 dihydrochloride hydrate	(Sigma Aldrich)
8-HA-cAMP	(BioLog Life Science Inst.)
4-(2-hydroxyethyl)-1-piperazineethanesulfonic acid (HEPES)	(Sigma Aldrich)
I^{125}human chorionic gonadotropin (I^{125}hCG)	(Izotop)
Kanamycin	(AppliChem)
KCl	(AppliChem)
Leupeptin	(Merck Millipore)
6-MBC-cAMP	(BioLog Life Science Inst.)
Methanol	(Sigma Aldrich)
$MgCl_2$	(AppliChem)
NaCl	(AppliChem)
NaOH	(Sigma Aldrich)
N,N,N',N'-Tetramethylenediamine (TEMED)	(Sigma Aldrich)
Ovine follicle stimulating hormone (oFSH)	(Dr. A. F. Parlow, National Hormone and Peptide Program (NHPP))
Ovine luteinizing hormone (oLH)	(Dr. A. F. Parlow, National Hormone and Peptide Program (NHPP))
8-PIP-cAMP	(BioLog Life Science Inst.)
Paraformaldehyde (PFA)	(Sigma Aldrich)
Phenylmethylsulfonyl fluoride (PMSF)	(Sigma Aldrich)
RNAse-free H_2O	(Qiagen)
Rolipram	(Sigma Aldrich)
RP-8-Br-cAMPS	(BioLog Life Science Inst.)
RP-8-PIP-cAMPS	(BioLog Life Science Inst.)
Sodium dodecyl sulfate (SDS)	(AppliChem)
Sephadex G-25	(GE Healthcare)

Sp-5,6-DCL-cBIMPS   (BioLog Life Science Inst.)

Tris (hydroxymethyl)-aminomethan (Tris)   (AppliChem)

TRITC   (Life Technologies)

Triton X-100 peroxide-free   (AppliChem)

Tween-20   (Sigma Aldrich)

3.1.6. Materials for cell culture

Minimum Essential Medium alpha phenol-red free

(MEMα)   (Life Technologies)

Dulbecco´s Modified Eagle Medium: Nutrient Mixture

F-12 phenol-red free (DMEM/F12)   (Life Technologies)

Dulbecco´s Phosphate Buffer Saline (DPBS)   (Life Technologies)

Fetal Bovine Serum, FBS Superior (FBS)   (Biochrom AG)

Penicillin / Streptomycin (100 U/ml / 100 µg/ml)   (Life Technologies)

Insulin-Transferrin-Selenium-Sodium Pyruvate (ITS)   (Life Technologies)

Hank's Balanced Salt Solution (HBSS)   (Life Technologies)

L-Glutamine   (PAN biotech)

3.1.7. Kits and reagents

BCA Protein Assay Kit   (Thermo Scientific)

ECL Western Blotting Detection Reagent   (Amersham)

Effectene Transfection Reagent   (Qiagen)

LB-agar powder   (AppliChem)

LB-medium powder   (AppliChem)

1 kb DNA ladder   (New England Biolabs)

5x loading dye (for agarose gel electrophoresis)   (Applichem)

Protein ladder (Protein marker V)   (peqLab)

Lipofectamine 2000 Transfection Reagent   (Invitrogen)

NucleoSpin extract Kit   (Macherey-Nagel)

Qiagen Plasmid Mini Kit   (Qiagen)

Qiagen Plasmid Plus Midi Kit   (Qiagen)

10x Orange G DNA loading dye   (Thermo Scientific)

Polyvinylidene fluoride (PVDF) membrane   (Merck Millipore)

SuperScript® II Reverse Transcriptase   (Life Technologies)

SYBR Select Master Mix   (Life Technologies)

TRIzol   (Life Technologies)

10x TAE buffer   (AppliChem)

All oligonucleotides were purchased from Eurofins MWG Operon, diluted to 100 µM in ddH$_2$O and stored at –20°C.

3.2. METHODS

3.2.1. Genetic engineering

POLYMERASE CHAIN REACTION

The polymerase chain reaction (PCR) (Saiki et al., 1988) is a common method to amplify DNA. A typical PCR encloses three major steps: First, denaturation of the double-stranded template at 94°C, followed by a decrease in temperature to allow oligonucleotide annealing to the singlestranded DNA, and finally elongation by DNA polymerase at 72°C. These three steps are repeated 28-35 times for sequence amplification.

The PCR reaction mixture contained 1 U Pfu polymerase, 10 µl 10x Pfu reaction buffer, 2.5 µl forward primer (final conc. 25 µM), 2.5 µl reverse primer (final conc. 25 µM), 2 µL 10 mM desoxyribonucleotide triphosphates mix (dNTPs), 100–200 ng cDNA template and ddH_2O up to a total volume of 100 µl and then the reaction was run using a thermocycler (GeneAmp PCR system 9700, AB Applied Biosystems). The standard annealing temperature (T) was adapted to the melting temperature (T_m) of the oligonucleotides (2°C below the lowest primer´s T_m) and the elongation time (t) was depended on the length of the desired PCR product (*Pfu* polymerase replicates 1 kbp in 2 min). For real-time quantitative RT-PCR see **3.2.4**.

PCR program: (94°C – 5 min, 30x(94°C – 30 s, T°C – 30 s, 72°C - t), 72°C – 7 min, 4°C - ∞)

AGAROSE GEL ELECTROPHORESIS

Agarose gels (1% Agarose, 0.5% EtBr in TAE buffer) were used in this study to separate DNA fragments according to their size. DNA samples were mixed 9:1 with Orange G DNA loading dye and loaded onto the gel; 1 kb DNA ladder was used as DNA standard and TAE was used as running buffer. Gels were run at a constant voltage of 100 V. Gel electrophoresis was also performed for isolation of DNA fragments, which were needed for ligation reactions during molecular cloning. A documentation system (Transilluminator, herolab) was used for UV-detection. For DNA extraction and purification the NucleoSpin extraction kit was used, according to the manufacturer's protocol and DNA was eluted with 30-50 µl ddH_2O.

RESTRICTION DIGESTION

A typical restriction digestion requires 2 µg template supplemented with 1 µl of each restriction enzyme, 5 µl New England Biolabs buffer and ddH$_2$O up to a volume of 50 µl. The mixture was incubated at 37°C for 1 h and the digested products were separated by gel electrophoresis. The isolated DNA was extracted and eluted in 30 µl ddH$_2$O (vector fragment) or 30 µl ddH$_2$O (insert). These extracted DNA fragments were used for subsequent ligation reactions.

LIGATION REACTION

Ligation reaction allows the insertion of a DNA fragment of interest into a plasmid vector of choice. The reaction mixture consisted of 1 µl vector, 1 µl insert/or digested PCR product, 1.5 µl 10x ligase reaction buffer and 1 µl T4-DNA ligase and was then incubated overnight at 14°C. Different vector-to-insert ratios were run in parallel to increase the ligation efficiency.

TRANSFORMATION OF COMPETENT E.COLI

For the purpose of amplification, ligation products were introduced into competent *E.coli* bacteria (Top 10). 65 µl ddH$_2$O and 20 µl of 5x KCM buffer were mixed with 15 µl of the ligation product and incubated on ice for 5 min. At the same time, 100 µl competent bacteria were thawed on ice and added to the ligation mixture which then incubated for 20 min on ice followed by 10 min incubation at room temperature (RT). This was followed by addition of 1 ml Luria-Bertani (LB) medium (without antibiotics). Cells were then incubated at 37°C for 50 min in a shaker at 600 rpm. Afterwards, the cells were centrifuged at 14,000 rpm, plated on selective LB-agar plates containing appropriate selection antibiotics. Isolated colonies were obtained after an overnight incubation at 37°C.

- **KCM buffer**: 500 mM KCL, 150 mM CaCl$_2$, and 250 mM MgCl$_2$ in ddH$_2$O.
- **LB-medium**: 25 g LB-medium powder was dissolved in 1 l ddH$_2$O, autoclaved, and stored at 4°C.
- **Selective LB-agar plates**: LB-medium + 1.5% Agar and supplemented with selection antibiotics, e.g., Kanamycin or Ampicillin.

PLASMID PURIFICATION

Depending on the starting bacterial culture, plasmid DNA was either purified by Qiagen Plus Mini kit or by Qiagen Plus Midi kit according to the manufacturer's protocols. Concentration of purified DNA was measured using a UV/VIS spectrophotometer, Nano Drop 2000, followed by a concentration adjustment to 1 µg DNA/µl. Aliquots were then stored at -20°C.

3.2.2. Cell culture and transfection techniques

MOUSE BREEDING

Transgenic and wild-type FVB mice were housed in the SPF animal facility of the Institute of Pharmacology and Toxicology, University of Würzburg. Mice were sacrificed at the age of 23 days or 2-3 months for the isolation of ovarian follicles and mural granulosa cells or thyroid cells, respectively. The mouse lines were managed by technicians of the SPF animal facility. All animal experiments were performed according to institutional and governmental guidelines of Lower Franconia.

ISOLATION AND TRANSFECTION OF PRIMARY THYROID CELLS

To perform Fluorescence Resonance Energy Transfer (FRET) measurements in single cells, thyroid follicles were isolated from transgenic Epac1-cAMPs mice (Calebiro et al., 2009) or wild-type mice and cultured to eventually obtain single cells. Under a stereomicroscope, thyroid lobes were isolated from 2-3 months-old mice. The lobes were briefly washed by dipping them in sterile DPBS and were then collected in a 1.5 ml tube, containing 1 ml of digestion solution, which consisted 100 U/ml collagenase I (100 U/L), collagenase II (100 U/L), dispase I (1 U/L) and DMEM/F12 medium. Enzymatic digestion was carried out for ca. 90 min in a water bath maintained at 37°C, with manual shaking every 15 min. The digestion enzymes were removed by washing twice with complete culture medium (DMEM/F12 medium supplemented with 20% Fetal Bovine Serum (FBS), 100 U/ml penicillin G and 100 µg/ml streptomycin) centrifugation at $100x$ g for 3 min. Isolated thyroid follicles were maintained in complete culture medium at 37°C, 5% CO_2 until at least 7 days, which is the time they need to completely dissociate to single thyroid cells and recover from the digestion and proliferation.

In order to transfect primary thyroid cells, the commercially available transfection reagents were not successful and efficient. Thus, an electroporation protocol was developed to transfect these cells with fairly better efficiency. Electroporation is a transfection procedure based on a millisecond electrical pulse, leading to a short-term permeabilization of the plasma membrane resulting in cellular uptake of plasmid DNA.

7-11-day old thyroid cells were washed twice with prewarmed DPBS followed by addition of 2 ml trypsin for 10 min at 37°C, a time which is sufficient for detaching thyroid cells from the cell culture dish. To inactivate and remove trypsin, 10 ml of complete culture medium was added and the cell suspension was centrifuged for 3 min at $100x$ g at RT. The cell pellet was washed once with 10 ml DPBS and centrifuged again to remove the medium, which would impair the electroporation process and therefore the transfection efficiency. The pellet was then resuspended in 240 µl DPBS

and was divided equally into two separate electroporation cuvettes (BioRad, 4 mm) and mixed with 40 µg plasmid DNA. Electroporation was carried out using the BioRad Gene Pulsar electroporator with a Capacitance Extender set to 0.32 kV and 125 µF. Complete culture medium of 1 ml was added to each cuvette shortly after the electroporation process to allow recovery of the cells. Electroporated thyroid cells from one cuvette were distributed into 4 wells of a 6-well plate, each containing a 24-mm round glass coverslip covered with 2 ml complete culture medium. Transfection efficiency was 10-15%. FRET measurements were performed 48 h post-transfection if not mention differently.

ISOLATION OF OVARIAN FOLLICLES

Ovarian follicles were isolated from a transgenic mouse with ubiquitous expression of a FRET sensor for cAMP (Epac1-camps) (Nikolaev et al., 2004). Ovaries were removed from 23-26 days-old transgenic Epac1-camps mice (Calebiro et al., 2009). Thereafter, antral follicles were isolated with the help of two 30-gauge needles under a stereomicroscope. Follicles were plated on Millicell culture plates in phenol-red-free MEMα medium supplemented with 100 U/ml penicillin G, 100 µg/ml streptomycin, 5% FBS and 10 ng/ml FSH (complete follicle medium) for 24 h at 37°C, 5% CO_2.

For germinal vesicle break down (GVBD) examination, only antral follicles with a clearly visible nucleus were used. Follicles were preincubated with 80 µM dynasore or DMSO for 1 h, followed by stimulation with LH or rolipram as indicated. At the end of stimulation, the disappearance of the nucleus, defined as GVBD, was assessed by microscopic examination.

ISOLATION AND TRANSFECTION OF PRIMARY MURAL GRANULOSA CELLS

Primary mural granulosa cells were isolated from two ovaries of an age between 23 days-2 months-old wild-type mice. Ovaries were removed and placed in a 30-mm cell culture dish containing 2 ml MEMα medium. Further steps were carried out under a stereomicroscope. The ovaries were punched with help of two 30-gauge needles to release mural granulosa cells. Large tissue fragments were removed from the plate and the remaining mural granulosa cell suspension was added to a 100-mm cell culture dish containing 8 ml of complete follicle medium. The cells were gently mixed and were distributed as a 2 ml cell suspension per well of a 6-well plate, with each well containing a 24-mm round glass coverslip and cultured at 37°C, 5% CO_2.

To achieve high transfection efficiency in primary mural granulosa cells several transfection methods were investigated and the highest efficiency was shown by Effectene, a liposome-based transfection reagent.

4-days old isolated mural granulosa cells were transfected via Effectene with a protocol that leads to a transfection efficiency of 30-40%. The transfection solution (100 µl buffer, 1 µg plasmid DNA and 8 µl Enhancer) was mixed and incubated for 5 min to condense the DNA molecules. 25 µl Effectene was added and then incubated for 10 min at RT to allow formation of a DNA-cationic-lipid complex, which interacts with the negatively charged cell membrane via its cationic surface. This formation finally allows DNA introduction by endocytosis. The mixture was filled up with 400 µl complete culture medium and then added to cells.

TRANSFECTION OF HEK 293 CELLS

HEK 293 cells were maintained in culture medium (DMEM containing 10% FBS, 2 mM L-glutamine, 100 U/ml penicillin, and 100 µg/ml streptomycin) at 37°C and 5% CO_2. Cells were subcultured at 70–90% confluency. For transient transfection in 6-well plates, cells were seeded onto clean poly-D-lysin-coated glass coverslips (24-mm, Hartenstein) at a density of 250,000 cells per well. Transfection with Effectene was carried out on the next day as described above. The transfection efficiency was 60-70%.

3.2.3. Biochemical techniques

Primary mouse thyroid cells were used for immunoblot experiments presented in this work. Cells were washed once with 1x TBS, lysed with D-Buffer (maintained at boiling temperature) and harvested with a cell scraper into a 1.5 ml tube. Next, 1 U/ml benzonase was added to the cell lysate and was placed on a shaker (1,500 rpm) for 1 h at 4°C, followed by 1 h at 4°C without shaking. Finally, the samples were sonicated for 30 sec (in a Sonicator water bath) and centrifuged at 14,000 rpm at 4°C for 30 min. The supernatant was transferred to a new 1.5 ml tube and stored at -80°C. Protein concentration was determined by Bicinchoninic Acid Assay (BCA assay).

- **10x TBS**: 0.1 M Tris (ph 7.4), 1 M NaCl in ddH$_2$O
- **D-Buffer**: 0.125 M Tris HCL (pH 6,8) and 5% SDS supplemented with a complete protease inhibitor cocktail tablet (1 tablet per 50 ml extraction solution), 0.1 M PMSF, 2 µg/ml Aprotinin and 0.5 mg/ml Leupeptin in ddH$_2$O.

PROTEIN ESTIMATION BY BICINCHONINIC ACID ASSAY

Protein amount was quantified with the Bicinchoninic Acid Assay (BCA), where Cu^{2+} is reduced to Cu^{1+} by protein bonds. Cu^{1+} together with bicinchoninic acid builds a purple-colored complex that can be detected at a wavelength of 562 nm (Smith et al., 1985). Lysates were diluted 1:5 with ddH$_2$O followed by addition of 200 µl assay reagent (BCA Protein Assay Kit, Thermo Scientific) to 25 µl sample or blank dilution and incubated at 37°C for 30 min. Samples and blank were run in triplicate in a 96-well format on a multi plate reader (SPECTRAmax Plus, Molecular Devices). The BSA standard curve was used to determine the protein concentrations by plotting absorbance against standard protein concentration.

SDS-POLYACRYLAMIDE GEL ELECTROPHORESIS

Proteins were separated according to their size by sodium dodecyl sulfate polyacrylamide gel electrophoresis (SDS-PAGE). Samples were supplemented with 5x SDS loading buffer and proteins were denatured by boiling at 99°C for 3 min. 6x9 cm SDS-PAGE gels were prepared in advance. Samples and protein ladder were run in an electrophoresis unit (Hoefer SE260, Amersham) filled with SDS running buffer first at constant voltage of 80 V, which was then switched to 150 V when the sample reached the separation gel. The stacking gel was discarded and the separation gel subjected to immunoblot analysis.

- **Stacking gel** (recipe sufficient for 4 gels): 1.5 ml Rotiphorese 30, 2.5 ml 4x Tris/SDS pH 6.8 (500 mM Tris, 0.4% SDS), 7.5 ml ddH$_2$O, 240 µl 1 M APS, 22.5 µl TEMED.
- **10% separating gel** (recipe sufficient for 4 gels): 7.2 ml Rotiphorese 30, 5.6 ml 4xTris/SDS pH 8.8 (1.5 M Tris, 0.4% SDS), 9.75 ml ddH$_2$O, 300 µl 1 M APS, 24 µl TEMED.
- **5x SDS loading buffer:** 200 mM Tris, 6% SDS, 15% glycerol, 0.3% bromophenol blue, 10% 2-mercaptoethanol in ddH$_2$O, pH 6.7.
- **SDS running buffer:** 25 mM Tris, 190 mM glycine, 1% SDS in ddH$_2$O, pH 8.3.

IMMUNOBLOT ANALYSIS

After gel separation, the proteins were transferred from the gel onto the blotting membrane and detected by immunostaining. PVDF membranes (6x9 cm) were activated in methanol for 5-7 min while gentle shaking and stored shortly in 1x Transfer buffer till the blot assembly was prepared. The blot sandwich consisted of three sheets of filter paper, followed by the gel and activated PVDF membrane and again by three sheets of filter paper. This blot sandwich was assembled in a blotting chamber (Criterion Blotter, BioRad), filled to the marked level with ice-cold 1x Transfer buffer. Blotting was carried out at constant voltage of 100 V for 50 min. At the end of the blot transfer, the gel was discarded and the membrane was transferred to blocking solution for 1 h at RT while gentle shaking to prevent unspecific binding. Afterwards, primary antibody incubation (P-CREB 1:1000) was done O/N at 4°C in blocking buffer. As protein loading control, an antibody against α-tubulin (1:40,000) was used to incubate for 1 h at RT. The membrane was washed three times with Wash buffer and incubated with a horseradish peroxidase (HRP)-coupled secondary antibody (1:10,000) in Wash buffer for 1 h at RT. After three further washing steps, the membrane was treated for 1 min with the enhanced chemiluminescence reagent (ECL prime Kit, Amersham), a substrate of HRP activity. Images of various exposure times (10 sec- 30 min) were acquired on films (Fuji Medical X-Ray Films, Fujifilm), which were scanned (1,200 dpi, Epson 1660) and analyzed using densiometric analysis of the protein signals from ImageJ (http://rsbweb.nih.gov/ij).

- **Blocking solution**: 5% BSA in 1x TBS buffer.
- **10x Transfer buffer**: 250 mM Tris, 660 mM glycine, 20% methanol in ddH$_2$O.
- **Wash buffer:** 50 mM Tris pH 7.4, 150 mM NaCl, 0.2% BSA, 0.2% NP-40 in ddH$_2$O.

IMMUNOFLUORESCENCE STUDIES

Immunostaining of PKA subunits was performed to localize the various isoforms of PKA in thyroid cells. 10-day-old thyroid cells seeded on glass coverslips were washed twice with prewarmed DPBS and fixed with 4% paraformaldehyde (PFA) in DPBS for 15 min at RT. This was followed by washing the cells with DPBS four times before permeabilizing the cells with 0.1% Triton X in DPBS for 3 min and incubation with 5% goat serum and 0.1% Triton X in DPBS for 1 h at RT to block unspecific binding. Cells were washed once with DPBS and incubated with primary mouse antibody against PKA Cα, PKA RIα, PKA RIIα, PKA RIIβ and primary rabbit antibody against GOLPH4 (1:200) overnight at 4°C, followed by triple washes with DPBS. Afterwards, the cells were treated with secondary antibodies Cy3-conjugated goat anti-mouse (1:100) and AlexaFluor594-conjugated goat anti-rabbit (1:100) for 2 h in an area protected from light. Nuclei were stained by adding DAPI to the cells for 5 min. Subsequently, the cells were washed three times with DPBS before they were stored at 4°C until imaging.

All blocking and incubation steps were performed in a humidified chamber at RT.

- **4% paraformaldehyde solution** (PFA): 0.4 g PFA was dissolved in 8 ml sterile DPBS and 5 µl of 1 mM NaOH and heated up 70°C in a closed tube while stirring. Once the solution appeared clear, it was allowed to cool down to room temperature and 10 ml sterile DPBS was added. The resulting solution was filtered through a 0.2 µm sterile filter and stored at –20°C.
- **Antibody dilutions for immunochemistry:** Antibodies were diluted in DPBS containing 1% goat serum and 0.1% Triton X.

3.2.4. Molecular biology techniques

RNA EXTRACTION

Primary thyroid cells of 2x 10-cm dishes were replated on 8x 6-cm plates. 1 day after, the cells were starved for 2 days with DMEM/F-12 medium supplemented with 1% P/S (starvation medium) before preincubation with 80 µM dynasore or DMSO for 30 min, followed by stimulation with or without 100 U/ml TSH for 30 min or 24 h. RNA isolation was done by the guanidinium thiocyanate-phenol chloroform method. First, medium was removed from thyroid cells followed by direct addition of 1.8 ml TRIzol reagent per plate. Cells were lysed by pipetting them up and down and were transferred to a new 2-ml tube followed by a 5-min incubation at RT to permit complete nucleoprotein complex breakdown. After lysis, 360 µl chloroform was added, and the lysate was allowed to separate into a clear upper aqueous phase (containing RNA), an interphase, and a red lower organic phase (containing the DNA and proteins). This was followed by centrifugation at 12,000x g for 15 min at 4°C. The upper aqueous phase was transferred carefully into a new 1.5-ml tube. RNA was precipitated by adding 900 µl isopropanol to the separated upper phase, followed by an incubation step for 10 min and centrifugation at 12,000x g for 10 min at 4°C. The supernatant was removed carefully without detaching the RNA pellet. Salts were removed by washing the pellet in 1.8 ml of 75% Ethanol (dissolved in DEPC-treated water) and centrifuged at 7,500x g for 5 min at 4°C, then discard the wash. The RNA pellet was air-dried for 10 min, resuspended in 20 µl RNase-free water and incubated for 10 min at 60°C before freezing to -80°C for storage. RNA concentration was measured with a UV/VIS spectrophotometer (Nano Drop 2000, Thermo Scientific). All steps were done under RNase-free conditions.

REVERSE TRANSCRIPTION

cDNA synthesis starting from RNA isolated from thyroid cell was carried out by using the SuperScript® II Reverse Transcriptase kit. 1 µg RNA was diluted with RNase-free H_2O to a final volume of 9 µl. The diluted RNA sample was mixed with 2 µl Oligo-dT-nucleotide primer (10 µM Oligo (dT)$_{15}$) and 1 µl deoxynucleotide triphosphates (10 mM dNTPseach) and incubated for 10 min at 70°C in a 1.5-ml tube to let the primers hybridize, the samples were slowly cooled down to 4°C on ice and then centrifuged shortly. Next, 4 µl 5x First-Strand Buffer, 2 µl DTT (0.1 M), 1 µl RNaseOUT (400 U/µl) and 1 µl SuperScript II (200 U/µl) were added per sample and mixed by gently pipetting up and down. As negative control, SuperScript II was replaced by 1 µl ddH$_2$O. The reaction mix was incubated for 60 min at 42°C followed by 15 min at 70°C to inactivate the SuperScript II. To use the newly synthesized cDNA as a template for amplification in PCR, RNA

complementary to the cDNA was removed by adding 1 µl RNase H (2 U/µl) per sample and incubating for 20 min at 37°C.

For real-time quantitative RT-PCR, the PCR mix contained 5 µl of 2x SYBR Select Master Mix, 1 µl forward (10 µM) and reverse primer (10 µM) each, 50 ng cDNA template created by reverse transcription and ddH$_2$O up to a volume of 8 µl. The mixture was then run on a thermocycler (C100 Real Time PCR system, BioRad). The SuperScript II control and ddH$_2$O control were amplified in parallel using the same mastermix and PCR protocol. For quantification of mRNA, the comparative Ct (cycle threshold) method also known as the 2ˆ$\Delta\Delta$Ct method was used. The Ct value represents the number of cycles, which the fluorescent signal needs to cross a defined threshold. The Ct values are reversed proportional to the amount of target nucleic acid in the sample. All genes in this study were normalized to the Ct value of β-actin, which represented housekeeping gene. The resulting ΔCt shows the difference of expression between the gene of interest and β-actin. Afterwards, the ΔCt$_{samples}$ were normalized to the corresponding non-treated sample (DMSO), which is referred as ΔCt$_{control}$.

The followed equation was used:

2ˆ $\Delta\Delta$Ct = 2ˆΔCt $_{sample}$/ 2ˆ ΔCt$_{control}$

Primer sequences:

mActin β forward	5' TTC TTT GCA GCT CCT TCG TT 3'
mActin β reverse	5' ATG GAG GGG AAT ACA GCC C 3'
mCdc2a forward	5' CTC CTG GGC AGT TCA TGG AT 3'
mCdc2a reverse	5' CGG GAG TGG CAA AAC ACA AT 3'
mEGR1 forward	5' GAG CGA ACA ACC CTA TGA GC 3'
mEGR1 reverse	5' TGG GAT AAC TCG TCT CCA CC 3'
mNr4a1 forward	5' AGT TGG GGG AGT GTG CTA GA 3'
mNr4a1 reverse	5' TTG AGC TTG AAT ACA GGG CA 3'
mNr4a3 forward	5' GTG TCT CAG TGT CGG GAT GG 3'
mNr4a3 reverse	5' TTG GTT TGG AAG GCA GAC GA 3'
mTop2a forward	5' ACT GTG GAA ACA GCC AGT AGA 3'
mTop2a reverse	5' ATG TCA CCA GCT CTC CCC AT 3'

PCR program:

for gene transcription: (50°C-2 min, 95°C-2 min, 40x(95°C-15 sec, 60°C-1 min))

3.2.5. I^{125}-hCG uptake

To confirm the efficiency of dynasore on LH receptor internalization in intact ovarian follicles, the radioligand I^{125}-hCG with a contraction of 3.5 µg/ml was used. First, the specific activity of I^{125}-hCG was determined by measuring 5 µl I^{125}-hCG in a γ-counter, which resulted in 255,749.6 cpm. To determine degree of receptor internalization via measuring I^{125}-hCG uptake, 10 follicles were preincubated for 1 h in 80 µM dynasore or DMSO dissolved in assay medium, followed by adding 2 µg/ml ($\triangleq$ 1,000,000 cpm) I^{125}-hCG and then incubating for 30 min at 37°C and 5% CO_2. For measuring the unspecific binding, 200-fold excess of unlabeled LH was simultaneously added together with I^{125}-hCG into a vial of 10 follicles. After the incubation, all three treatments were washed twice with assay medium in the presence or absence of dynasore and incubated the follicles subsequently for 5 min with acid solution. After washing the follicles again with assay medium they were transferred into new vials and I^{125}-hCG uptake was then counted with a γ-counter. The obtained counts of the unspecific binding were subtracted from the total counts of the two other groups at the end of the experiment.

- **Assay medium**: 0.1% BSA+ 98 mM NaCl+ 2 mM KCl in MEMα.
- **Acid solution**: 50 mM glycine, 100 mM NaCl in MEMα, pH 3.

3.2.6. LH labeling

To visualize LH receptor internalization in primary mural granulosa cells, LH was labeled with Tetramethylrhodamine isothiocyante (TRITC) (Brinkley, 1992). 3 mg of ovine LH (oLH) were dissolved in 300 µl of labeling buffer. To achieve a 5-fold excess of TRITC, 5.3 µl of 100 mM reactive dye dissolved in DMSO was added to the mixture then vortexing and the reaction was incubated for 18 h at 4°C in the dark. Unbound dye and labeled LH were separated by size exclusion column chromatography. The gel filtration was carried out on a Sephadex G25 column at 4°C in the dark. 1 M TRIS pH 7.4 was added to terminate the reaction and the collected fractions were analyzed with a UV spectrophotometer. Two well-separated peaks were visible on the chromatogram. Fractions corresponding to the first peak defined as protein conjugate (LH-TRITC) were combined. The obtained labeled-LH was then stored at –80°C.

- **Labeling buffer**: 150 mM NaCl, 8.4 mM $NaHPO_4$, 1.9 mM NaN_2PO, 50 mM BNa_3O_3 in DPBS, pH 9.3.

The degree of labeling was determined by Absorbance measurements (Brinkley, 1992).

$$C_d = A_{\lambda max} / \varepsilon_d$$

$$C_P = [A_{280} - (A_{\lambda max} * CF)] / \varepsilon_p$$

$$DOL = C_d / C_P$$

ε_d :	extinction coefficient of free dye	
C_d:	conc. of dye in conjugate (mol/l)	at λmax
$A_{\lambda max}$:	absorbance dye+ protein conjugate	

CF :	dye Correction Factor	
A_{280}:	absorbance dye + protein conjugate	at λ = 280
ε_p:	extinction coefficient of protein	
C_P:	conc. of protein in conjugate (mol/l)	

DOL	Degree of Labeling

Calculation:

CF (TRITC): **0.30**
ε_d (TRITC at 577 nm): **60,000** $M^{-1}cm^{-1}$
ε_p (LH at 280 nm): **20,440** $M^{-1}cm^{-1}$
A_{280}: **1.075**
$A_{\lambda max}$ (at 557 nm): **1.632**

C_d = 1.632 / 60,000 = 0.0000272

C_p = [1.075 – (1.632*0.30)] / 20,440 = 0.0000286

Degree of Labeling (DOL): Cd/Cp = 0.95

3.2.7. FRET-based measurements of cAMP levels and PKA activity

Typical systems for FRET-based imaging contain a source of light to excite donor fluorescence, a beam splitter to split the emission light into two independent channels and a camera to detect donor and acceptor channel intensities simultaneously (**Figure 14**). FRET data were acquired using two different imaging setups, one for single thyroid cells and another for isolated ovarian follicles.
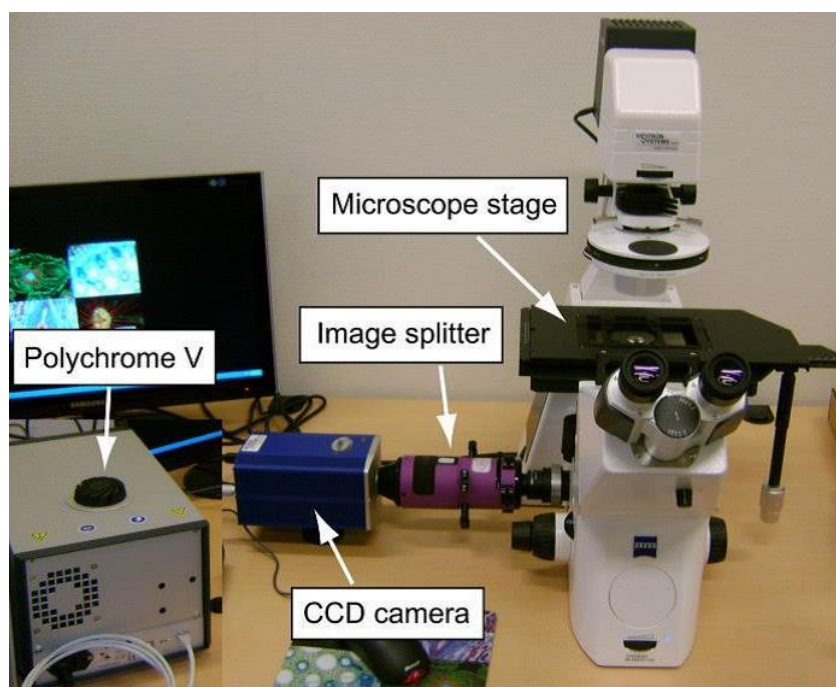
Figure 14: FRET setup.
An upright microscope (Zeiss Axiovert 200) equipped with a source of light (Polychrom V), an image splitter (Dual View beam splitter) to detect donor and acceptor intensities simultaneously, and a charge-coupled device (CCD) camera were used for acquiring FRET signals. Picture was taken from Börner et al., 2011.

For single thyroid cell experiments, a monochromator-based light source was used (Polychrome V) containing a 150 W xenon lamp (TILL photonics, Gräfelfing, Germany). The imaging setup was based on a standard inverted microscope (Zeiss Axiovert 200), equipped with a 63x/1.25 NA oil-immersion objective (Zeiss, Jena, Germany) and a wheel to switch excitation filter cubes. A filter cube equipped with a 436/20 excitation filter plus a 455LP dichroic mirror was used. The emission light was split into donor and acceptor channels using the Photometrics Dual View beam splitter (Photometrics), which uses a 505LP dichroic mirror and two emission filters: 480/15 for cyan (CFP) and 535/20 for yellow (YFP) fluorescent proteins. Images in the two channels were simultaneously collected with an electron multiplying charge-coupled device (EMCCD) camera (iXon ultra, Visitron System) and monitored online using the MetaFlour software (Molecular Devices/TILL photonics).

To perform imaging experiments, a coverslip containing transfected primary thyroid cells was mounted in an experimental chamber and placed onto the microscope. Complete culture medium was replaced by FRET buffer and changes in cAMP or PKA dynamics were monitored upon application of drugs at RT or 37°C. Donor and acceptor images were acquired simultaneously every 5 sec with 5-ms exposure, which resulted in negligible photobleaching over a period of 30-min acquisition. At the end of each experiment, an image of direct YFP-excitation with a 488/30 excitation filter was acquired.

- **FRET buffer**: 5.4 mM KCL,1 mM $MgCl_2$, 141 mM NaCl, 2 mM $CaCl_2$,10 mM Hepes in ddH_2O, pH 7,3

cAMP/FRET measurements in intact ovarian follicles isolated from transgenic Epac1-camps mice were exclusively performed on a TCS SP5 confocal microscope (Leica Microsystem) using a 20x/0.7 NA oil-immersion objective. CFP was excited with a 405-nm diode laser, while simultaneously acquiring at 460-485 nm (CFP emission) and 520-550 nm (YFP emission). The laser intensity was set to 13%, the scanner speed was 400 Hz and 12-bit images (1024x1024 pixels) were acquired every 10 sec. These parameters produced minimal photobleaching during long acquisition times (up to 90 min). FRET was monitored in real-time as the ratio between YFP and CFP emission intensities. At the end of each experiment, an image of direct YFP excitation with the 488-nm line of an argon-ion laser was acquired. The LASF software was used to control the system and to perform time-lapse image acquisition. Images were analyzed using ImageJ (http://rsbweb.nih.gov/ij).

For imaging cAMP dynamics in intact ovarian follicles of Epac1-camps mice, follicles were fixed between two glass coverslips separated by approximately 200 µm as previously described (Norris et al., 2008) and then placed in an imaging chamber. Imaging experiments were performed in phenol red-free MEMα medium supplemented with 0.1 mg/ml bovine serum albumin (MEMα/BSA) and changes in cAMP levels were observed at 37°C. For monitoring transient LH stimulation, a rapid superfusion system (Octaflow, ALA instruments) was used (**Figure 15**). The obtained raw intensity data in both FRET setups need further correction for emission spectra of donor (CFP) and acceptor (YFP) fluorescent proteins overlapping (bleed-through), and cross-excitation of YFP. Bleed-through and cross-excitation corrections were performed to calculate the corrected single channel intensities.
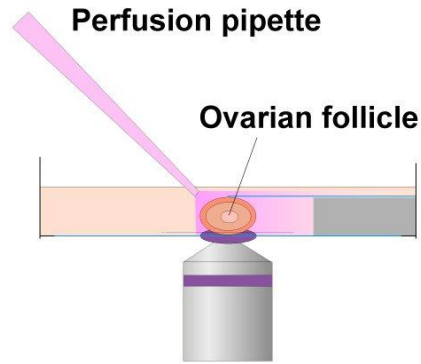
Figure 15: Ovarian follicle imaging setup.
Ovarian follicles isolated from Epac1-camps transgenic mice were fixed in a microchamber between two glass coverslips with the addition of a small quartz capillary placed in close proximity and connected to a fast superfusion system.

To calculate a bleed-through correction factor, CFP was expressed in HEK 293 cells and fluorescent intensities in CFP and YFP emission channels were measured upon CFP excitation. In this case, the ratio of YFP/CFP intensity represents the bleed-through coefficient A for CFP signal spillover into the YFP channel (the cross-excitation correction factor), YFP was expressed in HEK 293 cells to compare the fluorescent intensity in YFP emission channel upon CFP and YFP excitation. In this case, the ratio of YFP/CFP intensity represents the cross-excitation coefficient B for direct excitation of YFP at a wavelength used for CFP excitation. Determination of the correction factors is necessary for every microscopy setup due to the fact that the correction factors are depending on the light source and acquisition numbers used.

Corrected FRET ratios were calculated as follows:

$$\text{FRET}_{corr} = (\text{YFP}_{436} - A \times \text{CFP}_{436} - B \times \text{YFP}_{500}) / \text{CFP}_{436}$$

YFP_{436}: YFP intensity at 436 nm excitation (CFP)
CFP_{436}: CFP intensity at 436 nm excitation (CFP)
YFP_{500}: YFP intensity at 500 nm excitation (YFP)

Determined correction factors:

FRET setup:	A : 0.57	B : 0.07
TCS SP5:	A : 0.34	B : 0.11

The ratiometric traces were transferred into GraphPad Prism 5 software and corrected for photobleaching if necessary (Börner et al., 2011). FRET responses were quantified and statistics performed using GraphPad Prism 5 software.

3.2.8. Confocal microscopy

Confocal images were acquired using the Leica TCS SP5 laser scanning confocal microscope (Leica) equipped with a Plan-Apochromat 63x/1.4 NA oil-immersion objective, and analyzed using LASF software (Leica) and ImageJ. Excitation and detection parameters for simple confocal images and immunofluorescence studies were set as follows:

DAPI (405 nm diode laser excitation, detection 430-480 nm)
CFP (405 nm diode laser excitation, detection 460-485 nm)
YFP (488 nm argon ion laser excitation, detection 520-550 nm)
Cy3 (561 nm diode laser excitation, detection 569-641 nm)

LH receptor internalization in primary mural granulosa cells was visualized using two different approaches. In the first approach, TRITC-conjugated LH or AlexaFluor488-conjugated transferrin internalization in wild-type mural granulosa cells was monitored. 4-day-old mural granulosa cells were treated with either 10 µg/ml TRITC-conjugated LH or 50 µg/ml AlexaFluor488-conjugated transferrin in MEMα/BSA for 20 min before washing twice with MEMα/BSA and 5 min incubation in MEMα/BSA. Immediately after exchanging the medium with MEMα/BSA, mural granulosa cells were imaged by confocal microscopy.

In the second approach, LH receptor tagged with YFP was transiently expressed in mural granulosa cells. Two days after transfection, cells were imaged before and 60 min after 20 µg/ml LH stimulation to detect LH receptor internalization.

Imaging of transferrin internalization in wild-type ovarian follicles was carried out following standard procedures (Norris et al., 2008). Briefly, intact ovarian follicles were mounted between two coverslip (**Figure 15**) and treated with 50 µg/ml AlexaFluor488-conjugated transferrin in MEMα/BSA for 30 min, then washed twice with MEMα/BSA. Afterwards, the follicles were treated for 3 min with an acidic solution (0.5 M NaCl, pH 4.0) to remove membrane-bound transferrin, washed twice with DPBS and imaged immediately by confocal microscopy.

All above experiments including stimulation, washing and imaging were performed at 37°C.

3.2.9. Statistics

Data were analyzed with Graphpad Prism 5 and shown as mean ± standard error.
$P < 0.05$ was considered statistically significant.

The following equations were used to fit data in **Figures 16-18** and **24**:

$$Y(t) = Y_{top}; \quad t \le \Delta t$$

$$Y(t) = \left(Y_{top} - Y_{bottom}\right) e^{-\left[\frac{1}{\tau_{on}}(t-\Delta t)\right]} + Y_{bottom}; \quad t > \Delta t$$

Y_{top} : basal YFP/CFP ratio

Y_{bottom} : YFP/CFP ratio reached after LH stimulation

τ_{on} : tau value for the accumulation of cAMP (i.e. decrease of the YFP/CFP ratio)

Δt : time delay

The following equation was used to fit data in **Figures 19**, **20**, **25**, **31**, **33** and **34A**, **C**, **D**, and **F**:

$$Y(t) = Y_{top}\left(1 - e^{-\frac{1}{\tau_{top}}t}\right)$$

Y_{top} : YFP/CFP ratio at the end of the washout

τ_{top} : tau value of the increase of cAMP levels or PKA activation

The following equations were used to fit data in **Figures 27** and **32**:

$$Y(t) = Y_{bottom}; \quad t \le \Delta t$$

$$Y(t) = \left(Y_{bottom} - Y_{top}\right) e^{-\left[\frac{1}{\tau_{on}}(t-\Delta t)\right]} + Y_{top}; \quad t > \Delta t$$

Y_{bottom} : basal YFP/CFP ratio

Y_{top} : YFP/CFP ratio reached after TSH stimulation

τ_{on} : tau value for the accumulation of cAMP

Δt : time delay

The following equations were used to fit data in **Figure 28**, **31**, and **34B**, **E**:

$$Y(t) = Y_{top\_1}, Y_{top\_2}; \quad t \leq \Delta t$$

$$Y(t) = Y_{top\_1}\left(1 - e^{\left[-\frac{1}{\tau_1}t\right]}\right); \quad t > \Delta t$$

$$Y(t) = Y_{top\_1}\left(1 - e^{\left[-\frac{1}{\tau_1}t\right]}\right) + Y_{top\_2}\left(1 - e^{\left[-\frac{1}{\tau_2}(t-\Delta t)\right]}\right); \quad t > \Delta t$$

Y_{top_1} : 1st increase of YFP/CFP ratio after TSH stimulation

Y_{top_2} : 2nd increase of YFP/CFP ratio after TSH stimulation

τ_1 : tau value for 1st PKA activation

τ_2 : tau value for 2nd PKA activation

Δt : time delay between 1st and 2nd YFP/CFP ratio increase

4. Results

Besides the classical view of GPCR signaling at the cell membrane, a new pathway of GPCR signaling from the intracellular compartment has become a highly investigated topic in recent years. New findings have revealed a completely new scenario in which GPCR continues signaling via cAMP after ligand-induced internalization into the intracellular compartment (Calebiro et al., 2009;Ferrandon et al., 2009;Müllershausen et al., 2009;Kotowski et al., 2011;Werthmann et al., 2012;Feinstein et al., 2013;Irannejad et al., 2013;Kuna et al., 2013;Lohse and Calebiro, 2013;Merriam et al., 2013;Gidon et al., 2014;Tsvetanova and von Zastrow, 2014). However, the physiological relevance of GPCR signaling from this new pathway is largely unknown. The aim of my thesis is to investigate the mechanisms and the functional consequences of intracellular G protein-dependent signaling by using two different cellular models: intact ovarian follicles obtained from a transgenic mouse, which has ubiquitous expression of fluorescence resonance energy transfer (FRET) sensor for cAMP and primary mouse thyroid cells.

4.1. MEASUREMENTS OF LH RECEPTOR SIGNALING IN INTACT OVARIAN FOLLICLES

4.1.1. Real-time monitoring of cAMP signaling in ovarian follicles

In order to investigate cAMP signaling in intact ovarian follicles, a previously generated transgenic mouse (Calebiro et al., 2009) with ubiquitous expression of a FRET sensor for cAMP (Epac1-camps) was used (Nikolaev et al., 2004). This sensor allows monitoring cAMP signaling in real time and with high spatiotemporal resolution in both living cells and tissues (Calebiro et al., 2009;Calebiro et al., 2014).

Ovarian follicles isolated from Epac1-camps mice were immobilized in a custom-made chamber and imaged with a confocal microscope (**Figure 15**). Images revealed high expression of Epac1-camps in the outer theca cell layer, the adjacent mural granulosa and the inner cumulus oophorus cell layers (**Figure 16A**).
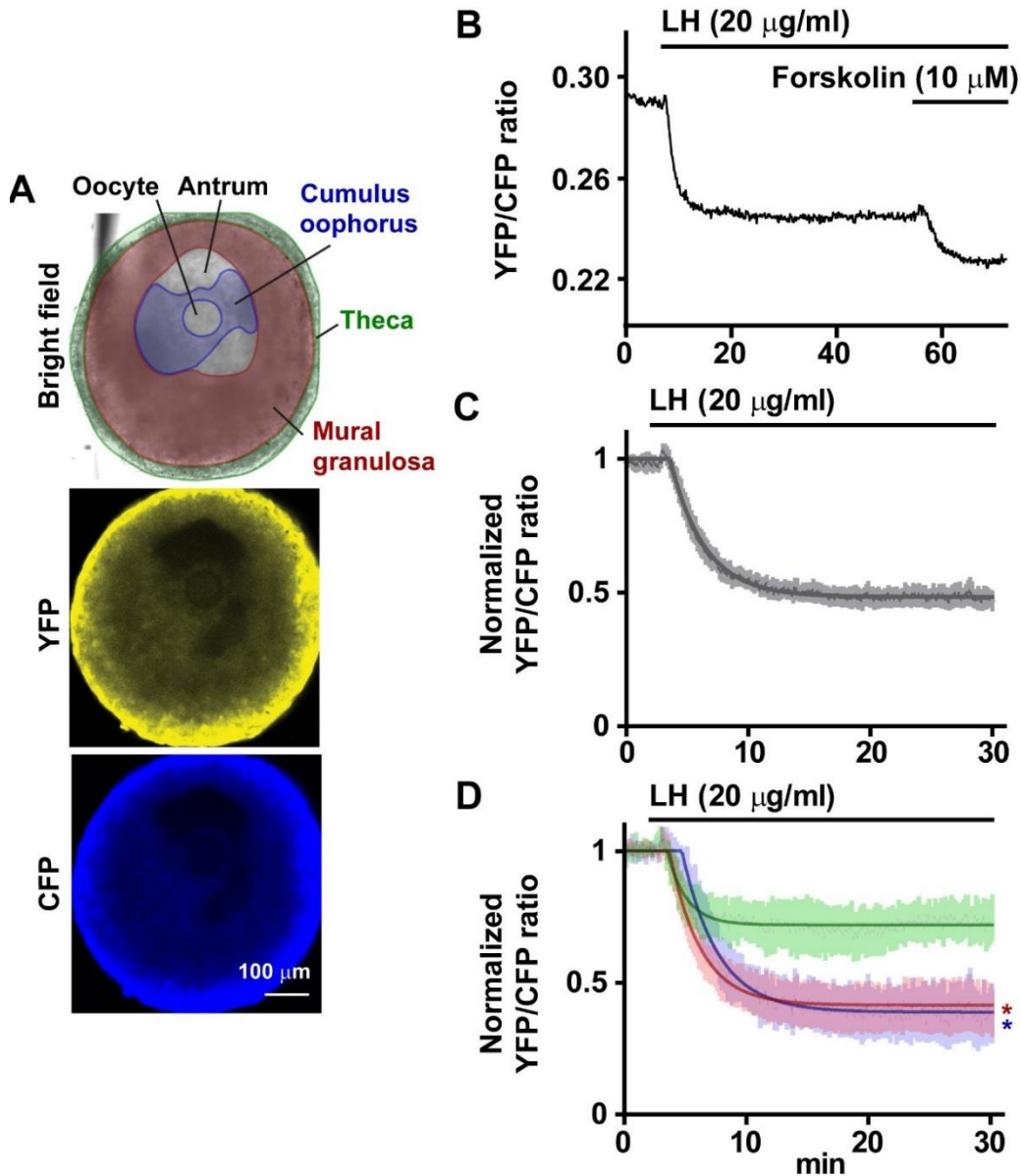
Figure 16: **FRET-based measurements of cAMP accumulation in ovarian follicles isolated from Epac1-camps transgenic mouse.**
(**A**) Confocal images of an antral follicle isolated from an Epac1-camps transgenic mouse.
(**B**) Real-time monitoring of cAMP levels in an intact ovarian follicle stimulated with 20 µg/ml LH, followed by treatment with 10 µM of the direct adenylyl cyclase activator forskolin. A decrease of the YFP/CFP ratio indicates an increase of the intracellular cAMP concentration. Shown is a representative trace.
(**C**) Shown are forskolin-normalized cAMP responses induced by LH measured in whole follicles.
(**D**) Comparison of LH receptor-mediated cAMP responses measured in subregions corresponding to theca (green), mural granulosa (red) and cumulus oophorus (blue) cells, defined as shown in **A**. FRET values in **C** and **D** were normalized to the basal level, set to 1, and the response to forskolin at the end of each experiment (as shown in **B**), set to 0. Data (mean ± S.E.M.) are from 6 independent experiments and were fitted as described in **3.2.9**. Differences in the LH receptor-mediated maximal cAMP responses between subregions (corresponding to the plateaus of the curves in **D**) are statistically significant by one-way ANOVA followed by Bonferroni´s post-hoc test. *, $P < 0.05$ vs. theca cells.

In contrast, the fluorescence of the central oocyte in both CFP and YFP channels too low for characterization. Thus, it was excluded for further analysis (**Figure 16A**).

A rapid and robust decrease of the FRET ratio was monitored after LH stimulation, indicating an increase of intracellular cAMP concentration. At the end of each experiment, forskolin - a direct activator of adenylyl cyclase - was added. The result showed a further decrease of the FRET signal indicating that LH stimulation did not saturate the Epac1-camps sensor. The cAMP signal was stable during constant LH stimulation, indicating that signal desensitization during the measurement (at least 40 min) was insignificant (**Figure 16B**).

In order to compare cAMP accumulation in different follicle compartments, the absolute FRET ratio was normalized to the maximal response of 10 µM forskolin stimulation.

cAMP accumulation was detectable in all follicle compartments upon LH stimulation. LH stimulation induced cAMP accumulation in different degree among follicle compartments (**Figure 16C, D**). In the outer layer (theca cells) a change of approx. 25% in the FRET ratio was detected, whereas in the middle (mural granulosa cells) and in the inner (cumulus oophorus cells) layers almost the double cAMP amount (approx. 50%) was detected (**Figure 16D**).

Remarkably, a FRET decrease in cumulus oophorus cell started approx. 2.5 min after LH stimulation, whereas in the other two compartments a delay of approx. 1.5 min was monitored (**Figure 17**).

Figure 17: Zoom-in of LH-induced cAMP signaling in different ovarian follicle compartments.
Shown are forskolin-normalized cAMP responses induced by LH in subregions corresponding to theca (green), mural granulosa (red) and cumulus oophorus (blue) cells. Cumulus oophorus cells show a longer delay in the cAMP response compared to theca and mural granulosa cells.

To investigate whether gap-junction closure has an effect on the LH-induced cAMP response in the analyzed compartments, especially the delayed cAMP response observed in the cumulus oophorus cells, follicles were pretreated with 200 μM carbenoxolone (CBX), a gap-junction inhibitor, prior to LH stimulation. The result showed that CBX pretreatment changes neither amplitude nor speed of cAMP accumulation in theca and mural granulosa cells (**Figure 18A, B and D**). In contrast, CBX significantly reduces the speed of cAMP accumulation in cumulus oophorus cells (**Figure 18C, D**). This data suggested that the observed cAMP response in cumulus oophorus cells is partially contributed by cAMP diffusion from mural granulosa cells to cumulus oophorus cells via gap-junctions.

To further evaluate kinetics of the cAMP diffusion within a follicle, derivatives of FRET data from CBX-pretreated and control follicles have been used to create pseudocolor images to show cAMP accumulation in space and time. The analysis shows that cAMP response occurs sequentially from the outer to the inner layers of a control follicle, which was finalized by a detectable cAMP rise in the central region corresponding to cumulus oophorus cells within 8 min after LH stimulation (**Figure 18E**). On the other hand, the cAMP increase in the CBX-treated follicle is visible only in the external cell layer including theca and mural granulosa cell layers. The signal remains below the detection limit of this analysis in the central region corresponding to cumulus oophorus cell layer (**Figure 18E**).

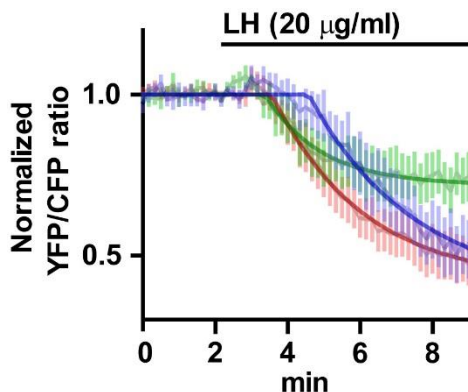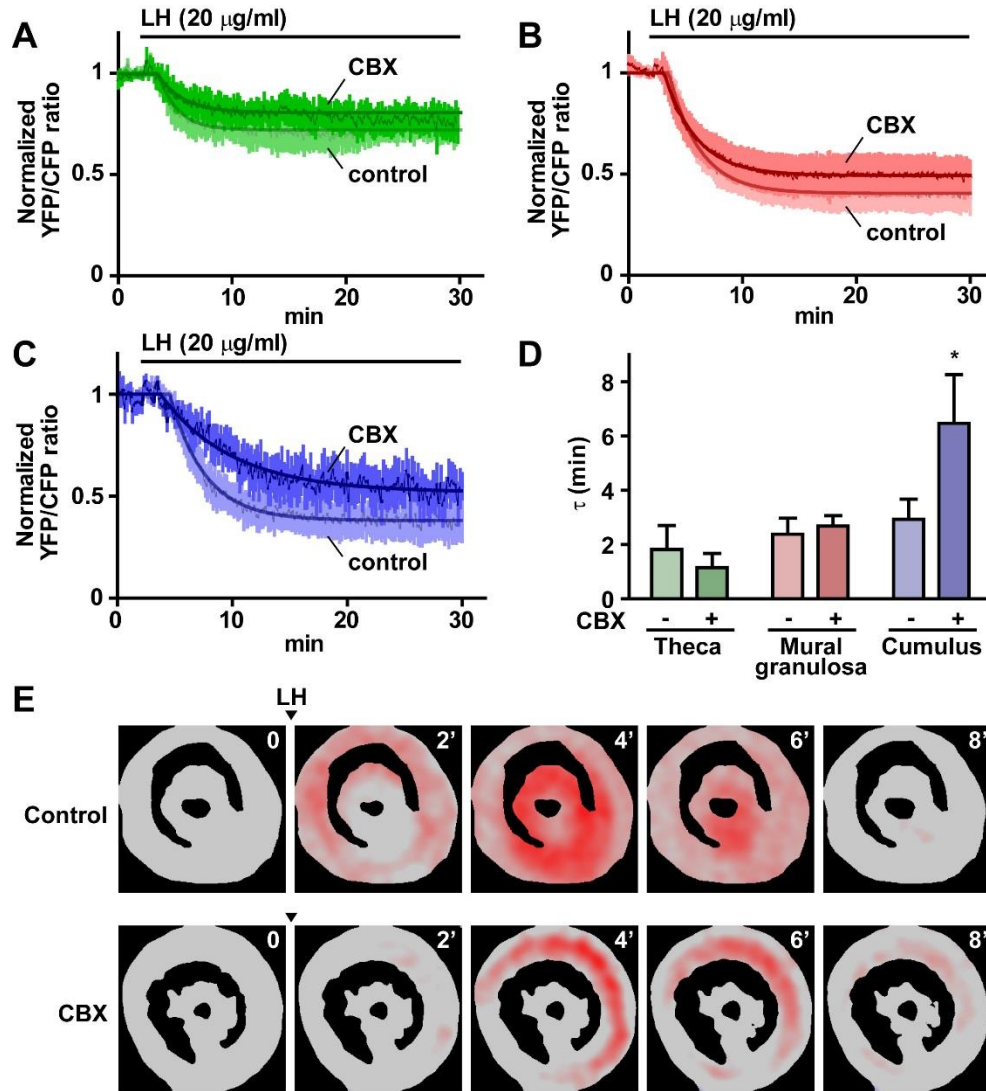**Figure 18: Effect of gap-junction inhibitor CBX on LH-induced cAMP dynamics in different ovarian follicle compartments.**
(**A-C**) Shown are forskolin-normalized cAMP responses induced by LH in subregions corresponding to theca (**A**), mural granulosa (**B**) and cumulus oophorus (**C**) cells with (dark color) or without (light color, control) 200 µM carbenoxolone (CBX) preincubation for 2 h. Data were analyzed as in **Figure 16**.
(**D**) Effect of CBX on the speed of LH-induced cAMP accumulation. Differences in **D** were statistically significant by two-way ANOVA. *, $P < 0.05$ vs. control by Bonferroni´s post-hoc test. Data in **A-D** (mean ± S.E.M.) are from 6 independent experiments.
(**E**) Derivative analysis of LH-induced cAMP accumulation in a whole follicle. Pseudocolor images (red color) represent the diffusion/generation of cAMP over time after LH stimulation comparing between a control (top) and CBX-pretreated (bottom) follicle.

4.1.2.   Persistent cAMP/LH receptor signaling in intact ovarian follicles

A fast exchange superfusion system was used for applying transient LH stimulation, which enables the reversibility study of LH-induced cAMP signaling in ovarian follicles (**Figure 15**).
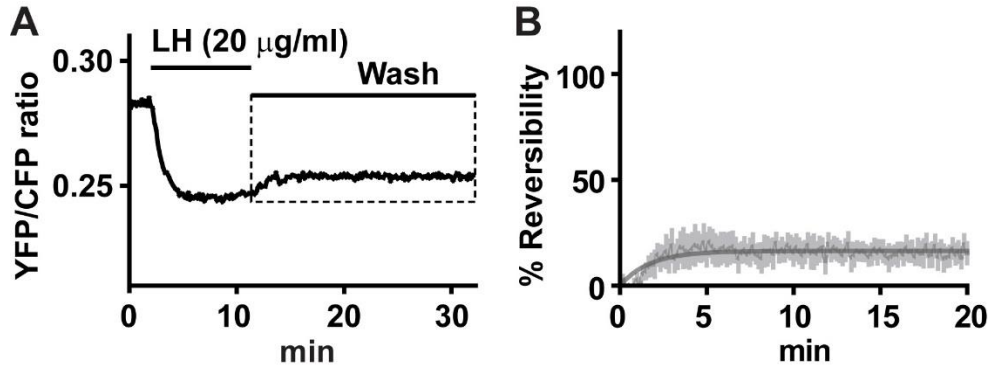
Figure 19: Real-time monitoring of cAMP levels in an intact ovarian follicle with a transient LH stimulus.
(**A**) Representative cAMP trace obtained in intact ovarian follicles stimulated with LH for 10 min followed by a 20-min wash.
(**B**) cAMP signal reversibility after LH removal. Data refer to the washout phase only (dashed box in **A**). Signal reversibility was calculated from the YFP/CFP ratio data of the washout phase, by setting the value at the end of LH stimulation equal to 0 and the value before LH stimulation equal to 100%. Shown are data (mean ± S.E.M.) from 8 independent experiments.

Intact ovarian follicles isolated from Epac1-camps mice were perfused with LH for 10 min resulting in an increase of cAMP. Stimulation with LH for 10 min is sufficient to allow LH receptors to undergo endocytosis (Jean-Alphonse et al., 2014).

A subsequent washout of LH for 20 min resulted in a maintain cAMP level with an incomplete return to basal level, which indicates that cAMP signaling in intact ovarian follicles was largely persistent after a transient stimulation with LH. The same signaling behavior was seen not just when measured in entire follicles (**Figure 19**), but also when measured in follicle subregions (**Figure 20**).
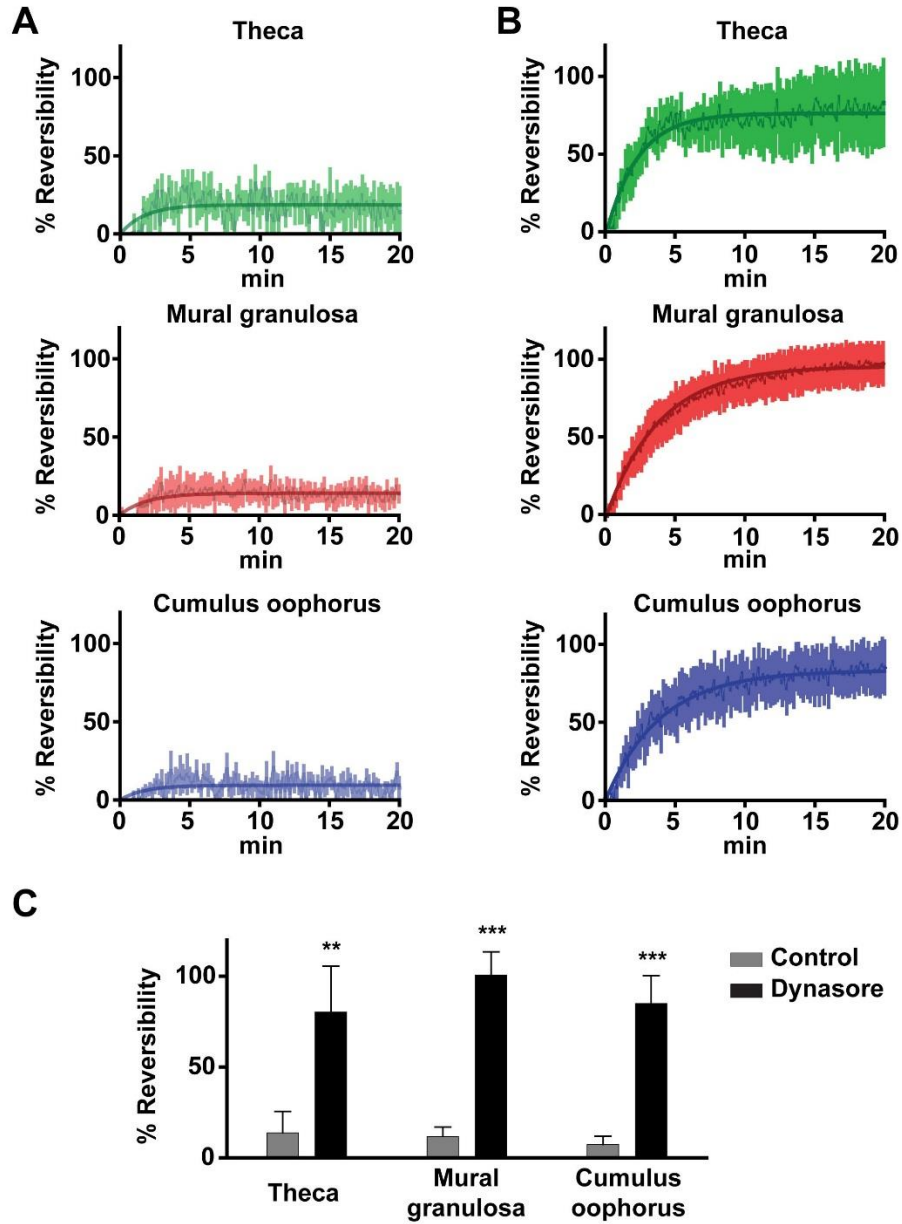
Figure 20: Effect of dynasore on the reversibility of cAMP signal during the washout phase in different subregions of intact ovarian follicles.
(**A, B**) Shown are cAMP signal reversibility of follicles pretreated with (**B**) or without (**A**) 80 µM dynasore for 1 h and thereafter, stimulated with LH for 10 min followed by a 20-min wash. Data represent cAMP signal after removal of LH in subregions corresponding to theca (green), mural granulosa (red) and cumulus oophorus (blue) cells.
(**C**) Comparison of the cAMP signal reversibility in the presence and absence of dynasore in the three subregions. Signal reversibility is calculated as described in **Figure 19**. Differences are statistically significant by two-way ANOVA followed by Bonferroni´s post-hoc test. **, $P < 0.01$; ***, $P < 0.001$ vs. control.
Data (mean ± S.E.M.) are from 8 (control) and 6 (dynasore) independent experiments.

4.1.3.   Visualization of LH receptor internalization in intact ovarian follicles

The lack of cAMP signal desensitization upon prolonged LH stimulation together with the persistent cAMP signaling induced by transient LH stimulation suggested the possibility that LH receptors were continuing stimulating cAMP production after internalization. A pharmacological approach was used to investigate whether endocytosis affect the LH receptor-mediated cAMP dynamics. We used dynasore, a small-molecule dynamin inhibitor that actually blocks clathrin-dependent internalization (Macia et al., 2006;Calebiro et al., 2009). To confirm the efficiency of dynasore on LH receptor internalization in intact ovarian follicles, fluorescently labeled LH was generated to visualize the endocytosis process. Unfortunately, the labeling process of LH with TRITC (Niswender et al., 1985;Brinkley, 1992) was not successful. TRITC-labeled LH did not show a specific binding upon addition to mural granulosa cells, which suggested that the covalent binding of the dye itself leads to inactivation of LH. Previous labeling attempts of LH with an AlexaFluor dye failed even though labeling of TSH, another glycoprotein hormone, with the same method was successful (Calebiro et al., 2009). This result indicated that the dye might cause inactivation of LH and consequently inability of the hormone in binding to the receptor.

Another possibility to visualize LH receptor internalization was to overexpress YFP-tagged LH receptors in mural granulosa cells and then stimulate with unlabeled LH. The result revealed a high expression of the YFP-tagged LH receptors on the cell-surface but upon stimulation with LH for 60 min, no vesicle formation and/or movement of the YFP-tagged LH receptor could be seen (**Figure 21**).

basal **20µg/ml LH**
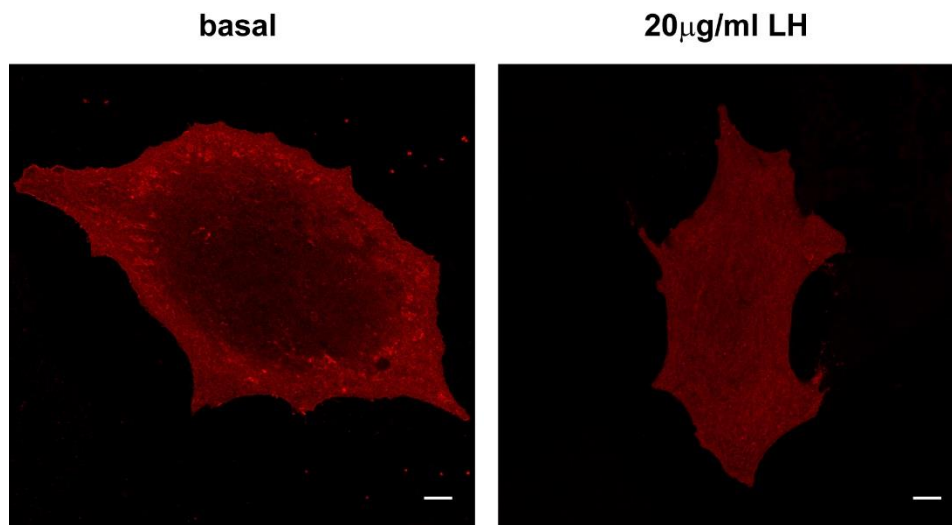
Figure 21: **Confocal images of mural granulosa cells transfected with YFP-tagged LH receptor**.
Mural granulosa cells obtained from wild-type mice were transfected with YFP-tagged LH receptor. Shown are representative confocal images of a mural granulosa cell before (basal) and after 60 min incubation with 20 µg/ml LH. Scale bars, 10 µm.

To evaluate the efficiency of the endocytosis machinery in ovarian follicles, another receptor, which undergoes clathrin-dependent endocytosis, was analyzed. The first choice was the transferrin/transferrin receptor complex, a classic marker of clathrin-dependent endocytosis (Ghosh et al., 1994;Jean-Alphonse et al., 2014). After fluorescently labeled transferrin stimulation of intact ovarian follicles for 30 min, transferrin-containing intracellular vesicles were visible. At the same time, dynasore effectively inhibited the clathrin-dependent internalization of fluorescently labeled transferrin by markedly reducing transferrin-containing intracellular vesicles in intact ovarian follicles (**Figure 22A**).

As an additional experiment the effect of dynasore on clathrin-dependent internalization was examined by measuring the uptake of ^{125}I-hCG in ovarian follicles. hCG is an agonist of the LH receptor with a similar affinity to the receptor as LH (Ascoli et al., 2002;Müller et al., 2003). The results demonstrate that dynasore pretreatment led to a significant reduction of internalized ^{125}I-hCG into the follicle compared to control, suggesting that dynasore can effectively inhibit the internalization of LH receptor in ovarian follicles (**Figure 22B**).
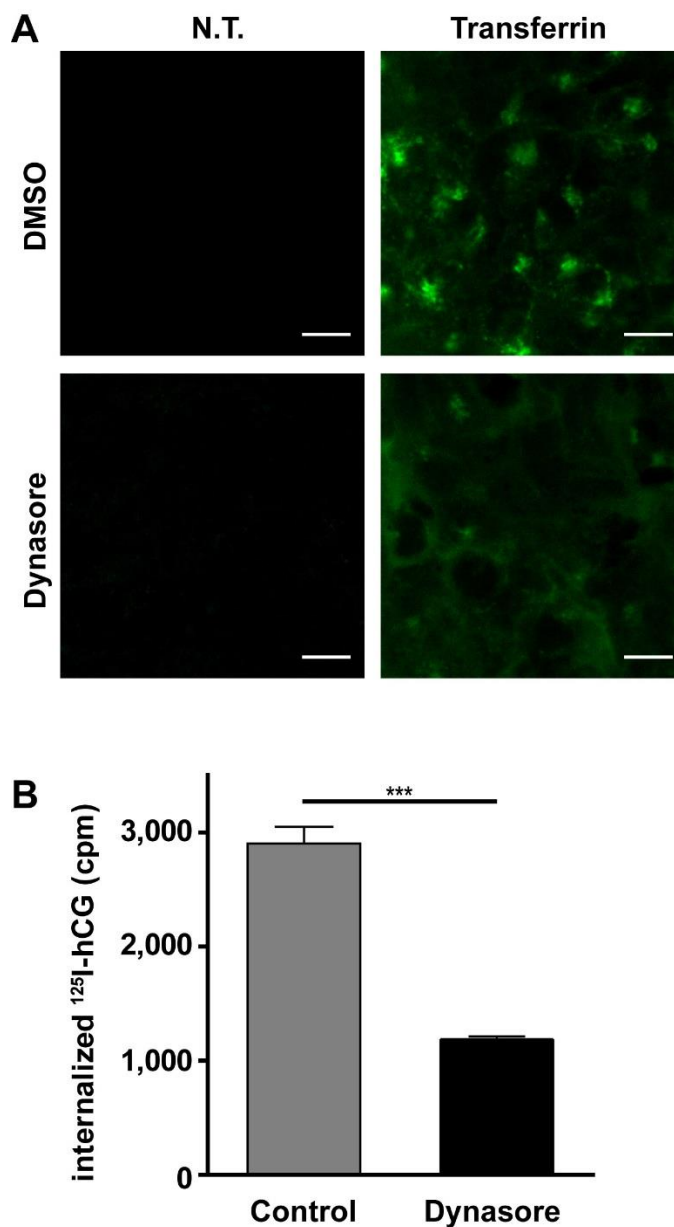
Figure 22: Effect of dynasore on clathrin-dependent internalization in intact ovarian follicles.
(**A**) Confocal images show the effect of dynasore on clathrin-dependent internalization of fluorescently labeled transferrin in intact ovarian follicles. Intact ovarian follicles obtained from wild-type mice were preincubated with either 80 µM dynasore or DMSO for 1 h before stimulation with Alexa488-conjugated transferrin for 30 min. Shown are representative confocal images of the mural granulosa cell layer of intact ovarian follicles with or without (control) transferrin treatment. A strong reduction of transferrin-containing intracellular vesicles is seen in the presence of dynasore. Scale bars, 10 µm.
(**B**) Follicles were pretreated with 80 µM dynasore or DMSO (control) for 1 h, followed by stimulation with 2 µg/ml ^{125}I-hCG for 30 min. Radioactivity that remained associated with the follicle was measured after acid treatment (internalized ^{125}I-hCG). Data (mean ± S.E.M.) are from 3 independent experiments per condition. ***, P < 0.001 by Student´s t-test.

4.1.4. Effect of LH receptor internalization on cAMP signaling

After proving the effective inhibition of endocytosis by dynasore in intact ovarian follicles, cAMP/FRET measurements were examined in real time in the presence of dynasore. Dynasore did not have any effect on cAMP dynamics in intact ovarian follicles induced by forskolin, a direct adenylyl cyclase activator (**Figure 23**), indicating that dynasore did not alter cAMP production and/or degradation.
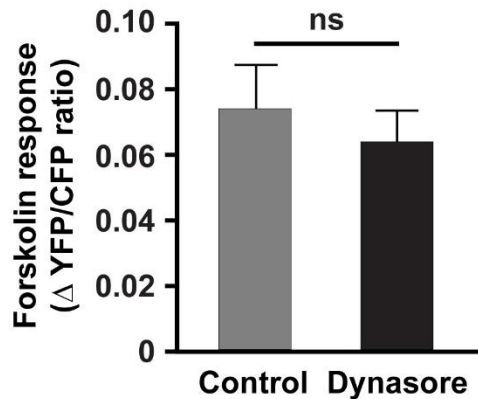
Figure 23: **Comparison of forskolin-dependent accumulation of cAMP in intact ovarian follicles in the absence and presence of dynasore.**
Shown are absolute changes of YFP/CFP ratio in whole follicles pretreated with 80 µM dynasore or DMSO (control) for 1 h, followed by stimulation with 10 µM forskolin. Data (mean ± S.E.M.) are from 8-10 independent experiments per condition. ns, no statistically significant difference by Student`s t-test.

Similarly, the initial phase of the cAMP response to LH bath application was not affected by dynasore pretreatment, either when considering whole follicles or different subregions (**Figure 24**; dots indicate P values).
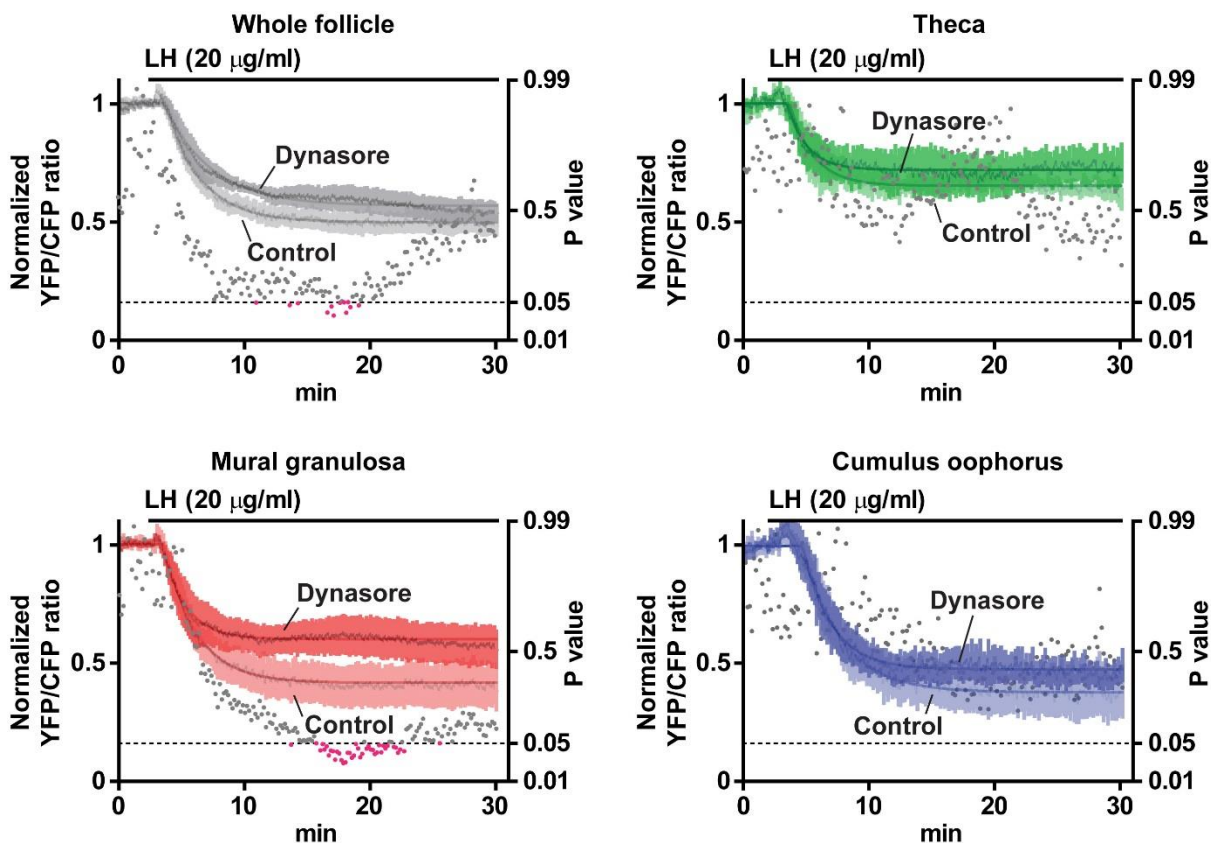
Figure 24: LH-dependent cAMP FRET traces observed in different compartments of intact ovarian follicles in the presence and absence of dynasore.
Shown are cAMP responses obtained in intact ovarian follicles pretreated with 80 μM dynasore or DMSO (control) for 1 h and stimulated with 20 µg/ml LH. The cAMP FRET traces were obtained in regions refer to whole follicles (grey) as well as to theca (green), mural granulosa (red) and cumulus oophorus (blue) cells. Data (mean ± S.E.M.) are from 6 independent experiments. They were normalized as described in **Figure 16**. For comparison, the results of **Figure 16** obtained in control follicles are shown in light colors. Data points between the two conditions were compared using the Holm-Šídák test for multiple comparisons. P values are shown as dots (pink, P < 0.05).

However, the obtained cAMP accumulation in the later phase was reduced in mural granulosa cells when the follicle was pretreated with dynasore. This, however, was not the case in other subregions (**Figure 24**). These data were consistent with two phases of cAMP signaling, an initial one occurring at the cell-surface and a later one induced by internalized receptors.

Acute endocytosis blockade of intact ovarian follicles with dynasore did not affect the cAMP signal upon 10 min of LH stimulation but as soon as LH was removed from the follicle surface, the cAMP levels returned almost completely back to the baseline. This was related to an increase of the reversibility of the cAMP signals induced by transient stimulation with LH (from approx. 15% to nearly 90%) compared to the control follicles (**Figure 20B, C** and **Figure 25**).
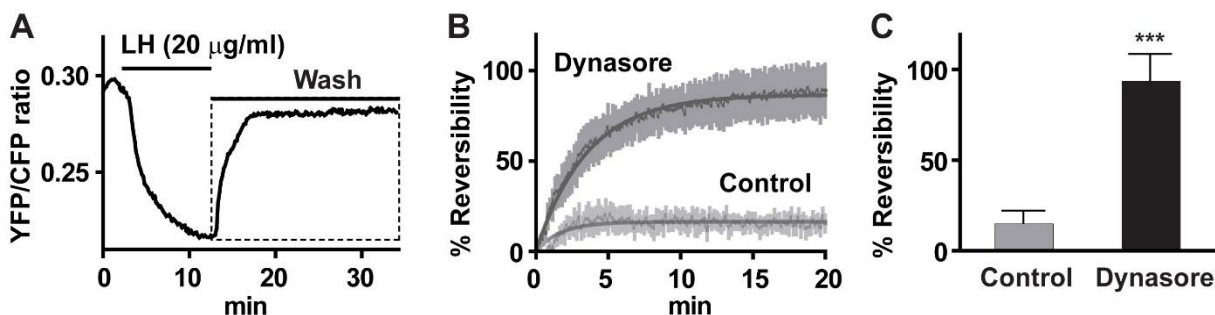
Figure 25: Effect of inhibiting internalization with dynasore on the reversibility of LH-induced cAMP signals.
(**A**)Representative cAMP trace obtained in an intact ovarian follicles pretreated with 80 µM dynasore and stimulated with LH for 10 min followed by a 20-min wash.
(**B**) cAMP signal reversibility after LH removal in the presence (dark grey) or absence (light grey) of dynasore obtained in whole follicles. Data refer to the washout phase only (dashed box in **A**). Signal reversibility was calculated as described in **Figure 19** and data were fitted as described in **3.2.9**. For comparison, the results of **Figure 19** obtained in control follicles are shown in light grey.
(**C**) Comparison of the cAMP signal reversibility in the presence or absence of dynasore.
***, P < 0.001 by Student´s t-test. Data in **B** and **C** (mean ± S.E.M.) are from 6 (dynasore) and 8 (control) independent experiments.

The decrease of cAMP level has a time constant of 3.5 min. This is similar to what is known for the dissociation kinetics of glycoprotein hormones from their receptors on the cell-surface (Werthmann et al., 2012). This was not only seen in whole follicles, but also in the different subregions of the follicle (**Figure 20**). Taken together, these data strongly suggested that inhibition of LH receptor internalization results in a reversible cAMP response upon LH dissociation from cell-surface receptors. This demonstrates that LH receptors continue signaling via cAMP after LH-induced internalization of LH/LH receptor complexes into the intracellular site.

4.1.5. Analysis of the effect of LH receptor internalization on meiosis resumption in intact ovarian follicles

The obtained results from the previous parts indicated that LH receptor internalization is responsible for persistent cAMP accumulation at intracellular sites, but whether the internalization of the LH receptor is required for biological effects is still not known. To investigate the physiological relevance of LH receptor signaling after internalization, the effect of dynasore on oocyte meiosis resumption induced by LH was evaluated. The most common way to analyze this event is to monitor the breakdown of the nuclear envelope of follicle-enclosed oocytes (known as germinal vesicle break down; GVBD) (Mehlmann et al., 2002) (**Figure 26A**).
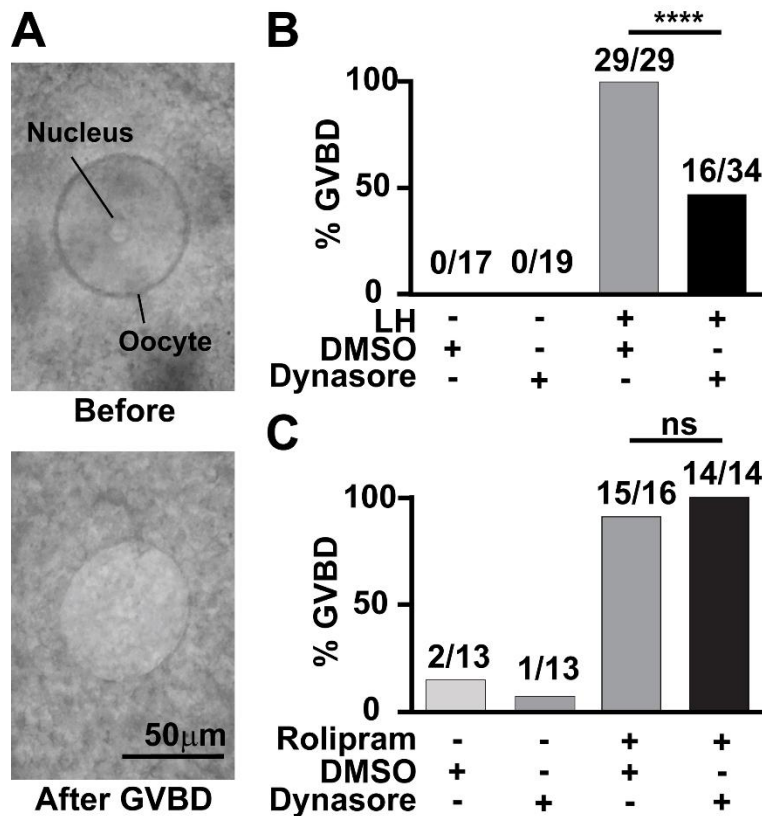
Figure 26: The effect of LH receptor internalization on efficient meiosis resumption in follicle-enclosed oocytes.
(**A**) Representative example of GVBD in follicle-enclosed oocyte. GVBD can be seen as the loss of the nuclear envelope in the oocyte.
(**B**) Ovarian follicles were pretreated with 80 µM dynasore or DMSO for 1 h and thereafter stimulated with 20 µg/ml LH for 6 h. Then, ovarian follicles were scored for GVBD. ****, P < 0.0001 by Fisher´s test.
(**C**) Ovarian follicles were pretreated with 80 µM dynasore or DMSO for 1 h, followed by stimulation with 2.5 µM rolipram for 24 h and then scored for GVBD. Data in **B** and **C** are from 4-6 independent experiments.

Remarkably, dynasore pretreatment led to a significant reduction of efficiency GVBD in response to LH from 100% to 47% (**Figure 26B**). To verify the specificity of dynasore on the LH-induced resumption of meiosis, a selective phosphodiesterase 4 (PDE4) inhibitor (rolipram) was used to directly increase cAMP levels in mural granulosa cells, thus bypassing receptor activation. Rolipram has been described to inhibit PDE4D, which is expressed in mural granulosa cells but not in the oocyte, thereby imitating the increase of cAMP caused by LH in mural granulosa cells and ultimately inducing meiosis resumption in follicle-enclosed oocytes (Tsafriri et al., 1996). Importantly, dynasore pretreatment did not affect the rolipram-induced meiosis resumption (**Figure 26C**). These data strongly indicated that LH receptor internalization in mural granulosa cells and cAMP production from intracellular sites were required for efficiently relaying the LH signal to the oocyte and thereby inducing meiosis resumption.

4.2. MEASUREMENTS OF TSH RECEPTOR SIGNALING IN PRIMARY THYROID CELLS

In this part of my thesis, the TSH receptor in thyroid cells was used as a second prototypical endocrine model to investigate the mechanisms and functional role of intracellular GPCR signaling. Previous studies demonstrated the occurrence intracellular cAMP/TSH receptor signaling upon transient TSH stimulation in primary thyroid cells (Calebiro et al., 2009). However, little information was available on the consequences of TSH receptor signaling in the intracellular compartment and downstream events such as protein kinase A (PKA) activation and gene transcription. For this purpose in the following section, the kinetics of cAMP and PKA activation were compared as well as the influence of TSH receptor internalization on nuclear signaling events.

4.2.1. FRET-based measurements of TSH-induced cAMP signaling in whole thyroid cells

FRET-based measurements of cAMP levels were performed in thyroid cells isolated from a transgenic mouse with ubiquitous expression of a FRET sensor for cAMP (Epac1-camps). This sensor allows monitoring cAMP signaling in real time and with high spatiotemporal resolution in both living cells and tissue (Calebiro et al., 2009). Images revealed high expression of Epac1-camps in the whole primary thyroid cells (**Figure 27A**). Epac1-camps expressing thyroid cells treated with TSH showed an increase of the cAMP signal with a delay of 47 ± 6 sec (**Figure 27B, C**; inverted FRET ratio, i.e. calculated as CFP emission/YFP emission). Subsequent treatment with forskolin led to a further increase of cAMP production, showing that the applied TSH concentration did not saturate the Epac1-camps sensor (**Figure 27B**). In order to analyze the obtained cAMP accumulation in single thyroid cells, the absolute FRET ratio was normalized to the maximal response to 10 µM forskolin stimulation. The increase of cAMP levels had a time constant of 156 ± 31 sec (**Figure 27C**).
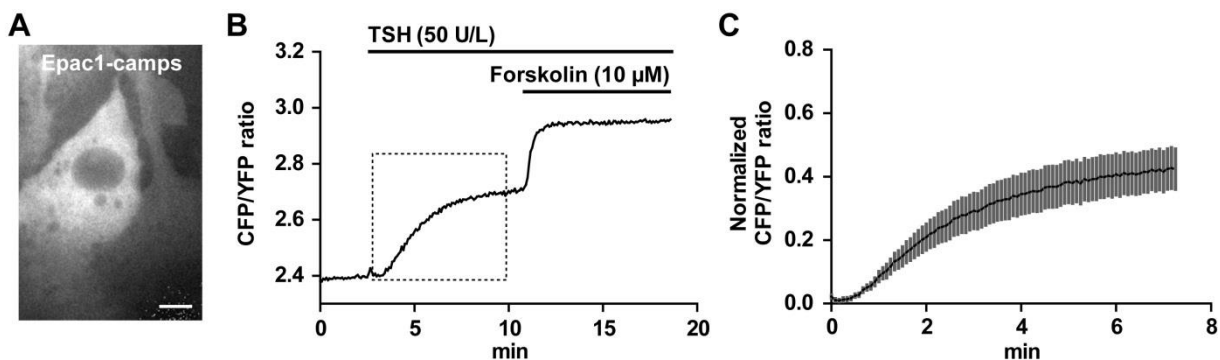
Figure 27: FRET-based measurements of cAMP accumulation in primary thyroid cells isolated from Epac1-camps transgenic mice.
(**A**) YFP image of primary thyroid cells isolated from an Epac1-camps transgenic mouse. Scale bar, 10 µM.
(**B**) Real-time monitoring of cAMP levels in primary thyroid cell stimulated with 50 U/L TSH, followed by treatment with 10 µM of the direct adenylyl cyclase activator forskolin. An increase of the CFP/YFP ratio indicates an increase of the intracellular cAMP concentration. Shown is a representative trace.
(**C**) Average cAMP/FRET response to stimulation with 50 U/L TSH measured in primary thyroid cells. FRET values in **C** were normalized to the basal level, set to 0, and the response to forskolin at the end of each experiment (as shown in **B**), set to 1. Data (mean ± S.E.M.) are from 15 independent experiments and were fitted as described in **3.2.9**.

4.2.2. FRET-based measurements of TSH-induced PKA signaling in whole thyroid cells

In order to investigate PKA signaling in primary thyroid cells, a FRET-based PKA sensor (AKAR2), which functions as an artificial substrate of PKA and detects changes in PKA activity in real-time with high temporal resolution (Zhang et al., 2005;Allen and Zhang, 2006), was used. Expression levels of AKAR2 in primary thyroid cells 48 h post-transfection was sufficient to perform FRET imaging (**Figure 28A**). Stimulation of thyroid cells with TSH resulted in a first rapid increase of the FRET ratio followed by a dominant second increase; the first one with a τ_1 of 37 ± 8 sec, the second one with a τ_2 of 72 ± 9 sec (**Figure 28B-E**). The delay between these two phases was 119 ± 13 sec (**Figure 28C, D**), suggesting that at least two distinct signaling events are involved in PKA activation.

Direct activation of adenylyl cyclase with forskolin led to a further increase in FRET ratio, indicating that TSH stimulation did not cause saturation of the AKAR2 sensor. At the end of every experiment, H-89, a selective, potent inhibitor of PKA, was added resulting in a decrease of the PKA signal, which reached its plateau below the basal PKA level (**Figure 28B**). In order to compare the two distinct PKA responses, the absolute FRET ratio was normalized to the maximal response of 10 µM forskolin stimulation and the minimal response of 20 µM H-89 (**Figure 28C- E**).
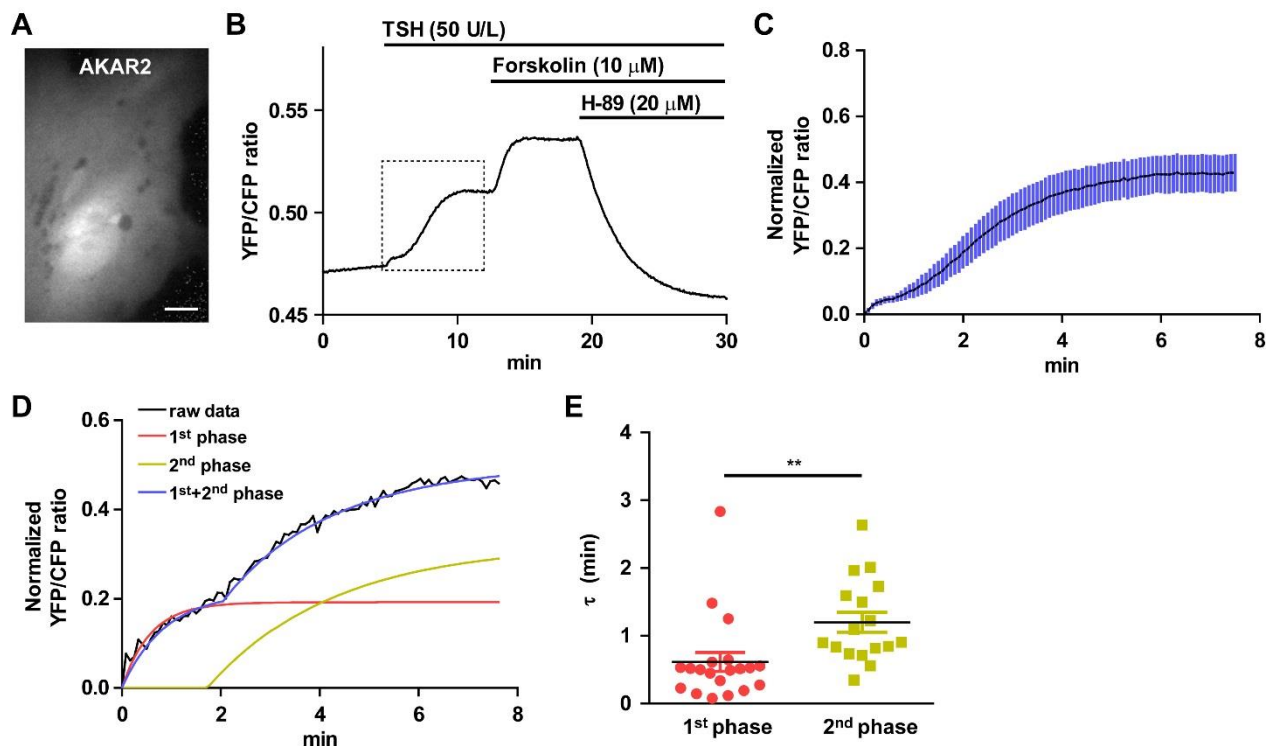
Figure 28: FRET-based measurements of PKA activity in primary thyroid cells transfected with AKAR2.
(**A**) YFP image of a primary thyroid cell expressing the PKA sensor AKAR2. Scale bar, 10 µM.
(**B**) Real-time monitoring of PKA activation in whole primary thyroid cells stimulated with 50 U/L TSH, followed by treatment with 10 µM forskolin and 20 µM PKA inhibitor H-89. A rise of the YFP/CFP ratio indicates an increase of the intracellular PKA activation. Shown is a representative trace.
(**C**) Average PKA/FRET response to stimulation with 50 U/L TSH measured in whole thyroid cells.
(**D**) Example of fitting the PKA response upon TSH stimulation with three different equations; the 1st fast, rapid curve (red), the 2nd delayed, slow curve (yellow) and the 3rd curve is the sum up of 1st and 2nd curve (blue).
(**E**) Comparison of the PKA kinetics in response to 50 U/L TSH. **, $P < 0.01$ by Student´s t-test. FRET values in **C, D** and **E** were normalized to the forskolin response by setting it to 1, and the response to H-89 at the end of each experiment (as shown in **B**) was set to 0. Data in **C** and **E** (mean ± S.E.M.) are from 18 independent experiments and were fitted as shown in **D** and described in **3.2.9**.

4.2.3. Characterization of the biphasic PKA activation

ANALYSIS OF PKA ISOFORM ACTIVATION IN THYROID CELLS

Studies in FRTL-5 cells, a well-differentiated thyroid cell line, suggested that the two PKA isoforms have different subcellular localization and carry out different biological functions (Calebiro et al., 2006). Thus, one could hypothesize that the two kinetically separated phases of PKA activation might involve different PKA isoforms.

To investigate this possibility, as a first step FRET measurements were performed to test the selectivity and specificity of existing PKA I and II inhibitors by stimulation of AKAR2 expressing thyroid cells with either PKA I or PKA II activators. Pairs of phosphodiesterase-resistant cAMP analogs, with different affinities for A and B sites on RI (8-HA-cAMP and 8-PIP-cAMP) and RII (6-MBC-cAMP and Sp-5,6-DCL-cBIMPS), were utilized to selectively activate PKA I and PKA II (Robinson-Steiner and Corbin, 1983;Beebe et al., 1984). A concentration-dependent reduction of PKA I and PKA II activation was examined upon using the corresponding inhibitors (Rp-8-Br-camps for PKA I and Rp-8-PIP-camps for PKA II). Both inhibitors effectively reduced PKA I or II activity (90-92%) at concentration of 0.5 mM (**Figure 29**).

PKA I activator (100µM)	+	+	+	+	+	+	+	+	+	-	-	-	-	-	-	-	-	-
PKA II activator (100µM)	-	-	-	-	-	-	-	-	-	+	+	+	+	+	+	+	+	+
PKA I inhibitor (mM)	-	0.1	0.2	0.5	1	-	-	-	-	-	0.1	0.2	0.5	1	-	-	-	-
PKA II inhibitor (mM)	-	-	-	-	-	0.01	0.1	0.2	0.5	-	-	-	-	-	0.01	0.1	0.2	0.5
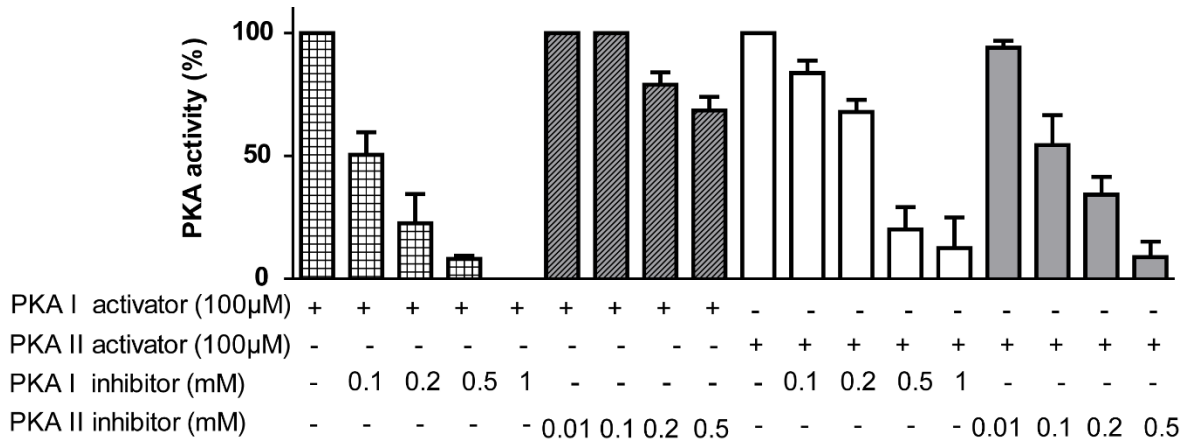
Figure 29: Effect of PKA I and II inhibitors on PKA I or II activation in thyroid cells.
AKAR2 expressing thyroid cells were stimulated with either PKA I or PKA II selective analogs followed by titration with PKA inhibitors (Rp-8-Br-camps for PKA I and Rp-8-PIP-camps for PKA II) at indicated concentrations. Shown are mean ± S.E.M. from three independent experiments.

In order to prove the selectivity of the used/available PKA inhibitors, primary thyroid cells were transfected with the AKAR2 sensor and stimulated with specific PKA isoform activators. It could be shown that at a concentration of 0.5 mM, the PKA II inhibitor caused a minimal reduction of the PKA I activity (32%) whereas PKA II activity was largely decreased (92%), which suggests that PKA II inhibitor specifically inhibits PKA II activity and has no effect on PKA I activity. In turn, the PKA I inhibitor at a concentration of 0.5 mM caused a large reduction of the PKA I activity (90%)

as well as the PKA II activity (80%), which indicates that the PKA I inhibitor blocks not only the PKA I activity but also the PKA II activity (**Figure 29**). Taken together, the PKA II inhibitor showed a good selectivity for PKA II activity while the PKA I inhibitor is not selective enough due to its inhibition of both isoforms. It could be possible that the experimental conditions are underestimating the PKA inhibitors, due to the effect that the used PKA activators could be also not selective for one PKA isoform.

ANALYSIS OF PKA SUBUNIT EXPRESSION/LOCALIZATION IN PRIMARY THYROID CELLS

So far, the obtained results showed two distinct phases of PKA signaling upon TSH stimulation in primary thyroid cells. A less significant characteristic pattern was seen in the cAMP response. The fact that the PKA subunits differ in their subcellular localization (Meoli et al., 2008;Sample et al., 2012) and promote different biological effects of TSH in FRTL-5 cells (Calebiro et al., 2006) might be a reason for the two distinct phases of PKA signaling. To verify this point, the expression of PKA subunits in primary thyroid cells was visualized via immunofluorescence experiments. Confocal images demonstrated that PKA Cα and PKA RIIα subunits were distributed throughout the whole thyroid cell, in both cytoplasm and nucleus (**Figure 30A**). However, the PKA RIα staining was observed only in the nucleus (**Figure 30A**). Interestingly, the PKA RIIβ subunit was localized mainly at a perinuclear tubular structure, most likely the Golgi compartment. To confirm this point, an antibody against Golgi integral membrane protein 4, GOLPH4, was used to stain the Golgi apparatus (Ozment et al., 2012;Franco et al., 2015). A high degree of co-localization was present between PKA RIIβ and GOLPH4 (**Figure 30B**), indicating that a significant fraction of PKA RIIβ was located on the membranes of the Golgi apparatus. This result is consistent with previous studies suggesting the Golgi apparatus is an important signaling compartment in primary thyroid cells (Calebiro et al., 2006;Calebiro et al., 2009). The visualization of the PKA RIβ and PKA Cβ subunits was so far not successful because of the lack of functional antibodies.
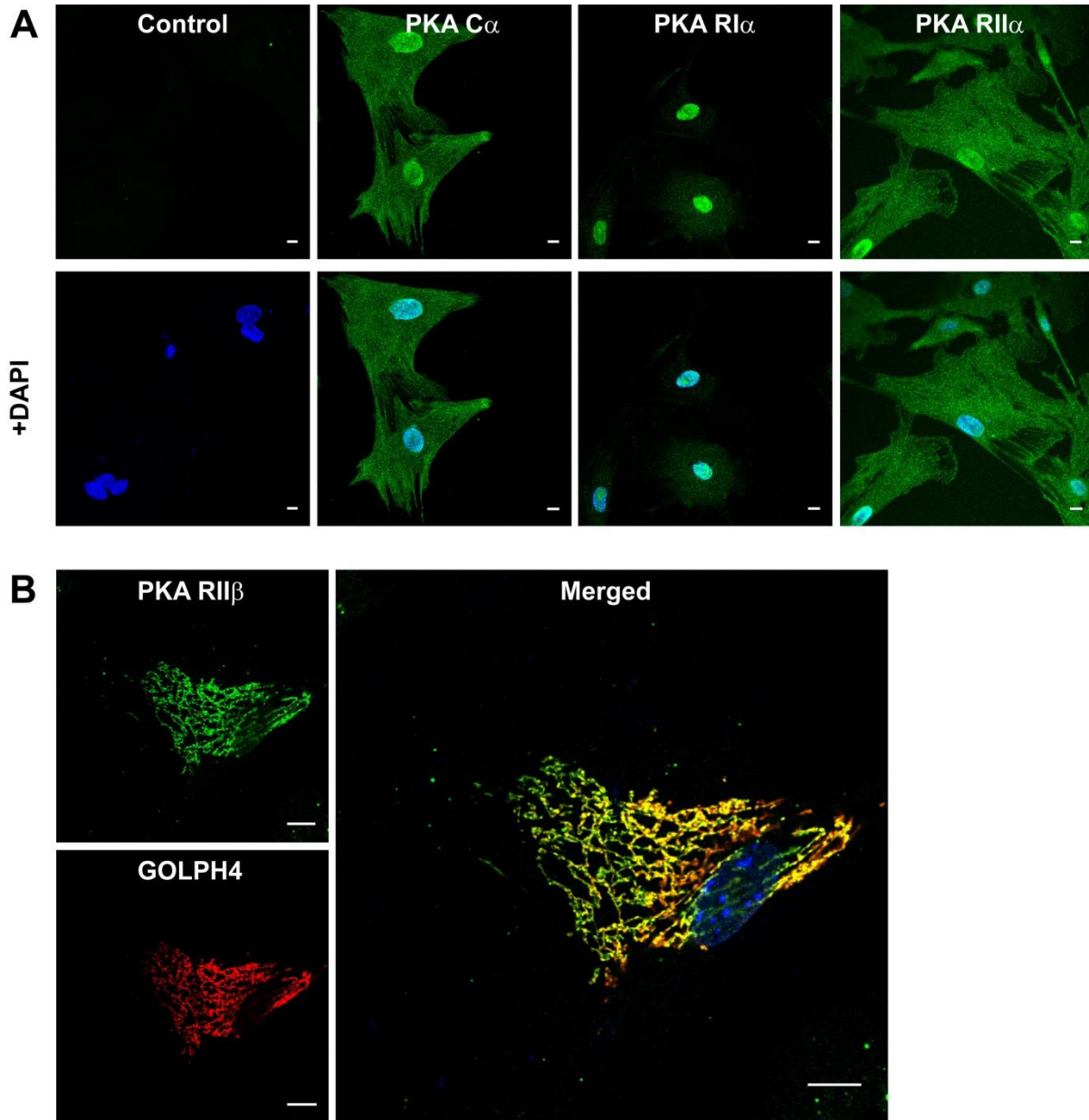
Figure 30: Localization of PKA isoforms in primary thyroid cells.
(**A, B**) Mouse primary thyroid cells were stained with antibodies against PKA Cα, RIα, RIIα and RIIβ isoforms (green) and visualized by confocal microscopy using a Cy3-labeled secondary antibody. The nucleus was stained with DAPI (blue) and the Golgi complex was stained with an antibody against GOLPH4 using an AlexaFluor594-conjugated secondary antibody (red). Yellow color indicates regions of overlapping intensities. Cα and RIIα are located in the cytosol as well as in the nucleus. RIα staining is present mostly in the nucleus. Note that the RIIβ isoform staining shows a high degree of co-localization (yellow) with the Golgi marker. Images in **A** and **B** are representatives of more than 15 cells per treatment from two independent experiments. Scale bars, 10 µM.

MEASUREMENTS OF COMPARTMENTALIZED PKA SIGNALING IN THYROID CELLS

Immunofluorescence of PKA subunits indicated that different cellular compartments might be responsible for the biphasic PKA signaling observed in the whole thyroid cell. To characterize this hypothesis, real-time measurements of PKA/TSH receptor signaling were obtained by using AKAR2 sensors located in different subcellular compartments. These sensors were generated by additions of specific targeting sequences, i.e., AKAR2 was targeted to the plasma membrane through a CAAX sequence derived from K-Ras (AKAR2-CAAX), to the cytosol via nuclear export signal (NES; AKAR2-NES) and to the nucleus via a nuclear localization signal (NLS; AKAR2-NLS) (DiPilato et al., 2004;Herbst et al., 2011) (**Figure 31A**). PKA activity in the plasma membrane and cytosol were measured 2 days post-transfection. In the nucleus a FRET ratio change could not be detected neither after TSH nor forskolin stimulation, even though the AKAR2-NLS sensor possessed an efficient expression. In order to monitor PKA activity in the nucleus, the experimental conditions were modified. Thyroid cells were additionally starved 2 days post-transfection with AKAR2-NLS for 1 day prior imaging, which was sufficient to detect FRET ratio changes of the AKAR2-NLS sensor after TSH stimulation.

Treating AKAR2-CAAX expressing thyroid cells with TSH resulted in a rapid and robust increase of the FRET ratio (τ_{PM} = 49 ± 9 sec), indicating an increase of PKA activity in the plasma membrane.

In contrast, PKA signaling observed in the cytosol showed a first, fast increase of the FRET ratio (τ_1 = 39 ± 8 sec) followed by a second, slow increase of the FRET ratio (τ_2 = 79 ± 21 sec). The speed of the two distinct phases was not significant different. The delay between these two phases was 115 ± 20 sec (**Figure 31B**), suggesting that at least two distinct signaling events are involved in PKA activation in the cytosol. Similar PKA activity was monitored in the whole thyroid cells after stimulation with TSH (**Figure 28**). Stimulation of AKAR2-NLS expressing thyroid cells with TSH showed a slow and small increase of the FRET ratio, which has also been detected after forskolin addition. Stimulation with TSH induced almost 14-fold faster PKA responses in the plasma membrane (τ_{PM} = 49 ± 9 sec) than in the nucleus (τ_N = 668 ± 187 sec) (**Figure 31B**). The slower nuclear PKA response is in line with previous findings that the PKA activity in the nucleus depends on passive/slow diffusion of the dissociated catalytic subunit from the cytosol into the nucleus (Harootunian et al., 1993).

Taken together, three kinetically and spatially distinct PKA responses were monitored upon TSH stimulation; a first, rapid phase of PKA activation occurs at the plasma membrane, a biphasic PKA signal in the cytosol and a third, slower PKA signal in the nucleus.
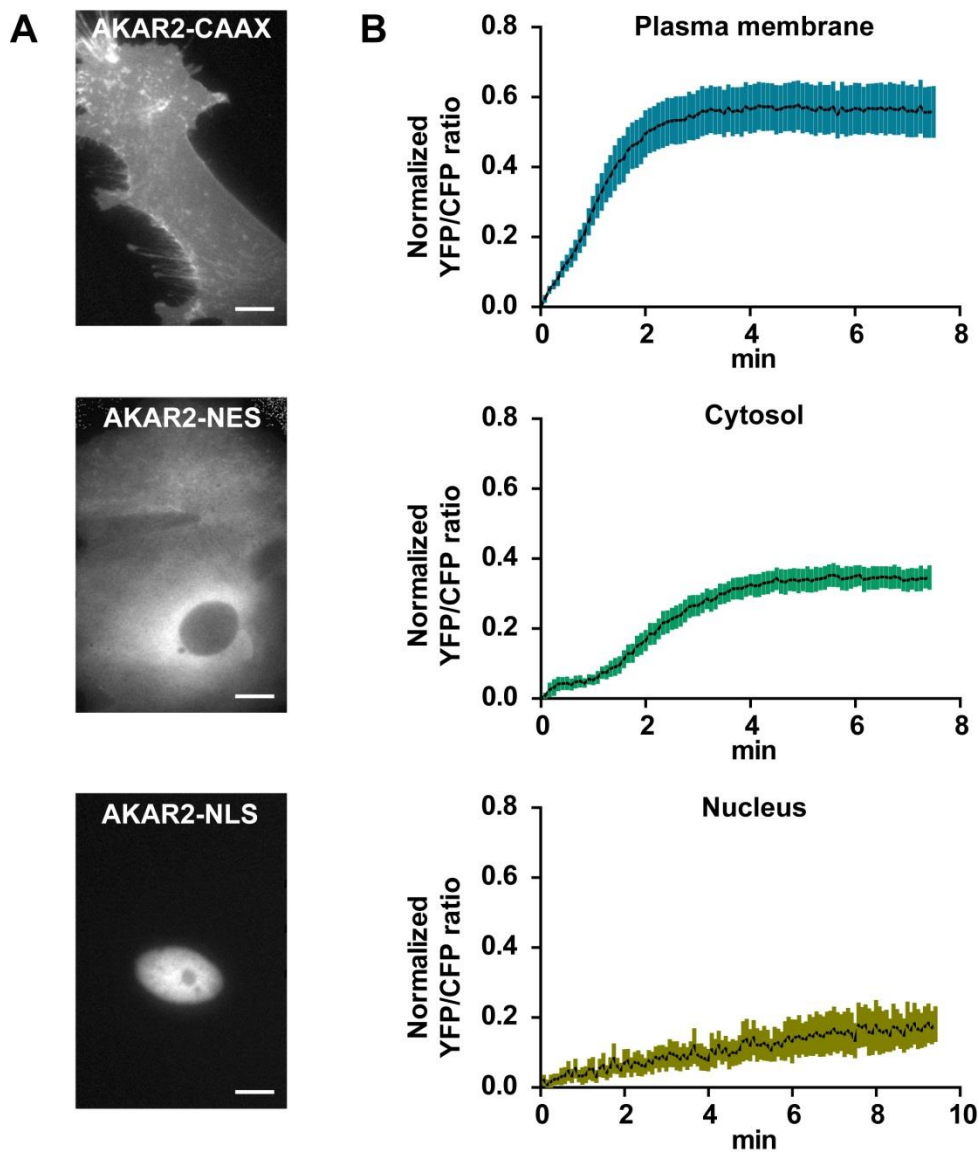
Figure 31: FRET-based measurements of PKA signaling in different compartments of primary thyroid cells.
(**A**) YFP images of primary thyroid cells expressing the PKA sensor in the plasma membrane (AKAR2-CAAX), cytosol (AKAR2-NES) and nucleus (AKAR2-NLS).
(**B**) Real-time FRET monitoring of PKA activity in primary thyroid cell in different compartments. A rise of the YFP/CFP ratio indicates an increase of PKA activation. Data (mean ± S.E.M.) shown here is the average from 16 (plasma membrane), 14 (cytosol) and 7 (nucleus) experiments. FRET values were normalized to the maximum forskolin response by setting it to 1, and the minimum response given by H-89 at the end of each experiment (as shown in **Figure 28**) by setting it to 0. Scale bars, 10 µM.

4.2.4. Analysis of the effect of TSH receptor internalization on G_S signaling in thyroid cells

Previous studies have demonstrated that the internalized TSH receptor continues to signal via cAMP after a transient TSH stimulation (Calebiro et al., 2009). This finding suggested the possibility that the biphasic PKA signaling might originate partially from the intracellular compartment. To investigate this possibility the kinetics of cAMP and PKA activation upon endocytosis inhibition were analyzed.

EFFECT OF TSH RECEPTOR INTERNALIZATION ON cAMP SIGNALING IN PRIMARY THYROID CELLS

To investigate the effect of endocytosis inhibition on TSH receptor signaling, dynasore, a small-molecule dynamin inhibitor, was used to block clathrin-dependent endocytosis (Macia et al., 2006). Dynasore pretreatment has already been shown to effectively inhibit TSH receptor internalization in primary thyroid cells (Calebiro et al., 2009). **Figure 32D** shows that dynasore did not affect direct adenylyl cyclase activation with forskolin in primary thyroid cells, indicating that dynasore did not interfere in cAMP production and/or degradation. Similarly, dynasore-treated cells showed no differences in the TSH-induced amplitude and/or speed of cAMP accumulation (dark grey; $\tau_{dynasore}$ = 133 ± 15 sec) compared to the control cell (light grey; $\tau_{control}$ = 156 ± 31 sec) (**Figure 32A-C**). The FRET increase in dynasore-treated cells started approx. 46 ± 8 sec upon TSH stimulation, which is similar to what was seen in control cells (delay = 47 ± 6 sec) (**Figure 32A, B**).
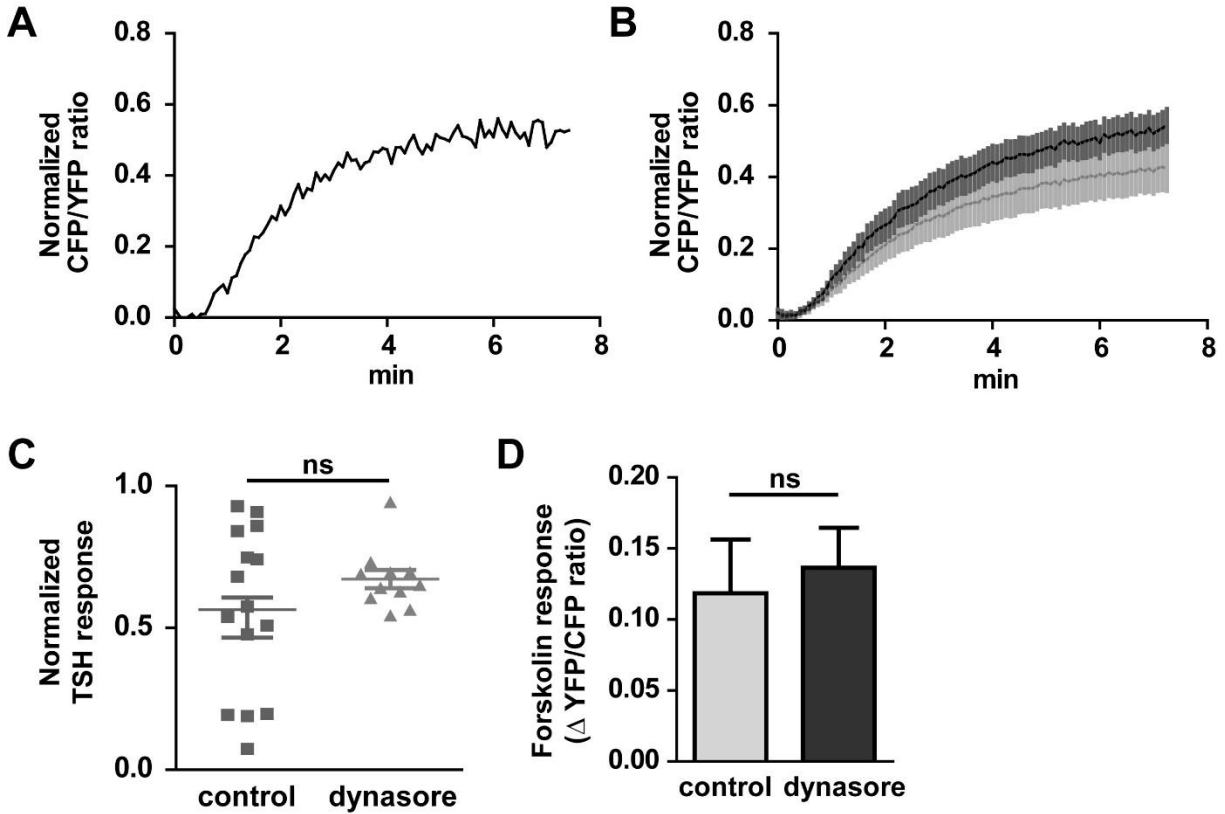
Figure 32: Effect of dynasore on cAMP accumulation in primary thyroid cells isolated from Epac1-camps transgenic mice.
(**A**) Representative time course of TSH-induced (50 U/L) cAMP/FRET changes in primary thyroid cells pretreated with 80 µM dynasore.
(**B**) Averaged time course of TSH-induced cAMP signaling in thyroid cells pretreated with 80 µM dynasore (dark) for 20 min. For comparison, the results of **Figure 27** obtained in control follicles are shown in light grey.
(**C**) Comparison of the amplitude of cAMP accumulation induced by TSH in the absence (control) and presence of dynasore in thyroid cells. Data in **A**, **B** and **C** were normalized as described in **Figure 27** and were fitted as described in **3.2.9**.
(**D**) Comparison of forskolin-dependent accumulation of cAMP in primary thyroid cells in the absence and presence of dynasore. Thyroid cells were pretreated with 80 µM dynasore or DMSO (control) for 20 min followed by stimulation with 10 µM forskolin.
Data in **B**, **C** and **D** (mean ± S.E.M.) are from 15 (control) and 11 (dynasore) independent experiments. ns, no statistically significant difference by Student`s t-test.

EFFECT OF TSH RECEPTOR INTERNALIZATION ON PKA SIGNALING IN PRIMARY THYROID CELLS

To understand in particular how TSH receptor internalization is involved in the production of a biphasic PKA response upon TSH stimulation, FRET-based measurements of PKA activity in primary thyroid cells were performed in the presence of dynasore.
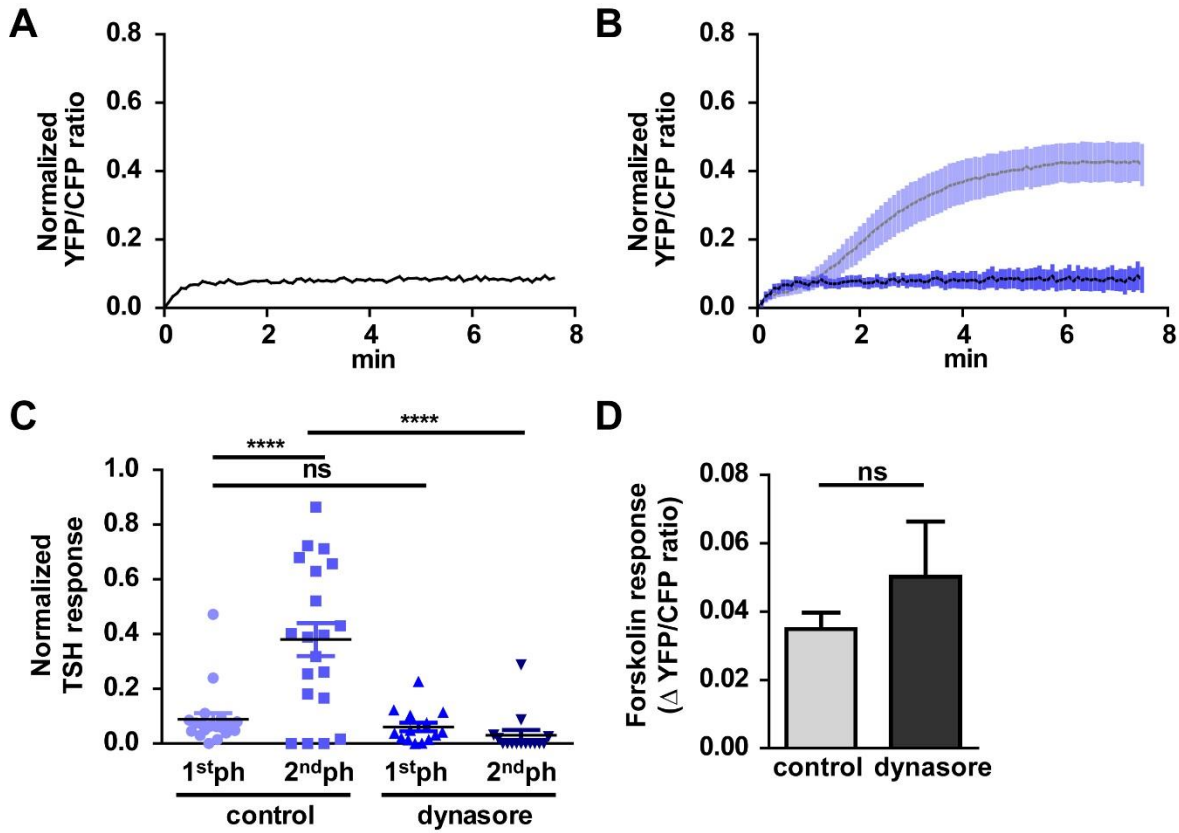
Figure 33: Effect of dynasore on PKA signaling in primary thyroid cells.
(**A**) Representative time course of TSH-induced (50 U/L) PKA/FRET changes in primary thyroid cells pretreated with 80 µM dynasore.
(**B**) Averaged time course of TSH-induced PKA signaling in thyroid cells pretreated with 80 µM dynasore (dark blue) for 20 min. For comparison, the results of **Figure 28** obtained in control cells are shown in light blue
(**C**) Comparison of the amplitude of PKA activity induced by TSH in the absence and presence of dynasore in thyroid cells. Data (mean ± S.E.M.) in **B** and **C** are from 18 (light blue, control) and 15 (dark blue, dynasore) independent experiments. Data in **A**, **B** and **C** were normalized as described in **Figure 28** and were fitted as described in **3.2.9**. Differences are statistically significant by one-way ANOVA followed by Bonferroni post-hoc test. ****, $P < 0.0001$.
(**D**) Comparison of forskolin-dependent PKA activity in thyroid cells in the absence and presence of dynasore. Thyroid cells were pretreated with 80 µM dynasore or DMSO (control) for 20 min, before stimulation with 10 µM forskolin. Data (mean ± S.E.M.) are from 18 (control) and 15 (dynasore) independent experiments per conditions. ns, statistically not significant difference by Student`s t-test.

Remarkably, acute inhibition of endocytosis significantly impaired PKA activation thereby almost completely abolishing the second phase in PKA signaling (**Figure 33A-C**).

This strongly indicates that the internalized-receptor plays a major role in the total PKA signal induced by TSH. Prevention of TSH receptor internalization showed no significant differences in the amplitude and speed of the first phase of TSH-induced PKA signaling (dark blue; $\tau_{1dynasore} = 31 \pm 12$ sec) compared of the first phase of PKA signaling in control cells (light blue; $\tau_{1control} = 37 \pm 8$ sec) (**Figure 33B, C**), suggesting that the first phase of PKA signaling is promoted by the cell-surface-localized TSH receptor. The fact that dynasore pretreatment did not affect direct adenylyl cyclase activation by forskolin in primary thyroid cells, indicating that dynasore treatment itself did not alter PKA activation (**Figure 33D**).

Blocking TSH receptor endocytosis led to no significant differences in the amplitude and speed of the PKA signaling at the plasma membrane ($\tau_{dynasore} = 61 \pm 22$ sec) (**Figure 34A, D**). This result suggests that PKA signaling from the plasma membrane is promoted by cell-surface-located TSH receptors and is not affected by receptor internalization.

In sharp contrast, an almost complete reduction in the amplitude of the second/dominant phase of the cytosolic PKA signaling was seen when endocytosis was blocked with dynasore. However, dynasore had no influence on the first fast phase of cytosolic PKA signaling ($\tau_{1dynasore} = 36 \pm 10$ sec) (**Figure 34B, E**), suggesting that the first phase of cytosolic PKA signaling is promoted by the cell-surface-localized TSH receptor. This might indicate that nuclear PKA activity has no impact on the first phase of cytosolic PKA signaling. To verify this point, nuclear PKA signaling in the presence of dynasore were performed in thyroid cells expressing AKAR2-NLS sensor. Preliminary experiments demonstrated that inhibition of TSH receptor internalization reduced a part of the nuclear PKA response induced by TSH (**Figure 34C, F**), suggesting that TSH receptor internalization is partially responsible for TSH-induced PKA signaling in the nucleus.
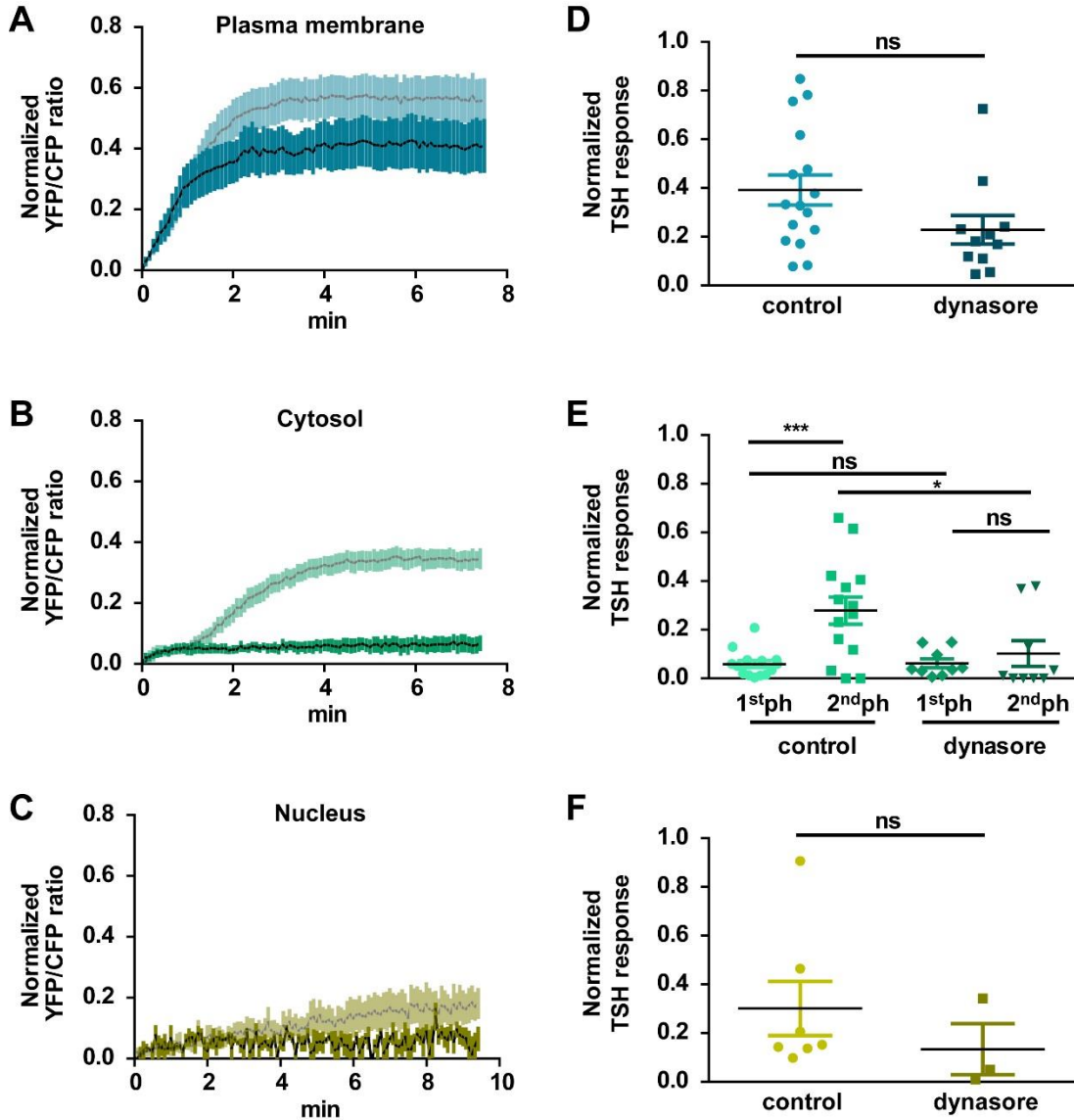
Figure 34: Effect of dynasore on TSH-dependent PKA signaling in primary thyroid cells expressing the PKA sensor AKAR2 in the plasma membrane, cytosol and nucleus.
(**A-C**) Averaged time course of TSH-induced PKA signaling in the plasma membrane (**A**), cytosol (**B**) and nucleus (**C**) of thyroid cells pretreated with 80 μM dynasore (dark colors) for 20 min. For comparison, the results of **Figure 28** obtained in control cells are shown in light colors.
(**D-F**) Comparison of the amplitude of PKA activity induced by TSH in the absence (control) and presence of dynasore in thyroid cells. Data (mean ± S.E.M.) in **A-F** are from 3-16 independent experiments and were normalized as described in **Figure 28** and were fitted as described in **3.2.9**. Data in **D** and **F** are statistically not significant as calculate using Student`s t-test. Differences in **E** are statistically significant by one-way ANOVA followed by Bonferroni post-hoc test. *, $P < 0.05$; ***, $P < 0.00.1$; ns, statistically not significant.

4.2.5. Impact of TSH receptor internalization on nuclear PKA signaling in primary thyroid cells

CREB PHOSPHORYLATION

To support the hypothesis that TSH receptor internalization affects the PKA response in the nucleus, the phosphorylation of the cAMP response element-binding protein (CREB) at Ser133, a major target of PKA in the nucleus and a key mediator of TSH effects in thyroid cells, was examined. CREB induces transcription of several cAMP regulated genes (Medina and Santisteban, 2000;Rivas and Santisteban, 2003;Calebiro et al., 2006). α-tubulin was used as loading control instead of total CREB due to the fact that no stripping protocol was successful. Treatment with TSH was associated with a 230 % increase in phosphorylated CREB, peaking at 10 min after stimulation (**Figure 35**), which was similarly observed in previous studies in FRTL-5 cells, a well differentiated rat thyroid cell line (Calebiro et al., 2006).
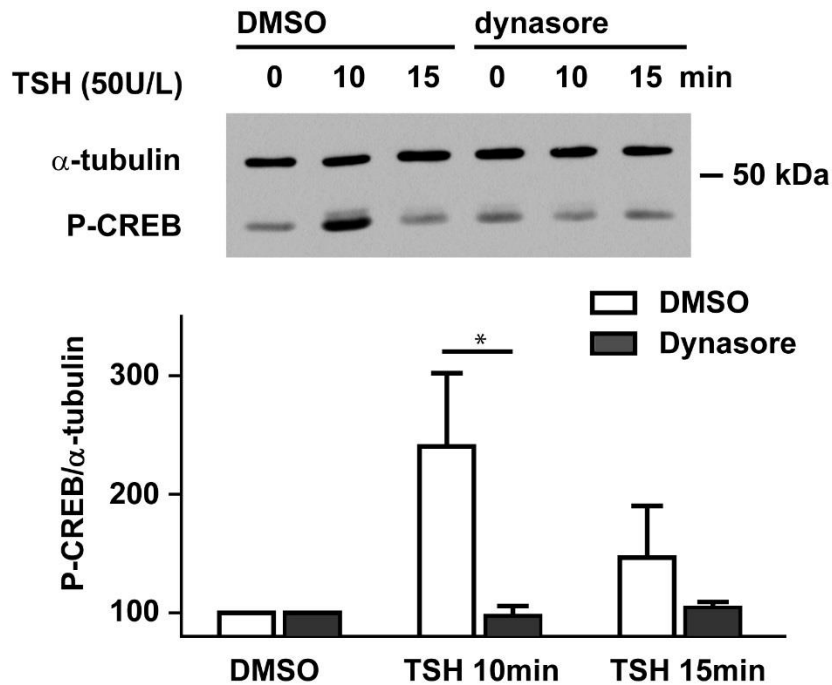
Figure 35: Effect of dynasore on TSH-induced CREB phosphorylation in primary thyroid cells.
Thyroid cells were starved 1 day, followed by preincubation with 80 µM dynasore or DMSO for 30 min and stimulated with 50 U/L TSH for indicated time points. CREB phosphorylation at Ser133 (P-CREB) and α-tubulin levels were evaluated by Western blot analysis, n = 4. The densitometric analysis of four independent experiments is reported shown above. y-Axis shows variations of P-CREB/α-tubulin ratio as percentage of the value in cells treated with DMSO or dynasore only. Differences are statistically significant by two-way ANOVA followed by Bonferroni post-hoc test. *, $P < 0.05$.

Interestingly, CREB phosphorylation was almost completely abolished when pretreating thyroid cells with the endocytosis inhibitor dynasore (**Figure 35**).

At the same time, dynasore pretreatment did not affect the CREB phosphorylation in primary thyroid cells induced by direct adenylyl cyclase activator forskolin (**Figure 36**), indicating that dynasore treatment by itself did not alter basal cAMP production and/or degradation.
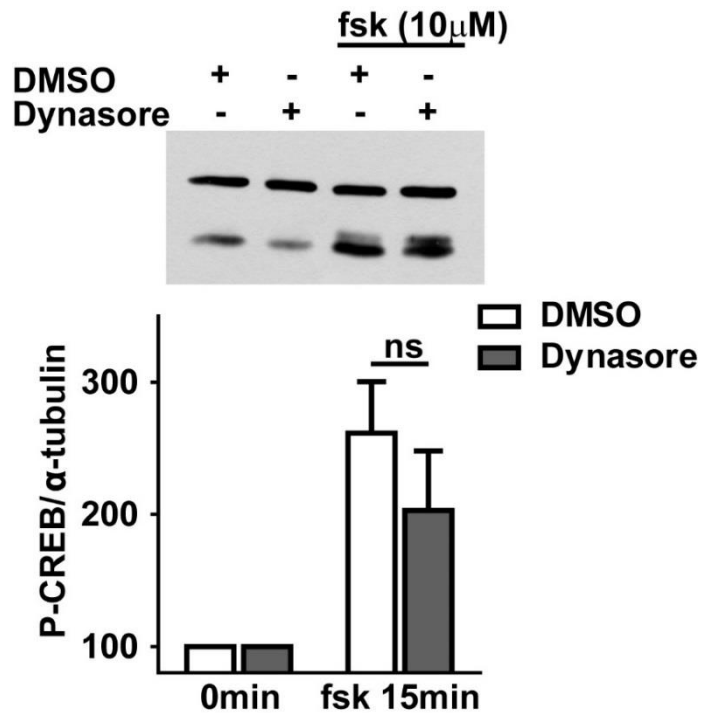
Figure 36: Effect of dynasore on forskolin-induced CREB phosphorylation in primary thyroid cells.
Thyroid cells were starved 1 d followed by preincubation with 80 µM dynasore or DMSO for 30 min and then stimulation with 10 µM forskolin (fsk) for 15 min. CREB phosphorylation at Ser133 (P-CREB) and α-tubulin levels were evaluated by Western blot analysis, n = 4. The densitometric analysis of four independent experiments is reported shown above. y-Axis shows variations of P-CREB/α-tubulin ratio as percentage of the value in cells treated with DMSO or dynasore only. ns, no statistically significant difference by two-way ANOVA followed by Bonferroni post-hoc test.

TSH-INDUCED GENE TRANSCRIPTION

To further confirm that the nuclear response is depending on internalized TSH receptor signaling, the effect of endocytosis inhibition was investigated on transcription of a subset of TSH-regulated genes based on microarray analysis of FRTL-5 cells from a previous study (Calebiro et al., 2006). These included early genes, such as early growth response 1 (*Egr1*), nuclear receptor 4A1 (*Nr4A1*) and 4A3 (*Nr4A3*) and late genes such as cell division cycle protein 2 (*Cdc2a*), a gene involved in cell cycle, and DNA topoisomerase 2α (*Top2a*), a gene involved in DNA replication.

A 30-min stimulation of TSH induced an 8-fold increase in *Nr4A1* expression and an 11-fold increase in *Egr1* expression, while *Nr4a3* did not show any induction by TSH stimulation. As expected, the late genes *Cdc2a* and *Top2a* did not show any induction after 30-min TSH stimulation (**Figure 37**). Unexpectedly, TSH stimulation for 24 h also did not induce *Cdc2a* or *Top2a* expression, possibly underlying sequence-specific differences in the genes that are regulated by TSH.

Inhibition of TSH receptor endocytosis by dynasore almost abolished the induction of *Egr1* and of *Nr4A1* (**Figure 37**).
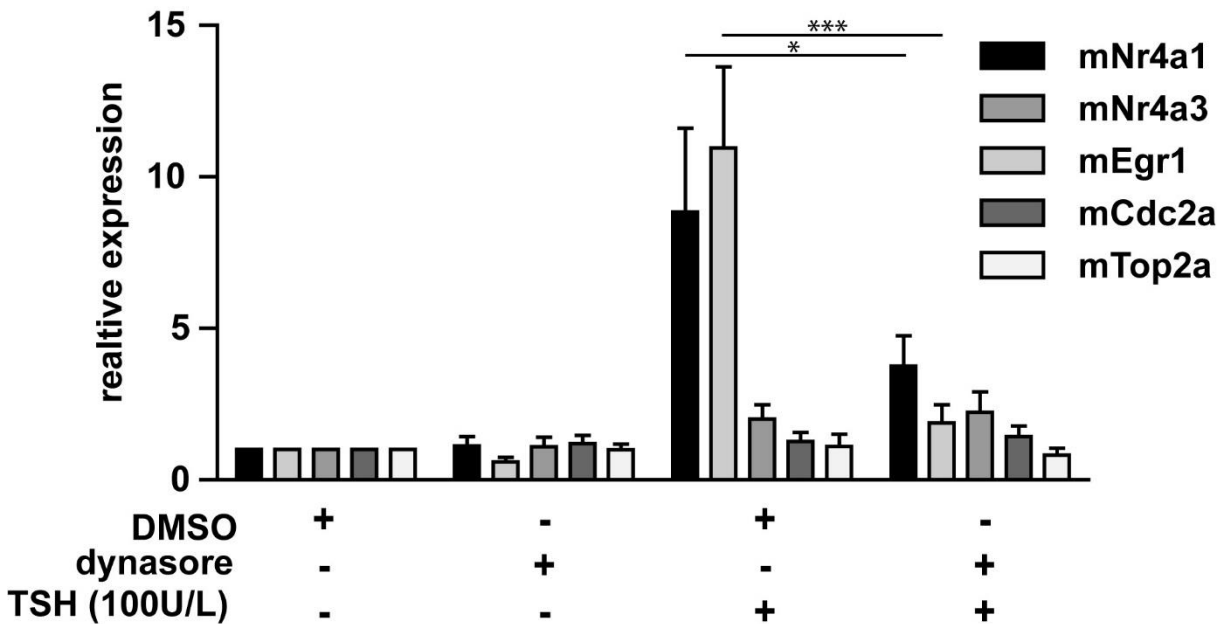
Figure 37: Effect of dynasore treatment on TSH-dependent induction of early genes in primary thyroid cells.
Thyroid cells were starved 1 day, followed by preincubation with 80 µM dynasore or DMSO for 30 min before addition of 100 U/L TSH for 30 min. y-Axis shows mRNA expression of 5 independent experiments relative to DMSO-treated cells. Differences are statistically significant by two-way ANOVA followed by Bonferroni post-hoc test. *, $P < 0.05$; ***, $P < 0.001$

5. Discussion

5.1. MEASUREMENTS OF LH RECEPTOR SIGNALING IN INTACT OVARIAN FOLLICLES

This study demonstrates that LH receptors can continue signaling via cAMP after internalization in follicle cells, and that this is required for transmission of the LH signal to the oocyte and triggers meiosis resumption.

5.1.1. Propagation of cAMP wave through/in different ovarian follicle compartments

The first real-time measurement of cAMP levels in different cell types of an intact ovarian follicle during the course of stimulation with LH was achieved by using isolated ovarian follicles from a transgenic mouse model with ubiquitous expression of a fluorescent sensor for cAMP. Differences in LH receptor signaling were seen between the theca, mural granulosa and cumulus oophorus cells (**Figure 16**). Moreover, the results revealed that a prolonged stimulation of the LH receptor with LH does not induce any detectable desensitization of cAMP signaling during at least 30 min of observation (**Figure 16B**). This is similar to what has been previously observed for the TSH receptor (Calebiro et al., 2009) and differs from what happens with other GPCRs, such as the β_2-AR, that rapidly desensitizes when chronically exposed to its agonists (Irannejad et al., 2013). In the literature, it is known that the LH receptor expression level differs amongst the subregions of the antral follicle with LH receptor being present in theca and mural granulosa cells, but only at very low levels in cumulus oophorus cells (Eppig, 1979;Peng et al., 1991;Russell and Robker, 2007). Consistently, preovulatory cumulus oophorus cells have been reported to respond poorly or not at all to LH stimulation (Eppig, 1979;Peng et al., 1991). Although pretreatment with FSH has been shown to increase the number of functional LH receptors in cumulus oophorus cells (Chen et al., 1994;Shimada et al., 2003), there is evidence supporting that the effects of LH on cumulus oophorus cells as well as on the oocyte are indirect and are mediated by additional factors released by mural granulosa cells in response to LH (Park et al., 2004;Russell and Robker, 2007;Hsieh et al., 2009). Surprisingly, LH induced a rapid and even stronger increase in cAMP in cumulus oophorus cells than in theca and mural granulosa cells (**Figure 16D**). Such an increase of cAMP in these cells that are in direct contact with the oocyte might play an important role in relaying the LH stimulus to the oocyte. Since cumulus oophorus cells possess virtually no LH receptors (Eppig, 1979;Peng et al., 1991;Russell and Robker, 2007), the cAMP increase in these cells presumably involved the gap junction-mediated diffusion of cAMP from mural granulosa cells

and/or the release of a paracrine mediator by mural granulosa cells. Both possibilities are consistent with the observed delay in the cAMP response (**Figure 17**).

To discriminate between these two possibilities, a gap junction inhibitor, carbenoxolone (CBX), was used to investigate if cAMP diffusion via gap junctions plays a role in mediating LH signaling between different subregions. Measurements of cAMP levels in the presence of CBX resulted in a slower kinetics of cAMP increase in cumulus oophorus cells compared to the non-treated cells (**Figure 18**). This result suggests that the cAMP increase in cumulus oophorus cells is at least partially dependent on the gap junction-mediated diffusion of cAMP from mural granulosa cells. Similar results were obtained in the study of Sela-Abramovich et al. (2006), demonstrating that post-LH stimulation, intraoocyte cAMP coming from the mural granulosa cells travels via gap junctions. Several reports have indicated that a reduction in gap junction communication between the somatic cells and the oocyte leads to a cAMP attenuation in the oocyte and consequent meiosis resumption (Sela-Abramovich et al., 2006;Norris et al., 2008). It has also been shown that removal of the oocyte from the follicle leads to decreased cAMP levels in the oocyte, which might indicate that the surrounding somatic cells contribute to the regulation of cAMP in the oocyte and consequent meiotic arrest (Pincus and Enzmann, 1935;Vivarelli et al., 1983).

The virtual lack of FRET signal in oocytes after treatment with LH and forskolin might be either due to the fact that the expression of the Epac1-camps sensor was too low or because of no cAMP signals in the oocyte. However, previous studies have detected FRET changes upon LH stimulation in the oocyte (Norris et al., 2009;Shuhaibar et al., 2015). In one of the mentioned works, Epac2-camps300 with a point mutation for increasing the affinity to cAMP was injected directly in oocytes (Norris et al., 2009) and in the other study, oocytes isolated from transgenic mice expressing the cGMP sensor, cGi500, were used (Shuhaibar et al., 2015). This suggests that the lack of FRET changes upon stimulation in this study is not because of the lack of LH receptor in the oocyte but due to the low expression level of the Epac1-camps sensor obtained in the oocyte compare to the other follicle compartments. This circumstance allows the proof of the capability of this method to distinctly analyze cAMP signaling in different follicle compartments without fluorescence overlying form one compartment to the other.

5.1.2. Persistent cAMP/LH receptor signaling in intact ovarian follicles

This study revealed that in intact ovarian follicles, LH receptor stimulation is associated with persistent cAMP signaling after LH removal and negligible desensitization of the cAMP signal (**Figure 16, 19** and **Figure 20**), suggesting that LH receptors might continue signaling after internalization. This is consistent with earlier studies done for other hormone receptors, e.g. PTH, S1P1 and TSH receptor (Calebiro et al., 2009;Ferrandon et al., 2009;Müllershausen et al., 2009).

To note is that persistent signaling is shown by LH receptor and TSH receptor both belonging to the glycoprotein hormone receptor family sharing structural homology and signaling pathways (Ascoli et al., 2002;Dias et al., 2002;Vassart et al., 2004). TSH receptors can continue to signal via G_s-cAMP from an intracellular compartment, causing persistent cAMP elevations in primary thyroid cells after removal of its endogenous ligand TSH. Conversely, these effects of the TSH receptor were not achieved by co-transfection of human TSH receptor and the FRET-based cAMP sensor Epac1-camps into HEK 293 cells neither 2 min nor 20 min transient stimulation with TSH (Werthmann et al., 2012). Overexpression of $\beta-$arrestin 2, which is known to mainly trigger internalization of human TSH receptors (Frenzel et al., 2006), did not change the rapid and reversible cAMP response upon transient TSH stimulation (Werthmann et al., 2012). Conflicting results have been obtained in HEK 293 cells stably expressing LH, TSH and FSH receptors where persistent signaling was not found for the LH and FSH receptor, whereas the TSH receptor continues signaling upon agonist removal (Neumann et al., 2010). Nonetheless, these experiments were conducted in a non-thyroidal or non-germinal cell line with no endogenous expression of LH receptor. In contrast, intact mouse ovarian follicles, which are composed of a network of structural and functional units and better mimic the ideal conditions allowed us to study GPCR signaling under highly physiological conditions (Jaffe et al., 2009).

5.1.3. LH receptor internalization is required for efficient cAMP signaling

The lack of receptor desensitization and persistent cAMP signaling in the absence of endocytosis inhibitors, suggests that LH receptors can continue stimulating cAMP production after their internalization. These observations are consistent with previous reports, providing growing evidence for intracellular GPCR signaling (Calebiro et al., 2009;Ferrandon et al., 2009;Müllershausen et al., 2009;Kotowski et al., 2011;Werthmann et al., 2012;Feinstein et al., 2013;Irannejad et al., 2013;Kuna et al., 2013;Merriam et al., 2013). To verify this hypothesis, LH receptor signaling was investigated after blocking clathrin-dependent endocytosis with the endocytosis inhibitor dynasore. Unfortunately, the effects of dynasore on the internalization of LH receptor could not be evaluated because, despite repeated efforts, LH labeling with different fluorophores such as TRITC and AlexaFluor594, was not successful. Either the fluorophore did not bind covalently to LH, even if a study of Niswender et al. (1985) showed successful labeling of LH-TRITC (Niswender et al., 1985), or labeling with AlexaFluor594 abolished the biological activity of LH. In content, the same labeling method and fluorophore used for the TSH achieved a high labeling efficiency while preserving biological activity (Calebiro et al., 2009;Calebiro et al., 2015).

Nevertheless, by using radioactive CG, an endogenous ligand of the LH receptor with similar binding affinities as LH in intact ovarian follicles (Marsh, 1976;Mock and Niswender, 1983;Roess et al., 2000), it could be shown that pretreatment with dynasore was capable of efficiently blocking the internalization of LH receptors in intact ovarian follicles (**Figure 22**). At the same time, the response to direct activation of AC with forskolin in ovarian follicles was not affected by dynasore treatment (**Figure 23**), indicating that dynasore did not affect cAMP production and/or degradation.

Surprisingly, prolonged LH stimulation induced no differences in the initial cAMP phase in presence of dynasore in all measured follicle compartments, except for a significant reduction in the overall amplitude of the cAMP response in mural granulosa cells (**Figure 24**). These results suggest that the initial cAMP response is produced by cell-surface LH receptors and the second cAMP response is elicited by internalized LH receptors. A reason for this specific difference in mural granulosa cells might be the distinct higher expression levels of LH receptors than in other follicular compartments (Russell and Robker, 2007).

Remarkably, a rapid reversibility of cAMP signaling upon LH washout was observed in the presence of dynasore in all follicular compartments (**Figure 20** and **Figure 25**), providing strong evidence that LH receptor internalization and the subsequent G_s protein-dependent signaling at intracellular sites was responsible for persistent cAMP generation after transient LH stimulation.

These experiments revealed also that at least two distinct cAMP waves are occurring in ovarian follicles after LH receptor stimulation. A first, transient-one is induced by receptors localized on the cell membrane and a second, sustained one is originating from endocytosed receptors. This is similar to what has been previously observed for two other protein/peptide receptors, i.e. the TSH (Calebiro et al., 2009) and the PTH (Ferrandon et al., 2009) receptor. In conclusion, also the LH receptor can be added to the list of GPCRs able to continue signaling from intracellular sites.

5.1.4. LH receptor internalization contributes to meiosis resumption in intact ovarian follicles

Recent investigations have challenged the traditional view of the role of receptor internalization in GPCR signaling. Most studies could show intracellular signaling at the level of cAMP but the functional consequences of this new phenomenon are still missing. In the case of the LH receptor, the functional consequences of internalized signaling were investigated by making use of the fact that LH surge at mid cycle leads to meiosis resumption and ovulation. As readout meiosis resumption was employed for visual detection of the disappearance of the nuclear envelope, which is a key physiological event that prepares the oocyte for fertilization (Russell and Robker, 2007;Conti et al., 2012).

Our results demonstrated that dynasore treatment is associated with a significant reduction of the fraction of follicles undergoing GVBD after continuous exposure to LH (**Figure 26B**). Application of rolipram to selectively block PDE4 activity, which is expressed in mural granulosa cells but not in the oocyte, mimics cAMP increase caused by LH in mural granulosa cells (Tsafriri et al., 1996). Thereby, the content of cAMP in the oocyte decreases and meiosis resumes by avoiding signaling via LH receptors, leading to 100% GVBD in the presence and absence of dynasore **(Figure 26C)**.
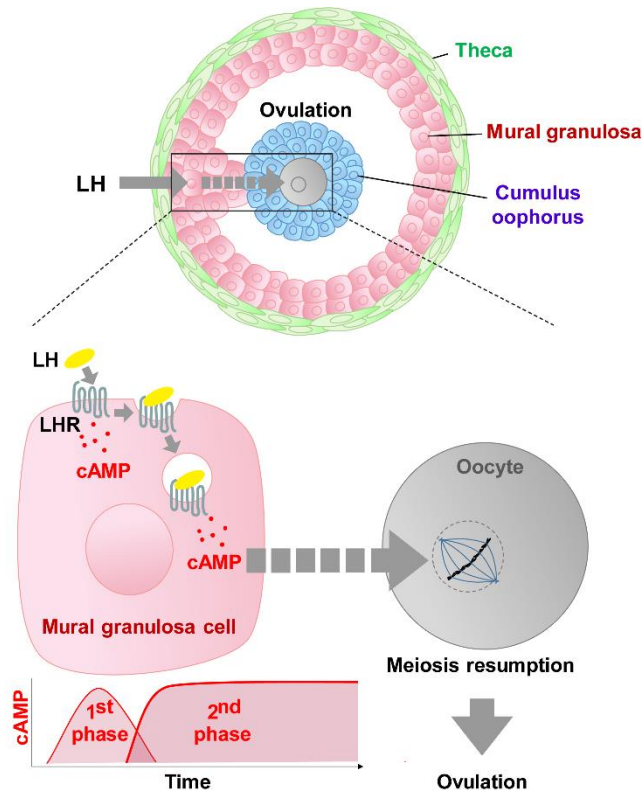
Figure 38: Proposed model of persistent cAMP signaling by internalized LH receptors in ovarian follicles.
Upon stimulation with luteinizing hormone (LH) the LH receptor (LHR) mediates two distinct cAMP signals. First cAMP phase is occurring at the cell-surface and is transient. The second subsequent is produced by the internalized receptor from intracellular sites of mural granulosa cells. The second phase of cAMP production at intracellular sites triggers a cascade of events, presumably involving extracellular and/or intracellular mediators, which contributes to promoting meiosis resumption in the oocyte.

Remarkably, LH receptor internalization in mural granulosa cells appears to be required for efficient induction of meiosis resumption in follicle-enclosed oocytes. Paradoxically, dynasore inhibits spontaneous GVBD also in isolated mouse oocyte where the LH receptor is not present (Lowther et al., 2011), suggesting that the dynasore effect on LH-induced GVBD could be due to a non-specific effect on the oocyte and not caused by LH receptor internalization.

There are several aspects that might help to explain the divergent results. First, the signaling behavior of the model used in Lowther et al., 2011, isolated oocyte, is not comparable with the follicle-enclosed oocyte used in this study, because of the fact that denude oocytes already undergo GVBD without LH stimulation (Vivarelli et al., 1983) or PDE3 inhibitor treatment (Tsafriri et al., 1996). Second, just a partially inhibition of GVBD could be achieved in follicle-enclosed oocytes in this study, whereas a complete reduction is seen in isolated oocytes after 6 h in the study of Lowther et al., 2011 , indicating that the LH-induced cAMP signal obtained at the cell membrane of mural granulosa cells might also contribute to meiosis resumption (Lowther et al.,

2011). Indeed, 100% GVBD was obtained with rolipram in presence of dynasore in follicle-enclosed oocytes (**Figure 26C**), indicating that dynasore does not have any effect on signals mediated independently of LH receptor signaling in the somatic cells surrounding the oocyte.

A possible experiment to complete this would be to do real-time cAMP/FRET measurements upon PDE4 inhibitor stimulation in the presence and absence of dynasore to show that PDE4 inhibitor-induced cAMP signal reach similar levels as LH.

Moreover, blocking LH receptor internalization lead to a significant reduction of the cAMP level in mural granulosa cells and to a partially inhibition of meiosis resumption but the cAMP level in cumulus oophorus cells is not affected (**Figure 24, Figure 26B**). Since it is known that the LH-induced signals from the outer cell layers of ovarian follicles are relayed to the oocyte and trigger meiosis resumption one could ask why the cAMP level in cumulus oophorus cells is not changed as seen in mural granulosa cells upon inhibition of the LH receptor internalization.

One aspect that might help to explain the divergent results could be that the decrease in LH receptor signaling in mural granulosa cells blunts one or more of the numerous other signals known to be involved in the LH action. One possible signal could be elicited by the second messenger cGMP. It is known that meiosis resumption is triggered by a decrease of intraoocyte cAMP level induced by a reduction of cGMP (Shuhaibar et al., 2015). This phenomenon could be explained by the general task of cGMP to inhibit the cAMP phosphodiesterase PDE3A present in the oocyte and thus prevents the degradation of cAMP in the oocyte (Solc et al., 2010;Conti et al., 2012). Therefore a decrease in cGMP levels lead to a decrease of cAMP levels in the oocyte. In particular, such a decrease of cGMP could be elicited by inactivation of the NPR2 guanylyl cyclase by reducing the ovarian content of the NPR2 agonist C-type natriuretic peptide due to LH signaling (Zhang et al., 2010;Kawamura et al., 2011;Egbert et al., 2014), which is responsible for cGMP production in mural granulosa cells. However, levels of this peptide decrease only after the decrease in oocyte cGMP (Robinson et al., 2012).

Since cGMP diffuses through gap junctions from outer cell layers to the core of the follicle, a LH-induced decrease of cGMP levels in mural granulosa cells lead also to a decrease of cGMP in COC (Törnell et al., 1991;Kawamura et al., 2011;Shuhaibar et al., 2015).

Another mechanism involved in the cGMP decrease could be the PKA-dependent activation of the cGMP phosphodiesterase PDE5 (Corbin et al., 2000), which degrades cGMP and has been shown to become phosphorylated in ovarian follicles in response to LH (Egbert et al., 2014). Thus, LH-dependent decrease in cGMP concentration in the cells surrounding the oocyte (Vaccari et al., 2009) serve as a possible explanation of cAMP signal transmitting from mural granulosa cells to the oocyte.

Taken together, LH receptor endocytosis is involved in efficient induction of meiosis resumption in intact ovarian follicles. This demonstrates that cAMP signaling by internalized GPCRs is biologically distinct from the one occurring at the cell-surface, and has a relevant functional role in a complex and intact biological model (**Figure 38**). Thus, these findings provide strong evidence that signaling by internalized receptors is physiologically relevant.

5.2. Measurements of TSH receptor signaling in primary thyroid cells

This study demonstrates that TSH receptor signaling occurs in temporally and spatially distinct PKA phases and signaling by internalized TSH receptors is required for efficient PKA and nuclear signaling in primary thyroid cells.

5.2.1. TSH induces multiple waves of spatially and kinetically distinct PKA signaling

Measurements of PKA dynamics in intact cells are highly demanding and little is known about the spatiotemporal organization in thyroid cells. In order to investigate spatiotemporal dynamics of PKA/TSH receptor signaling, primary thyroid cells were transiently transfected to express the PKA sensor AKAR2. TSH receptor stimulation with TSH is associated with a rapid initial phase followed by a subsequent acute phase of PKA activation with a delay of approximately 2 min (**Figure 28**), suggesting that at least two distinct signaling events are involved in PKA activation.

One could speculate that the first, rapid PKA signal is elicited via TSH binding to its receptor located on the cell-surface, while the second, slower PKA signal is generated from TSH/TSH receptor complex located in the cell interior of the thyroid cell. According to a previous study showing persistent cAMP signaling in thyroid follicles after TSH removal, the perinuclear compartment contains the internalized TSH/TSH receptor, G_s protein and AC III (Calebiro et al., 2009) and serves as a new signaling hot spot. This suggests that the internalized TSH receptor might signal via PKA from the perinuclear compartment and therefore might be responsible for the second PKA response obtained in primary thyroid cells.

The delay of the second PKA response might be due to the G protein-independent signaling via β-arrestin. In particular, β-arrestin binds to the GRK-phosphorylated receptor and initiates the internalization process via clathrin-coated pits. The binding of β-arrestin to the receptor activates the MAPK pathway (Diaz Anel, 2007). During β-arrestin binding to the receptor, signaling via G protein is believed to stop and therefore β-arrestin signaling might be an explanation of the delayed second PKA response. β-arrestin signaling between to signaling waves was already shown for the β2-AR at the level of cAMP by the group of Mark von Zastrow. They could show that β-arrestin binds to β2-AR before and during clathrin-coated pit formation without the presence of G protein binding to the receptor (Irannejad et al., 2013;Lohse and Calebiro, 2013)(**Figure 39**).
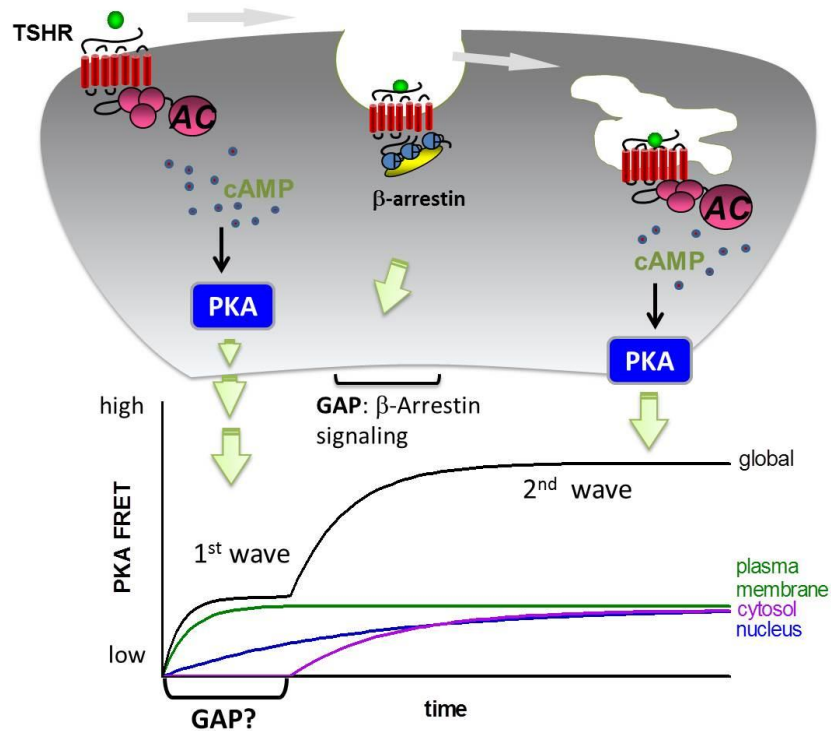
Figure 39: Working model of PKA/TSH receptor signaling.
TSH receptor (TSHR) in thyroid cells produces two distinct waves of PKA signaling. The first wave is generated by receptors located at the cell-surface and the second, late wave is generated at intracellular sites after the clathrin-dependent internalization of TSH-stimulated receptors. The gap between the first and the second PKA wave could be the time where β-arrestin signals.

One can assume the possibility that the obtained temporal distinct PKA responses might be due to the different subcellular localization of PKA isoforms. For instance, the PKA I isoforms can freely diffuse in the cytosol and therefore can be easily reached and activated by the TSH-induced cAMP. Therefore the PKA I isoform signaling might be responsible for elicit the first, rapid PKA response. While, PKA II isoforms are targeted via AKAPs to cell membranes of the cytoskeleton and the Golgi (Rios et al., 1992;Rubin, 1994;Skalhegg and Tasken, 2000) it might take longer for cAMP to reach the anchored PKA II isoforms, which might result in a delayed second PKA response.

Additionally, earlier studies for TSH receptor in FRTL-5 cells, showing that different PKA isoforms mediate distinct downstream effects of PKA signaling. The analysis showed that PKA II, but not PKA I, is required and sufficient for cAMP to exert its effects in the nucleus, whereas PKA I seems to mediate the effects on cAMP on cytosolic targets (Calebiro et al., 2006). Independent from the fact that PKA I and PKA II activation results in the release of otherwise identical catalytic subunits, only PKA II signaling from the Golgi area, and thus close to the nucleus, is required for TSH-dependent CREB phosphorylation peaking after 10 min (Calebiro et al., 2006). This observation

suggests that also the monitored second, delayed PKA response might be produced by the PKA II activation located in the Golgi compartment.

Taken together, this might allow the hypothesis that the TSH-induced spatially and kinetically distinct PKA signaling is mediated through different PKA isoforms from distinct cellular compartments.

To investigate whether the PKA signaling is compartmentalized and how it is involved in the biphasic PKA signaling observed in the whole thyroid cell, PKA activity was measured at the plasma membrane, cytosol and in the nucleus. This could be achieved by using AKAR2 sensor tagged with localization signals for the plasma membrane (CAAX sequence derived from K-Ras, AKAR2-CAAX), for the cytosol (nuclear export signal, AKAR2-NES) and for the nucleus (nuclear localization signal, AKAR2-NLS) (**Figure 31A**). As expected, TSH stimulation led to a rapid and monophasic response at the plasma membrane (**Figure 31B**), which has a higher amplitude than the global PKA response. A reason might be that the AKAR2-CAAX sensor is enriched close to the non-raft portions of the plasma membrane (Depry et al., 2011). Hence, AKAR2-CAAX sensor is able to detect more active PKAs located close to the plasma membrane, than the global sensor which is expressed everywhere in the thyroid cell.

In addition, the CAAX sequence derived from K-Ras that was used for targeting the PKA sensor to the plasma membrane might be not specific for the cell-surface membrane and consequently the AKAR2-CAAX can be found on every membrane in the cell (Philips, 2005). Nevertheless, the used localization tag is one of the most common sequence to target a protein to the plasma membrane (Ananthanarayanan et al., 2005;Allen and Zhang, 2006;Zhou et al., 2012).

The cytosolic PKA response showed almost the same biphasic pattern as the global PKA response (**Figure 31B**), but with slightly reduced amplitude indicating that this might refer to the missing nuclear PKA activity. In comparison to the plasma membrane and cytosolic PKA responses, a small PKA response with slow kinetics and without a lag time was detected in the nucleus (**Figure 31B**).

In particular, monitoring of PKA activation in the nucleus was challenging. Without 24 h starvation of the thyroid cells no PKA activation could be detected upon TSH and/or forskolin stimulation in the nucleus. However, a decrease of the FRET ratio was obtained by using the PKA inhibitor H-89 suggesting that the PKA activity in the nucleus at basal level was already very high and thus the sensor was saturated.

The absence of a lag time in the nuclear PKA response was unexpected because of the common knowledge that the nuclear PKA response depends on the catalytic subunit dissociation from the regulatory subunit in an isoform-specific manner upon cAMP generation (Martin et al., 2007) and translocation of the catalytic subunit to the nucleus by slow diffusion (Harootunian et al., 1993).

A possible explanation could be that the PKA catalytic subunit might be already located in the nucleus in basal conditions. This theory is consistent with the immunofluorescence data of PKA catalytic subunit obtained in this study (**Figure 30A**), which showed a staining of the catalytic subunit also in the nucleus.

This theory is in agreement with a study of Sample et al. (2012) in HEK 293 cells showing a rapid nuclear PKA response generated by the PKA holoenzyme without a lag time, which resides inside the nucleus and is not depending on the passive diffusion of the catalytic PKA subunit into the nucleus (Sample et al., 2012).

Interestingly, the obtained immunofluorescence results using antibodies against different PKA isoforms, $C\alpha$, $RI\alpha$ and $RII\alpha$, showed strong staining in the nuclei of thyroid cells, whereas no staining was seen against $RII\beta$ in the nucleus (**Figure 30**). These data indicate that the PKA holoenzyme resides not exclusively outside of the nucleus but also inside the nucleus. Therefore, the obtained nuclear PKA response is not dependent on passive diffusion of the catalytic PKA subunit into the nucleus, which might also explain the negligible lag time.

Also the diffusion rate of the PKA catalytic subunit from distinct PKA regulatory subunits was shown to be different upon cAMP elevation. While PKA catalytic subunit may not diffuse far when released from PKA $RI\alpha$, PKA catalytic subunit is capable of diffusing far away from $RII\alpha$ (Martin et al., 2007;Manni et al., 2008).

Based on these facts and the immunofluorescence staining of PKA $RI\alpha$ and $C\alpha$ in the nucleus suggest that the nucleus might comprises a novel PKA signaling microdomain in thyroid cells. To better understand the PKA signaling machinery translocation experiments of the PKA catalytic subunit could be done, which might help to explain the events happening inside and outside the nucleus of thyroid cells.

Furthermore, immunofluorescence staining of PKA $RII\beta$ was seen in the Golgi (**Figure 30B**). This high degree of co-localization indicates that a significant fraction of PKA $RII\beta$ resides on the membrane of the Golgi. This is consistent with several studies showing that the PKA II isoform is localized through AKAPs to the Golgi membranes (Rios et al., 1992;Rubin, 1994). A study of the TSH receptor signaling in thyroid cells showed that the TSH receptor/TSH complex after internalization is located together with AC and G_s protein on a perinuclear compartment (Calebiro et al., 2009).

These findings together with the immunofluorescence staining of PKA $RII\beta$ in this study implicate that the Golgi/ trans-Golgi network might serve as a specialized intracellular platform not only for TSH receptor but also for other GPCRs like the S1P1 receptor (Müllershausen et al., 2009) and

somatostatin receptor type 2 receptor (Csaba et al., 2007) and should be taken more in consideration for further experiments.

Taken together, the results in this study indicate that TSH-induced biphasic PKA response is composed of three spatial and temporal distinguished phases: a first, rapid phase of PKA activation occurs at the plasma membrane, followed by a second phase in the cytosol and a third, slower phase in the nucleus, which is hidden by the two other phases (**Figure 31, Figure 39**).

5.2.2. Blocking TSH receptor internalization abolishes the second phase of PKA signaling in thyroid cells

It has been demonstrated that cAMP signals induced by a transient TSH receptor stimulation remain persistent even after TSH removal in primary thyroid follicles, whereas in presence of dynasore a rapid reversibility in cAMP signaling upon TSH washout was detected. These results provide strong evidence that TSH receptor internalization and the subsequent G_s protein-dependent signaling at intracellular sites were responsible for persistent cAMP generation after transient TSH stimulation (Calebiro et al., 2009). However, inhibition of TSH receptor internalization did not impair the cAMP response induced by prolonged TSH stimulation in thyroid cells (**Figure 32A-C**). This is consistent with limited or no PDE activation under the experimental conditions in this study. In the case of LH receptors, blocking receptor endocytosis yielded a reduced second cAMP response, while the initial phase of cAMP was not affected in mural granulosa cells (Lyga et al., 2016). This is also true for another G_s protein-coupled receptor the β_2-AR in HEK 293, which subsequent cAMP accumulation was significantly reduced upon blocking receptor endocytosis (Irannejad et al., 2013).

In conclusion, TSH receptor internalization do not contribute to the total cAMP accumulation upon persistent TSH stimulation.

Furthermore, the PKA isoforms as well as PKA signaling were identified to be compartmentalized in thyroid cells (**Figure 30, Figure 31**). In particular, TSH receptor signaling upon TSH stimulation was related to a biphasic PKA response in the global thyroid cell (**Figure 28**). Remarkably, the second, acute wave of TSH-mediated PKA signaling was largely abolished in the presence of an endocytosis inhibitor in the whole thyroid cell (**Figure 33A-C**). This phenomenon provides strong evidence that TSH receptor internalization and the subsequent G_s protein-dependent signaling at intracellular sites is required for the acute PKA response upon TSH stimulation. These data suggest that at least two distinct PKA waves are occurring after TSH-induced receptor activation in thyroid cells. A first, fast one induced by receptors localized on the cell-surface and a second, sustained one induced by endocytosed TSH receptors.

As expected, the plasma membrane PKA response was not impaired by blocking TSH receptor endocytosis (**Figure 34A, D**), which indicates that indeed the initial phase in the global PKA response is most likely initiated by TSH receptor activation on the plasma membrane.

Measurements of PKA signal in the cytosol in the presence of dynasore showed a fast but small PKA response lacking the subsequent second phase (**Figure 34B, E**) as seen prior for the global PKA response (**Figure 33**). This might suggests that the initial PKA phase obtained in the global thyroid cell does not contain PKA signals obtained in the nucleus.

Moreover, it was of interest to investigate the effect on the nuclear PKA response in the presence and absence of receptor internalization. Apparently, the PKA activity is very high in the nucleus of thyroid cells (see discussion **5.2.1**), which delayed the analysis of the effects of endocytosis inhibitors in this compartment. Preliminary data demonstrate that the nuclear PKA response is impaired by blocking receptor internalization (**Figure 34C, F**), suggesting that the nuclear PKA response contributes to the second phase of the global PKA response. The endocytosed receptor/ligand complex continues signaling via PKA from the intracellular site, which is required for efficient PKA signaling in the nucleus.

Taken together, these findings provide for the first time direct evidence that GPCR signaling can occur in temporally and spatially distinct phases and signaling by internalized GPCRs is required for the efficient activation of PKA.

5.2.3. TSH receptor internalization is required for efficient CREB phosphorylation and gene transcription in thyroid cells

Very recently, it could be shown that signaling outcomes produced by internalized receptors indeed differ from those that originate at the cell-surface (Calebiro et al., 2009;Tsvetanova and von Zastrow, 2014;Lyga et al., 2016). An interesting possibility is that intracellular TSH receptor activity could contribute to PKA-dependent CREB phosphorylation in thyroid cells. Indeed, inhibition of TSH receptor internalization was associated with a lack of CREB phosphorylation, while TSH stimulation in control cells induced CREB phosphorylation peaking 10 min after stimulation (**Figure 35**). Due to the fact that CREB phosphorylation is induced by the catalytic subunit of PKA in the nucleus (Skalhegg and Tasken, 2000), the nuclear PKA response and CREB phosphorylation should have similar kinetics. Actually, the nuclear PKA response reaches a maximum after ca. 8 min and the CREB phosphorylation after 10 min stimulation with TSH. However, the nuclear PKA response remains stable for at least further 10 min, whereas the induction of CREB phosphorylation is reduced after 15 min stimulation with TSH (**Figure 35)**.

One has to refer to the possibility that phosphates in the nucleus might have different affinities on PKA and on CREB phosphorylation (Hunter, 1995), which might be a reason for the differences among nuclear signaling kinetics. Another aspect that might help to explain the divergent result could be that the compartmentalization of PKA isoforms might contribute to the distinct temporal signaling events. Given the fact that PKA II exclusively promotes CREB phosphorylation in FRTL-5 cells, which is a transient event (Calebiro et al., 2006), one could assume that the nuclear PKA response, which is persistent, might be elicited by both PKA isoforms.

In conclusion, PKA II anchoring to the Golgi compartment and now also the internalization of TSH receptor, which is located in a preinuclear region, is required for efficient nuclear signaling (TSH-dependent CREB phosphorylation) suggesting that the Golgi region might be a new signaling platform and need to be further investigated.

Another approach to investigate the involvement of TSH receptor endocytosis further downstream of PKA on nuclear targets was to analyze receptor-mediated regulation of gene expression. Remarkably, the presence of an endocytosis inhibitor largely impaired the TSH-dependent induction of early genes in thyroid cells (**Figure 37**) providing strong evidence that TSH receptor internalization and the subsequent G_s protein-dependent signaling at intracellular sites is required for efficient transcriptional activation. The investigated late genes, *Cdc2* and *Top2a*, which are known to be induced by TSH receptor activation in FRTL-5 cells (Calebiro et al., 2006), showed no differential changes upon TSH stimulation in thyroid cells.

There are several aspects that might help to explain the divergent results. First, the different TSH incubation time points varied from 24 hours in primary thyroid cells (this work) to 17 hours in FRTL-5 cells (Calebiro et al., 2006). Seven hours discrepancy might already be enough for the gene expression to return to basal levels. Second, the use of a divergent thyroid cell system could be responsible for such a difference in the expression of late genes. Since it was demonstrated that thyroid cells of different animal models show divergent signaling behavior (Allgeier et al., 1997;Medina and Santisteban, 2000;Kimura et al., 2001), a comparison between a stable cell line derived from rat and primary mouse thyroid cells, which additionally belong to different species might limit the comparison of such findings (Dumont et al., 1992).

Taken together, the data suggest that TSH-induced PKA signaling in primary thyroid cells is composed of two temporally and spatially distinct phases. In particular, internalization of TSH/TSH receptor complex to a perinuclear compartment is responsible for the second PKA response and for efficient phosphorylation of CREB and induction of early gene transcription.

5.3. STRENGTHS, LIMITATIONS AND POSSIBLE IMPROVEMENTS

In this study, real-time measurements of GPCR signaling in living cells were achieved by using an optical method based on Förster/Fluorescence resonance energy transfer (FRET). FRET provides great advantages in analysis of the complex mechanistic of GPCR signaling compared to traditionally biochemical approaches (Zaccolo et al., 2000;Nikolaev et al., 2004;Lohse et al., 2008).

In particular, FRET allows the monitoring of dynamic processes of GPCR activation and signaling, such as ligand specific conformational change of GPCR, G protein activation and cellular signals within milliseconds (Arshavsky et al., 2002). In contrast, traditional methods for analyzing GPCR activation using membrane-based biochemical assays or detecting downstream physiological events cannot provide the ability of FRET to resolve the kinetics and spatiotemporal dynamics of receptor activation and signaling.

Using intact ovarian follicles or primary thyroid cells isolated from transgenic mouse expressing a FRET sensor for cAMP provide the advantage to perform real-time experiments in a highly physiologically relevant environment without the need of overexpressing proteins, which could interfere with the cell biology.

However, no genetically modified organisms with ubiquitous expression of PKA-based sensors are available so far in an adequate quality for measuring PKA activity (Lissandron et al., 2007). To obtain real-time measurements of PKA activity a transient transfection of primary thyroid cells with the PKA sensor AKAR2 was necessary. Electroporation was used to transfect primary thyroid cells, although it is known to induce substantial cell death initiated by high voltage as well as only partially successful membrane repair, which require the use of high amount of cells. Nevertheless, it was the only method to achieve high level of cell quality combined with good expression efficiency in primary thyroid cells.

To investigate the effects of receptor internalization a pharmacological inhibitor, a small dynamin inhibitor dynasore, was used. Dynasore treatment was capable of efficiently blocking the internalization of LH receptors in intact ovarian follicles (**Figure 22**) as well the internalization of TSH receptors in mouse primary thyroid cells (Calebiro et al., 2009) without having any effect on the cellular response induced by forskolin (**Figure 23, Figure33**). As an alternative to dynasore, dynamin dominant-negative mutant (K44A) or wild-type dynamin as a control was expressed together with the PKA sensor but due the too low or no transfection efficiency in primary thyroid cells this alternative could not be fully tested in the given time-frame. As a further outlook or possible solution to confirm the obtained results by another method for inhibition of receptor internalization one could try to optimize the transfection (by making adenoviruses for increased

efficiency) or use other pharmacological options like inhibiting receptor internalization in the presence of high concentrations of sucrose (Calebiro et al., 2009). Since clathrin and dynamin are implicated in other physiological processes besides GPCR internalization, on could attempt to selectively inhibit GPCR internalization by silencing β-arrestin 1 and 2 expression, which has been already applied with success to other GPCRs (Ahn et al., 2003).

In order to characterize the two distinct phases of PKA signaling regarding the involvement of different PKA isoforms, PKA I and II inhibitors were evaluated for their selectivity. PKA II inhibitor (Rp-8-PIP-camps) showed a good degree of selectivity, whereas PKA I inhibitor (Rp-8-Br-camps) did not show the expected level of selectivity in primary thyroid cells despite its effectiveness in other cells/conditions/labs (Schwede et al., 2000b). Although the selective activation of PKA I or II was achieved by using PDE-resistant cAMP analog pairs (Robinson-Steiner and Corbin, 1983;Beebe et al., 1984;Calebiro et al., 2006), which have different affinities for activation of type PKA RI or RII, the use of these cAMP analog pairs could lead to an underestimation of the efficiency of PKA isoform inhibitors. Nevertheless, the estimated selectivity for PKA I:II obtained under this experimental conditions was approximately 5:1 for PKA RI and 1:60 for PKA RII (Dostmann et al., 1990;Skalhegg et al., 1992;Schwede et al., 2000a). To avoid the use of pharmacological inhibitors a possibility could be the knockdown of genes encoding the PKA RI (*Prkar1a*, *Prkar1b*) and RII (*Prkar2a*, *Prkar2b*) by gene silencing with small interfering RNAs.

Taken together, the techniques used in the study, especially the FRET, provide the possibility to capture fast signaling events and at the same time, define their subcellular location in living cells/organism. Expression of FRET-based DNAs in primary cells is still challenging and required time consuming optimization, nevertheless it represents just a small limitation compared to biochemical methods.

5.4. OUTLOOK

The findings of this study shed new light in the mechanisms of GPCR signaling at intracellular sites and its physiological relevance. The investigations of two endocrine models, primary thyroid cells and intact ovarian follicles, provide strong evidence that GPCRs signaling occurs in at least two temporal and spatial distinct waves. A first, rapid one derived from receptors at the cell-surface and a second, sustained one is induced by internalized receptors, which are required for the specific effects of TSH and LH.

In particular, the data suggest that the Golgi/trans-Golgi network may serve as a hot spot for GPCR signaling as proposed by the study of Calebiro et al., 2009. However, the exact nature of the intracellular signaling compartment still needs to be answered. To investigate this question, live-cell imaging experiments could be performed to visualize the trafficking of the signaling machinery and downstream signaling in the Golgi/trans-Golgi network could be monitored. For this purpose, Golgi-targeted AKAR2 sensor containing the GRIP domain (Munro and Nichols, 1999) was generated in our laboratory and preliminary experiments are already ongoing.

Furthermore, the results of this study indicate that GPCR internalization is required to mediate the biological effects of LH in intact ovarian follicles, but so far the functional relevance for TSH receptor internalization remains to be fully elucidated. To fill this gap, experiments considering the effect of cell-surface vs. intracellular TSH receptor signaling on thyroid hormone production, which is a major functional outcome of TSH receptor activation in thyroid cells, could be done. In particular, thyroglobulin reuptake and thyroid hormone release (T4 and T3) could be evaluated by a commercially available radioimmunoassay in the presence or absence of endocytosis inhibitors.

The data indicate that besides the TSH receptor, a second glycoprotein hormone receptor, the LH receptor is able to continue signaling via cAMP from the intracellular sites. A raising question is, whether also the FSH receptor, which shares structural homology with LH and TSH receptors, can also signal from the intercellular sites. To investigate this question, similar experiments on cAMP/FSH receptor signaling could be repeated in intact ovarian follicles by using FSH instead of LH, since FSH receptors have the same tissue localization as LH receptors, i.e., in theca and mural granulosa cells. These investigations might also allow better understanding how the different cell layers of an ovarian follicle communicate and transmit signals to the oocyte and consequently understand the regulation of female fertility leading to ovulation.

The obtained results could have a variety of possible implications. On the one hand, alteration in pathophysiology, e.g. hyperthyroidism and/or hypothyroidism, might be caused by defects of receptor internalization. In particular, mutations of each component of the TSH signaling pathway are known to be implicated in various diseases such as benign and malignant endocrine tumors

or TSH resistance. These mutations might change the ability of GPCR to undergo internalization and/or to signal from the intercellular sites and thus cause functional disorders. On the other hand, the data of this study suggest that novel pharmacological therapies, e.g. for contraception or the treatment of infertility, could be established by interfering with receptor internalization and/or signaling at intracellular sites. As a perspective, the findings of this study might pave the way to a new generation of ligands selectively inducing cell-surface vs. intracellular GPCR signaling.

6. Summary

G protein-coupled receptors (GPCRs) are the major group of cell-surface receptors that transmit extracellular signals via classical, G protein-dependent pathways into the cell. Although GPCRs were long assumed to signal exclusively from the cell-surface, recent investigations have demonstrated a possibly completely new paradigm. In this new view, GPCR continues signaling via 3´,5´-cyclic adenosine monophosphate (cAMP) after their agonist-induced internalization of ligand/receptor complexes into an intracellular compartment, causing persistent cAMP elevation and apparently specific signaling outcomes. The thyroid stimulating hormone (TSH) receptor is one of the first GPCRs, which has been reported to show persistent signaling after ligand removal (Calebiro et al., 2009). In the meantime, signaling by internalized GPCR become a highly investigated topic and has been shown for several GPCRs, including the parathyroid hormone receptor (Ferrandon et al., 2009), D_1 dopamine receptor (Kotowski et al., 2011) and β_2-adrenergic receptor (Irannejad et al., 2013). A recent study on the β_2-adrenergic receptor revealed that internalized receptor not only participates in cAMP signaling, but is also involved in gene transcription (Tsvetanova and von Zastrow, 2014). However, a biological effect of GPCR signaling at intracellular sites, which would demonstrate its physiological relevance, still remained to be shown.

To investigate GPCR signaling from intracellular compartment under physiological condition, two different cellular models were utilized in the present study: intact ovarian follicles expressing luteinizing hormone (LH) receptors and primary thyroid cells expressing TSH receptors.

Intact ovarian follicles were obtained from a transgenic mouse expressing, a Förster/Fluorescence Resonance Energy Transfer (FRET) sensor for cAMP to monitor cAMP/LH receptor signaling. This study provides the first accurate spatiotemporal characterization of cAMP signaling, which is derived from different cell layers of an intact ovarian follicle. Additionally, it could be shown that cAMP diffusion via gap junctions is implicated in spreading the LH-induced cAMP signals from one the outermost (mural granulosa) to the innermost (cumulus oophorus) cell layer of an ovarian follicle. Interestingly, LH receptor stimulation was associated with persistent cAMP signaling after LH removal and negligible desensitization of the cAMP signal. Interfering with receptor internalization with a dynamin inhibitor dynasore did not only prevent persistent LH-induced cAMP signaling, but also impaired the resumption of meiosis in follicle-enclosed oocytes, a key biological effect of LH.

In order to investigate the downstream activation of protein kinase A (PKA) in primary thyroid cells, FRET sensors with different subcellular localization (plasma membrane, cytosol and nucleus) were transiently transfected into primary thyroid cells of wild-type mice via electroporation.

Interestingly, TSH stimulation causes at least two distinct phases of PKA activation in the global primary thyroid cell, which are temporally separated by approximately 2 min. In addition, PKA activation in different subcellular compartments are characterized by dissimilar kinetics and amplitudes. Pharmacological inhibition of TSH receptor internalization largely prevented the second (i.e. late) phase of PKA activation as well as the subsequent TSH-dependent phosphorylation of CREB and TSH-dependent induction of early genes. These results suggest that PKA activation and nuclear signaling require internalization of the TSH receptor.

Taken together, the data of the present study provide strong evidence that GPCR signaling at intracellular sites is distinct from the one occurring at the cell-surface and is highly physiologically relevant.

Zusammenfassung

G-Protein-gekoppelte Rezeptoren (GPCR) umfassen die größte Gruppe von Rezeptoren in der Zellmembran und übermitteln extrazelluläre Signale via G-Protein-abhängige Signalwege in das Zellinnere. Obwohl lange Zeit die Wissenschaft davon ausging, das GPCR ausschließlich an der Zelloberfläche Signale weiterleiten, zeigen Studien der letzten Jahre eine vollkommen neuartige Signalweiterleitung aus dem Zellinneren. In dieser neuen Sichtweise, vermitteln GPCR nach Agonist-induzierter Internalisierung des Liganden/Rezeptor-Komplexes in das Zellinnere weiterhin zyklische Adenosin-3´,5´-monophosphat (cAMP)-Signale, was zu einer dauerhaften cAMP-Erhöhung und einem spezifischen Ergebnis der Signaltransduktion führt. Einer der ersten GPCR, für den gezeigt wurde, dass Signale aus dem Zelleninneren übertragen werden können, war der Thyreoidea-stimulierendes Hormon (TSH) Rezeptor. In der Zwischenzeit wurde die Signalübertagung von bereits internalisierten Rezeptoren für weitere GPCR gezeigt, inklusive des β_2-adrenergen Rezeptors. Vor kurzem demonstrierte eine Studie des β_2-adrenerge Rezeptors, dass die intrazellulare GPCR-Signalübertragung nicht nur an der cAMP-Weiterleitung sondern auch an der Gentranskription beteiligt ist. Bis jetzt konnte jedoch noch kein Zusammenhang zwischen der GPCR-Signaltransduktion aus dem Zellinneren und einem biologischen Effekt mit physiologischer Relevanz hergestellt werden.

Um GPCR-Signaltransduktion im Zellinneren unter physiologischen Bedingungen zu untersuchen, wurden in der aktuellen Arbeit zwei unterschiedliche zelluläre Modelle verwendet: Intakte Follikel eines Ovars, welche luteinisierende Hormon (LH) Rezeptoren exprimieren und TSH-Rezeptoren-exprimierende primäre Schilddrüsenzellen.

Die Follikel wurden aus einer transgenen Maus, die einen Förster/Fluoreszenz Resonanz Energie Transfer (FRET) Sensor für cAMP exprimiert, gewonnen, um cAMP/LH-Signaltransduktion zu messen. Diese Arbeit zeigt die erste exakte, zeitliche und räumliche Charakterisierung der LH-induzierten cAMP-Signaltransduktion in intakten Follikeln des Ovars. Des Weiteren konnte gezeigt werden, dass die Diffusion von cAMP via Gap Junctions ein wichtiger Bestandteil bei der Übermittlung des LH-induzierten cAMP-Signals von der äußeren (Mural granulosa) zur inneren (Cumulus oophorus) Zellebene eines Follikels darstellt. Interessanterweise ergab die LH-Rezeptor Stimulation nach Entfernung des Liganden LH ein anhaltendes cAMP-Signal sowie eine unwesentliche Desensitization des cAMP-Signals. Die Inhibition der Rezeptorendozytose mit Dynasore verhinderte nicht nur das LH-induzierte anhaltende cAMP-Signal sondern beeinflusste auch die Wiederaufnahme der Meiose durch die Follikel-eingeschlossene Oozyte, einer der wichtigsten biologischen Aufgaben von LH.

Summary

Um den Einfluss der TSH-Rezeptorinternalisierung auf die PKA-Aktivität zu untersuchen, wurden primäre Schilddrüsenzellen von FVB-Mäusen, mit FRET-basierenden Protein Kinase A (PKA) Sensor exprimiert werden, via Elektroporation transfiziert. Die Ergebnisse zeigen, dass eine TSH-vermittelte Stimulation des Rezeptors mindestens zwei kinetisch und räumlich unterschiedliche PKA-Signale in Schilddrüsenzellen auslöst, die zeitlich voneinander getrennt sind. Durch die Inhibierung des TSH-Rezeptorinternalisierung konnte gezeigt werden, dass das zweite PKA-Signal sowie die darauffolgende TSH-abhängige Phosphorylierung des Trankriptionsfaktors CREB und die TSH-abhängige Regulierung von Gen Expression vermindert ist. Diese Befunde geben Aufschluss über die Notwendigkeit der Internalisierung des Rezeptors in das Zellinnere für eine effektive PKA- und Zellkern-Signaltransduktion.

Zusammenfassend lässt sich sagen, dass die Ergebnisse dieser Arbeit neue, und wichtige Erkenntnisse über den Mechanismus der GPCR-Signalweiterleitung im Zellinneren und erstmals einen Einblick über die biologische Relevanz der Rezeptorinternalisierung liefern.

7. Bibliography

Adams, S.R., Harootunian, A.T., Buechler, Y.J., Taylor, S.S., and Tsien, R.Y. (1991). Fluorescence ratio imaging of cyclic AMP in single cells. *Nature* 349**,** 694-697.

Ahn, S., Nelson, C.D., Garrison, T.R., Miller, W.E., and Lefkowitz, R.J. (2003). Desensitization, internalization, and signaling functions of beta-arrestins demonstrated by RNA interference. *Proc Natl Acad Sci U S A* 100**,** 1740-1744.

Albertini, D.F., Combelles, C.M., Benecchi, E., and Carabatsos, M.J. (2001). Cellular basis for paracrine regulation of ovarian follicle development. *Reproduction* 121**,** 647-653.

Allen, M.D., and Zhang, J. (2006). Subcellular dynamics of protein kinase A activity visualized by FRET-based reporters. *Biochemical and Biophysical Research Communications* 348**,** 716-721.

Allgeier, A., Laugwitz, K.L., Van Sande, J., Schultz, G., and Dumont, J.E. (1997). Multiple G-protein coupling of the dog thyrotropin receptor. *Mol Cell Endocrinol* 127**,** 81-90.

Allgeier, A., Offermanns, S., Van Sande, J., Spicher, K., Schultz, G., and Dumont, J.E. (1994). The human thyrotropin receptor activates G-proteins Gs and Gq/11. *J Biol Chem* 269**,** 13733-13735.

Amsterdam, A., Koch, Y., Lieberman, M.E., and Lindner, H.R. (1975). Distribution of binding sites for human chorionic gonadotropin in the preovulatory follicle of the rat. *J Cell Biol* 67**,** 894-900.

Ananthanarayanan, B., Ni, Q., and Zhang, J. (2005). Signal propagation from membrane messengers to nuclear effectors revealed by reporters of phosphoinositide dynamics and Akt activity. *Proc Natl Acad Sci U S A* 102**,** 15081-15086.

Anderson, E., and Albertini, D.F. (1976). Gap junctions between the oocyte and companion follicle cells in the mammalian ovary. *J Cell Biol* 71**,** 680-686.

Apter, D. (1997). Development of the hypothalamic-pituitary-ovarian axis. *Ann N Y Acad Sci* 816**,** 9-21.

Arshavsky, V.Y., Lamb, T.D., and Pugh, E.N., Jr. (2002). G proteins and phototransduction. *Annu Rev Physiol* 64**,** 153-187.

Ascoli, M. (1984). Lysosomal accumulation of the hormone-receptor complex during receptor-mediated endocytosis of human choriogonadotropin. *J Cell Biol* 99**,** 1242-1250.

Ascoli, M., Fanelli, F., and Segaloff, D.L. (2002). The lutropin/choriogonadotropin receptor, a 2002 perspective. *Endocr Rev* 23**,** 141-174.

Ascoli, M., and Puett, D. (1978). Inhibition of the degradation of receptor-bound human choriogonadotropin by lysosomotropic agents, protease inhibitors, and metabolic inhibitors. *J Biol Chem* 253**,** 7832-7838.

Avivi, A., Tramontano, D., Ambesiimpiombato, F.S., and Schlessinger, J. (1982). Direct Visualization of Membrane Clustering and Endocytosis of Thyrotropin into Cultured Thyroid-Cells. *Molecular and Cellular Endocrinology* 25**,** 55-71.

Baratti-Elbaz, C., Ghinea, N., Lahuna, O., Loosfelt, H., Pichon, C., and Milgrom, E. (1999). Internalization and recycling pathways of the thyrotropin receptor. *Molecular Endocrinology* 13**,** 1751-1765.

Beebe, S.J. (1994). The cAMP-dependent protein kinases and cAMP signal transduction. *Semin Cancer Biol* 5**,** 285-294.

Beebe, S.J., Holloway, R., Rannels, S.R., and Corbin, J.D. (1984). Two classes of cAMP analogs which are selective for the two different cAMP-binding sites of type II protein kinase demonstrate synergism when added together to intact adipocytes. *J Biol Chem* 259**,** 3539-3547.

Börner, S., Schwede, F., Schlipp, A., Berisha, F., Calebiro, D., Lohse, M.J., and Nikolaev, V.O. (2011). FRET measurements of intracellular cAMP concentrations and cAMP analog permeability in intact cells. *Nat. Protocols* 6**,** 427-438.

Bos, J.L. (2003). Epac: a new cAMP target and new avenues in cAMP research. *Nat Rev Mol Cell Biol* 4**,** 733-738.

Bibliography

Brabant, G., Prank, K., Ranft, U., Schuermeyer, T., Wagner, T.O., Hauser, H., Kummer, B., Feistner, H., Hesch, R.D., and Von Zur Muhlen, A. (1990). Physiological regulation of circadian and pulsatile thyrotropin secretion in normal man and woman. *J Clin Endocrinol Metab* 70**,** 403-409.

Breen, S.M., and Knox, R.V. (2012). The impact of dose of FSH (Folltropin) containing LH (Lutropin) on follicular development, estrus and ovulation responses in prepubertal gilts. *Anim Reprod Sci* 132**,** 193-200.

Brinkley, M. (1992). A brief survey of methods for preparing protein conjugates with dyes, haptens, and cross-linking reagents. *Bioconjug Chem* 3**,** 2-13.

Brown, R.A., Al-Moussa, M., and Beck, J. (1986). Histometry of normal thyroid in man. *J Clin Pathol* 39**,** 475-482.

Büch, T.R., Biebermann, H., Kalwa, H., Pinkenburg, O., Hager, D., Barth, H., Aktories, K., Breit, A., and Gudermann, T. (2008). G13-dependent activation of MAPK by thyrotropin. *J Biol Chem* 283**,** 20330-20341.

Bünemann, M., Frank, M., and Lohse, M.J. (2003). Gi protein activation in intact cells involves subunit rearrangement rather than dissociation. *Proc Natl Acad Sci U S A* 100**,** 16077-16082.

Calebiro, D., De Filippis, T., Lucchi, S., Martinez, F., Porazzi, P., Trivellato, R., Locati, M., Beck-Peccoz, P., and Persani, L. (2006). Selective modulation of protein kinase A I and II reveals distinct roles in thyroid cell gene expression and growth. *Mol Endocrinol* 20**,** 3196-3211.

Calebiro, D., Godbole, A., Lyga, S., and Lohse, M.J. (2015). Trafficking and function of GPCRs in the endosomal compartment. *Methods Mol Biol* 1234**,** 197-211.

Calebiro, D., Nikolaev, V.O., Gagliani, M.C., De Filippis, T., Dees, C., Tacchetti, C., Persani, L., and Lohse, M.J. (2009). Persistent cAMP-signals triggered by internalized G-protein-coupled receptors. *PLoS Biol* 7**,** e1000172.

Calebiro, D., Sungkaworn, T., and Maiellaro, I. (2014). Real-time monitoring of GPCR/cAMP signalling by FRET and single-molecule microscopy. *Horm Metab Res* 46**,** 827-832.

Castro, M., Dicker, F., Vilardaga, J.P., Krasel, C., Bernhardt, M., and Lohse, M.J. (2002). Dual regulation of the parathyroid hormone (PTH)/PTH-related peptide receptor signaling by protein kinase C and beta-arrestins. *Endocrinology* 143**,** 3854-3865.

Chen, L., Russell, P.T., and Larsen, W.J. (1994). Sequential effects of follicle-stimulating hormone and luteinizing hormone on mouse cumulus expansion in vitro. *Biology of Reproduction* 51**,** 290-295.

Conner, S.D., and Schmid, S.L. (2003). Regulated portals of entry into the cell. *Nature* 422**,** 37-44.

Conti, M. (2002). Specificity of the cyclic adenosine 3',5'-monophosphate signal in granulosa cell function. *Biol Reprod* 67**,** 1653-1661.

Conti, M., Hsieh, M., Zamah, A.M., and Oh, J.S. (2012). Novel signaling mechanisms in the ovary during oocyte maturation and ovulation. *Mol Cell Endocrinol* 356**,** 65-73.

Corbin, J.D., Keely, S.L., and Park, C.R. (1975). The distribution and dissociation of cyclic adenosine 3':5'-monophosphate-dependent protein kinases in adipose, cardiac, and other tissues. *J Biol Chem* 250**,** 218-225.

Corbin, J.D., Turko, I.V., Beasley, A., and Francis, S.H. (2000). Phosphorylation of phosphodiesterase-5 by cyclic nucleotide-dependent protein kinase alters its catalytic and allosteric cGMP-binding activities. *Eur J Biochem* 267**,** 2760-2767.

Csaba, Z., Lelouvier, B., Viollet, C., El Ghouzzi, V., Toyama, K., Videau, C., Bernard, V., and Dournaud, P. (2007). Activated somatostatin type 2 receptors traffic in vivo in central neurons from dendrites to the trans Golgi before recycling. *Traffic* 8**,** 820-834.

Daaka, Y., Luttrell, L.M., Ahn, S., Della Rocca, G.J., Ferguson, S.S., Caron, M.G., and Lefkowitz, R.J. (1998). Essential role for G protein-coupled receptor endocytosis in the activation of mitogen-activated protein kinase. *J Biol Chem* 273**,** 685-688.

Day, R.N., and Davidson, M.W. (2012). Fluorescent proteins for FRET microscopy: monitoring protein interactions in living cells. *Bioessays* 34, 341-350.

Depry, C., Allen, M.D., and Zhang, J. (2011). Visualization of PKA activity in plasma membrane microdomains. *Mol Biosyst* 7**,** 52-58.

Dias, J.A., Cohen, B.D., Lindau-Shepard, B., Nechamen, C.A., Peterson, A.J., and Schmidt, A. (2002). Molecular, structural, and cellular biology of follitropin and follitropin receptor. *Vitam Horm* 64**,** 249-322.

Diaz Anel, A.M. (2007). Phospholipase C beta3 is a key component in the Gbetagamma/PKCeta/PKD-mediated regulation of trans-Golgi network to plasma membrane transport. *Biochem J* 406**,** 157-165.

Dipilato, L.M., Cheng, X., and Zhang, J. (2004). Fluorescent indicators of cAMP and Epac activation reveal differential dynamics of cAMP signaling within discrete subcellular compartments. *Proc Natl Acad Sci U S A* 101**,** 16513-16518.

Doherty, G.J., and Mcmahon, H.T. (2009). Mechanisms of endocytosis. *Annu Rev Biochem* 78**,** 857-902.

Dostmann, W.R., Taylor, S.S., Genieser, H.G., Jastorff, B., Doskeland, S.O., and Ogreid, D. (1990). Probing the cyclic nucleotide binding sites of cAMP-dependent protein kinases I and II with analogs of adenosine 3',5'-cyclic phosphorothioates. *J Biol Chem* 265**,** 10484-10491.

Dremier, S., Coulonval, K., Perpete, S., Vandeput, F., Fortemaison, N., Van Keymeulen, A., Deleu, S., Ledent, C., Clement, S., Schurmans, S., Dumont, J.E., Lamy, F., Roger, P.P., and Maenhaut, C. (2002). The role of cyclic AMP and its effect on protein kinase A in the mitogenic action of thyrotropin on the thyroid cell. *Ann N Y Acad Sci* 968**,** 106-121.

Du Plessis, S.S., Cabler, S., Mcalister, D.A., Sabanegh, E., and Agarwal, A. (2010). The effect of obesity on sperm disorders and male infertility. *Nat Rev Urol* 7**,** 153-161.

Dumont, J.E., Lamy, F., Roger, P., and Maenhaut, C. (1992). Physiological and pathological regulation of thyroid cell proliferation and differentiation by thyrotropin and other factors. *Physiol Rev* 72**,** 667-697.

Dunn, J.T. (1996). Seven deadly sins in confronting endemic iodine deficiency, and how to avoid them. *J Clin Endocrinol Metab* 81**,** 1332-1335.

Dunn, T.A., Wang, C.T., Colicos, M.A., Zaccolo, M., Dipilato, L.M., Zhang, J., Tsien, R.Y., and Feller, M.B. (2006). Imaging of cAMP levels and protein kinase A activity reveals that retinal waves drive oscillations in second-messenger cascades. *J Neurosci* 26**,** 12807-12815.

Edwards, R.G. (1965). Maturation in vitro of mouse, sheep, cow, pig, rhesus monkey and human ovarian oocytes. *Nature* 208**,** 349-351.

Egbert, J.R., Shuhaibar, L.C., Edmund, A.B., Van Helden, D.A., Robinson, J.W., Uliasz, T.F., Baena, V., Geerts, A., Wunder, F., Potter, L.R., and Jaffe, L.A. (2014). Dephosphorylation and inactivation of NPR2 guanylyl cyclase in granulosa cells contributes to the LH-induced decrease in cGMP that causes resumption of meiosis in rat oocytes. *Development* 141**,** 3594-3604.

Eppig, J.J. (1979). Gonadotropin stimulation of the expansion of cumulus oophori isolated from mice: general conditions for expansion in vitro. *J Exp Zool* 208**,** 111-120.

Eppig, J.J., Chesnel, F., Hirao, Y., O'brien, M.J., Pendola, F.L., Watanabe, S., and Wigglesworth, K. (1997). Oocyte control of granulosa cell development: how and why. *Hum Reprod* 12**,** 127-132.

Fan, Q.R., and Hendrickson, W.A. (2005). Structure of human follicle-stimulating hormone in complex with its receptor. *Nature* 433**,** 269-277.

Feinstein, T.N., Yui, N., Webber, M.J., Wehbi, V.L., Stevenson, H.P., King, J.D., Jr., Hallows, K.R., Brown, D., Bouley, R., and Vilardaga, J.P. (2013). Noncanonical control of vasopressin receptor type 2 signaling by retromer and arrestin. *J Biol Chem* 288**,** 27849-27860.

Feliciello, A., Gallo, A., Mele, E., Porcellini, A., Troncone, G., Garbi, C., Gottesman, M.E., and Avvedimento, E.V. (2000). The localization and activity of cAMP-dependent protein kinase affect cell cycle progression in thyroid cells. *J Biol Chem* 275**,** 303-311.

Feliciello, A., Giuliano, P., Porcellini, A., Garbi, C., Obici, S., Mele, E., Angotti, E., Grieco, D., Amabile, G., Cassano, S., Li, Y., Musti, A.M., Rubin, C.S., Gottesman, M.E., and Avvedimento, E.V. (1996). The v-

Ki-Ras oncogene alters cAMP nuclear signaling by regulating the location and the expression of cAMP-dependent protein kinase IIbeta. *J Biol Chem* 271**,** 25350-25359.

Ferrandon, S., Feinstein, T.N., Castro, M., Wang, B., Bouley, R., Potts, J.T., Gardella, T.J., and Vilardaga, J.P. (2009). Sustained cyclic AMP production by parathyroid hormone receptor endocytosis. *Nat Chem Biol* 5**,** 734-742.

Förster, T. (1948). Zwischenmolekulare Energiewanderung und Fluoreszenz. *Annalen der Physik* 437**,** 55-75.

Franco, C.A., Jones, M.L., Bernabeu, M.O., Geudens, I., Mathivet, T., Rosa, A., Lopes, F.M., Lima, A.P., Ragab, A., Collins, R.T., Phng, L.K., Coveney, P.V., and Gerhardt, H. (2015). Dynamic endothelial cell rearrangements drive developmental vessel regression. *PLoS Biol* 13**,** e1002125.

Frenzel, R., Voigt, C., and Paschke, R. (2006). The human thyrotropin receptor is predominantly internalized by beta-arrestin 2. *Endocrinology* 147**,** 3114-3122.

Galet, C., Min, L., Narayanan, R., Kishi, M., Weigel, N.L., and Ascoli, M. (2003). Identification of a transferable two-amino-acid motif (GT) present in the C-terminal tail of the human lutropin receptor that redirects internalized G protein-coupled receptors from a degradation to a recycling pathway. *Mol Endocrinol* 17**,** 411-422.

Gerard, C.M., Roger, P.P., and Dumont, J.E. (1989). Thyroglobulin gene expression as a differentiation marker in primary cultures of calf thyroid cells. *Mol Cell Endocrinol* 61**,** 23-35.

Ghinea, N., Vu Hai, M.T., Groyer-Picard, M.T., Houllier, A., Schoëvaërt, D., and Milgrom, E. (1992). Pathways of internalization of the hCG/LH receptor: immunoelectron microscopic studies in Leydig cells and transfected L-cells. *The Journal of Cell Biology* 118**,** 1347-1358.

Ghosh, R.N., Gelman, D.L., and Maxfield, F.R. (1994). Quantification of low density lipoprotein and transferrin endocytic sorting HEp2 cells using confocal microscopy. *J Cell Sci* 107 (Pt 8)**,** 2177-2189.

Gidon, A., Al-Bataineh, M.M., Jean-Alphonse, F.G., Stevenson, H.P., Watanabe, T., Louet, C., Khatri, A., Calero, G., Pastor-Soler, N.M., Gardella, T.J., and Vilardaga, J.P. (2014). Endosomal GPCR signaling turned off by negative feedback actions of PKA and v-ATPase. *Nature Chemical Biology* 10**,** 707-709.

Gilman, A.G. (1987). G proteins: transducers of receptor-generated signals. *Annu Rev Biochem* 56**,** 615-649.

Goodman, O.B., Jr., Krupnick, J.G., Gurevich, V.V., Benovic, J.L., and Keen, J.H. (1997). Arrestin/clathrin interaction. Localization of the arrestin binding locus to the clathrin terminal domain. *J Biol Chem* 272**,** 15017-15022.

Haraguchi, K., Saito, T., Kaneshige, M., Endo, T., and Onaya, T. (1994). Desensitization and Internalization of a Thyrotropin Receptor Lacking the Cytoplasmic Carboxy-Terminal Region. *Journal of Molecular Endocrinology* 13**,** 283-288.

Harootunian, A.T., Adams, S.R., Wen, W., Meinkoth, J.L., Taylor, S.S., and Tsien, R.Y. (1993). Movement of the free catalytic subunit of cAMP-dependent protein kinase into and out of the nucleus can be explained by diffusion. *Mol Biol Cell* 4**,** 993-1002.

Herbst, K.J., Allen, M.D., and Zhang, J. (2011). Spatiotemporally regulated protein kinase A activity is a critical regulator of growth factor-stimulated extracellular signal-regulated kinase signaling in PC12 cells. *Mol Cell Biol* 31**,** 4063-4075.

Hillier, S.G., Whitelaw, P.F., and Smyth, C.D. (1994). Follicular oestrogen synthesis: the 'two-cell, two-gonadotrophin' model revisited. *Mol Cell Endocrinol* 100**,** 51-54.

Hsieh, M., Zamah, A.M., and Conti, M. (2009). Epidermal Growth Factor-Like Growth Factors in the Follicular Fluid: Role in Oocyte Development and Maturation. *Seminars in Reproductive Medicine* 27**,** 52-61.

Hsueh, A.J., Adashi, E.Y., Jones, P.B., and Welsh, T.H., Jr. (1984). Hormonal regulation of the differentiation of cultured ovarian granulosa cells. *Endocr Rev* 5**,** 76-127.

Hunter, T. (1995). Protein kinases and phosphatases: the yin and yang of protein phosphorylation and signaling. *Cell* 80**,** 225-236.

Irannejad, R., Tomshine, J.C., Tomshine, J.R., Chevalier, M., Mahoney, J.P., Steyaert, J., Rasmussen, S.G.F., Sunahara, R.K., El-Samad, H., Huang, B., and Von Zastrow, M. (2013). Conformational biosensors reveal GPCR signalling from endosomes. *Nature* 495**,** 534-+.

Jaffe, L.A., Norris, R.P., Freudzon, M., Ratzan, W.J., and Mehlmann, L.M. (2009). Microinjection of follicle-enclosed mouse oocytes. *Methods Mol Biol* 518**,** 157-173.

Janetopoulos, C., Jin, T., and Devreotes, P. (2001). Receptor-mediated activation of heterotrimeric G-proteins in living cells. *Science* 291**,** 2408-2411.

Jean-Alphonse, F., Bowersox, S., Chen, S., Beard, G., Puthenveedu, M.A., and Hanyaloglu, A.C. (2014). Spatially restricted G protein-coupled receptor activity via divergent endocytic compartments. *J Biol Chem* 289**,** 3960-3977.

Jiang, X., Dias, J.A., and He, X. (2014). Structural biology of glycoprotein hormones and their receptors: Insights to signaling. *Molecular and Cellular Endocrinology* 382**,** 424-451.

Kappos, L., Antel, J., Comi, G., Montalban, X., Radue, E.W., De Vera, A., Pohlmann, H., and O'connor, P. (2006). Oral fingolimod (FTY720) in relapsing multiple sclerosis: 24-month results of the Phase II study. *Multiple Sclerosis* 12**,** S101-S101.

Kawamura, K., Cheng, Y., Kawamura, N., Takae, S., Okada, A., Kawagoe, Y., Mulders, S., Terada, Y., and Hsueh, A.J. (2011). Pre-ovulatory LH/hCG surge decreases C-type natriuretic peptide secretion by ovarian granulosa cells to promote meiotic resumption of pre-ovulatory oocytes. *Hum Reprod* 26**,** 3094-3101.

Kero, J., Ahmed, K., Wettschureck, N., Tunaru, S., Wintermantel, T., Greiner, E., Schutz, G., and Offermanns, S. (2007). Thyrocyte-specific Gq/G11 deficiency impairs thyroid function and prevents goiter development. *J Clin Invest* 117**,** 2399-2407.

Kimura, T., Van Keymeulen, A., Golstein, J., Fusco, A., Dumont, J.E., and Roger, P.P. (2001). Regulation of thyroid cell proliferation by TSH and other factors: a critical evaluation of in vitro models. *Endocr Rev* 22**,** 631-656.

Kishi, M., Liu, X., Hirakawa, T., Reczek, D., Bretscher, A., and Ascoli, M. (2001). Identification of two distinct structural motifs that, when added to the C-terminal tail of the rat LH receptor, redirect the internalized hormone-receptor complex from a degradation to a recycling pathway. *Mol Endocrinol* 15**,** 1624-1635.

Klaushofer, K., Varga, F., Glantschnig, H., Fratzl-Zelman, N., Czerwenka, E., Leis, H.J., Koller, K., and Peterlik, M. (1995). The Regulatory Role of Thyroid Hormones in Bone Cell Growth and Differentiation. *The Journal of Nutrition* 125**,** 1996S-2003S.

Kleinau, G., Neumann, S., Gruters, A., Krude, H., and Biebermann, H. (2013). Novel insights on thyroid-stimulating hormone receptor signal transduction. *Endocr Rev* 34**,** 691-724.

Koenig, J.A., and Edwardson, J.M. (1997). Endocytosis and recycling of G protein-coupled receptors. *Trends Pharmacol Sci* 18**,** 276-287.

Köhrle, J. (2000). Thyroid Hormone Metabolism and Action in the Brain and Pituitary

Schilddrüsenhormonstoffwechsel und -wirkung in Gehirn und Hypophyse. *Acta Medica Austriaca* 27**,** 1-7.

Kotowski, S.J., Hopf, F.W., Seif, T., Bonci, A., and Von Zastrow, M. (2011). Endocytosis Promotes Rapid Dopaminergic Signaling. *Neuron* 71**,** 278-290.

Krueger, K.M., Daaka, Y., Pitcher, J.A., and Lefkowitz, R.J. (1997). The role of sequestration in G protein-coupled receptor resensitization. Regulation of beta2-adrenergic receptor dephosphorylation by vesicular acidification. *J Biol Chem* 272**,** 5-8.

Krupnick, J.G., and Benovic, J.L. (1998). The role of receptor kinases and arrestins in G protein-coupled receptor regulation. *Annu Rev Pharmacol Toxicol* 38**,** 289-319.

Kuna, R.S., Girada, S.B., Asalla, S., Vallentyne, J., Maddika, S., Patterson, J.T., Smiley, D.L., Dimarchi, R.D., and Mitra, P. (2013). Glucagon-like peptide-1 receptor-mediated endosomal cAMP generation promotes glucose-stimulated insulin secretion in pancreatic beta-cells. *Am J Physiol Endocrinol Metab* 305**,** E161-170.

Lagerström, M.C., and Schioth, H.B. (2008). Structural diversity of G protein-coupled receptors and significance for drug discovery. *Nat Rev Drug Discov* 7**,** 339-357.

Lahuna, O., Quellari, M., Achard, C., Nola, S., Meduri, G., Navarro, C., Vitale, N., Borg, J.P., and Misrahi, M. (2005). Thyrotropin receptor trafficking relies on the hScrib-betaPIX-GIT1-ARF6 pathway. *EMBO J* 24**,** 1364-1374.

Laporte, S.A., Oakley, R.H., Zhang, J., Holt, J.A., Ferguson, S.S.G., Caron, M.G., and Barak, L.S. (1999). The beta(2)-adrenergic receptor/beta arrestin complex recruits the clathrin adaptor AP-2 during endocytosis. *Proceedings of the National Academy of Sciences of the United States of America* 96**,** 3712-3717.

Laugwitz, K.L., Allgeier, A., Offermanns, S., Spicher, K., Van Sande, J., Dumont, J.E., and Schultz, G. (1996). The human thyrotropin receptor: a heptahelical receptor capable of stimulating members of all four G protein families. *Proc Natl Acad Sci U S A* 93**,** 116-120.

Lawrence, T.S., Dekel, N., and Beers, W.H. (1980). Binding of human chorionic gonadotropin by rat cumuli oophori and granulosa cells: a comparative study. *Endocrinology* 106**,** 1114-1118.

Ledent, C., Demeestere, I., Blum, D., Petermans, J., Hamalainen, T., Smits, G., and Vassart, G. (2005). Premature ovarian aging in mice deficient for Gpr3. *Proc Natl Acad Sci U S A* 102**,** 8922-8926.

Lee, C.-L., Linton, J., Soughayer, J.S., Sims, C.E., and Allbritton, N.L. (1999). Localized measurement of kinase activation in oocytes of Xenopus laevis. *Nat Biotech* 17**,** 759-762.

Lefkowitz, R.J. (1998). G protein-coupled receptors. III. New roles for receptor kinases and beta-arrestins in receptor signaling and desensitization. *J Biol Chem* 273**,** 18677-18680.

Levy, O., Dai, G., Riedel, C., Ginter, C.S., Paul, E.M., Lebowitz, A.N., and Carrasco, N. (1997). Characterization of the thyroid Na+/I- symporter with an anti-COOH terminus antibody. *Proc Natl Acad Sci U S A* 94**,** 5568-5573.

Li, Y., Ndubuka, C., and Rubin, C.S. (1996). A kinase anchor protein 75 targets regulatory (RII) subunits of cAMP-dependent protein kinase II to the cortical actin cytoskeleton in non-neuronal cells. *J Biol Chem* 271**,** 16862-16869.

Lissandron, V., Rossetto, M.G., Erbguth, K., Fiala, A., Daga, A., and Zaccolo, M. (2007). Transgenic fruit-flies expressing a FRET-based sensor for in vivo imaging of cAMP dynamics. *Cell Signal* 19**,** 2296-2303.

Lohse, M.J. (1993). Molecular mechanisms of membrane receptor desensitization. *Biochim Biophys Acta* 1179**,** 171-188.

Lohse, M.J., and Calebiro, D. (2013). Cell biology: Receptor signals come in waves. *Nature* 495**,** 457-458.

Lohse, M.J., Nikolaev, V.O., Hein, P., Hoffmann, C., Vilardaga, J.P., and Bunemann, M. (2008). Optical techniques to analyze real-time activation and signaling of G-protein-coupled receptors. *Trends Pharmacol Sci* 29**,** 159-165.

Lowther, K.M., Nikolaev, V.O., and Mehlmann, L. (2011). Endocytosis in the mouse oocyte and its contribution to cAMP signalling during meiotic arrest. *Reproduction*.

Ludwig, M., Felberbaum, R.E., Diedrich, K., and Lunenfeld, B. (2002). Ovarian stimulation: from basic science to clinical application. *Reprod Biomed Online* 5 Suppl 1**,** 73-86.

Lunenfeld, B. (2002). Development of gonadotrophins for clinical use. *Reprod Biomed Online* 4 Suppl 1**,** 11-17.

Lunenfeld, B. (2004). Historical perspectives in gonadotrophin therapy. *Hum Reprod Update* 10**,** 453-467.

Lyga, S., Volpe, S., Werthmann, R.C., Gotz, K., Sungkaworn, T., Lohse, M.J., and Calebiro, D. (2016). Persistent cAMP signaling by internalized LH receptors in ovarian follicles. *Endocrinology***,** en20151945.

Macia, E., Ehrlich, M., Massol, R., Boucrot, E., Brunner, C., and Kirchhausen, T. (2006). Dynasore, a cell-permeable inhibitor of dynamin. *Developmental Cell* 10**,** 839-850.

Magner, J.A. (1990). Thyroid-stimulating hormone: biosynthesis, cell biology, and bioactivity. *Endocr Rev* 11**,** 354-385.

Manni, S., Mauban, J.H., Ward, C.W., and Bond, M. (2008). Phosphorylation of the cAMP-dependent protein kinase (PKA) regulatory subunit modulates PKA-AKAP interaction, substrate phosphorylation, and calcium signaling in cardiac cells. *J Biol Chem* 283**,** 24145-24154.

Marsh, J.M. (1976). The role of cyclic AMP in gonadal steroidogenesis. *Biol Reprod* 14**,** 30-53.

Martin, B.R., Deerinck, T.J., Ellisman, M.H., Taylor, S.S., and Tsien, R.Y. (2007). Isoform-specific PKA dynamics revealed by dye-triggered aggregation and DAKAP1alpha-mediated localization in living cells. *Chem Biol* 14**,** 1031-1042.

Mauras, N. (1996). Effects of estrogen therapy on whole body proteins. *J Clin Endocrinol Metab* 81**,** 431.

Mcknight, G.S., Cadd, G.G., Clegg, C.H., Otten, A.D., and Correll, L.A. (1988). Expression of wild-type and mutant subunits of the cAMP-dependent protein kinase. *Cold Spring Harb Symp Quant Biol* 53 Pt 1**,** 111-119.

Medina, D.L., and Santisteban, P. (2000). Thyrotropin-dependent proliferation of in vitro rat thyroid cell systems. *Eur J Endocrinol* 143**,** 161-178.

Mehlmann, L.M., Jones, T.L., and Jaffe, L.A. (2002). Meiotic arrest in the mouse follicle maintained by a Gs protein in the oocyte. *Science* 297**,** 1343-1345.

Mehlmann, L.M., Saeki, Y., Tanaka, S., Brennan, T.J., Evsikov, A.V., Pendola, F.L., Knowles, B.B., Eppig, J.J., and Jaffe, L.A. (2004). The Gs-linked receptor GPR3 maintains meiotic arrest in mammalian oocytes. *Science* 306**,** 1947-1950.

Meoli, E., Bossis, I., Cazabat, L., Mavrakis, M., Horvath, A., Stergiopoulos, S., Shiferaw, M.L., Fumey, G., Perlemoine, K., Muchow, M., Robinson-White, A., Weinberg, F., Nesterova, M., Patronas, Y., Groussin, L., Bertherat, J., and Stratakis, C.A. (2008). Protein kinase A effects of an expressed PRKAR1A mutation associated with aggressive tumors. *Cancer Res* 68**,** 3133-3141.

Merriam, L.A., Baran, C.N., Girard, B.M., Hardwick, J.C., May, V., and Parsons, R.L. (2013). Pituitary adenylate cyclase 1 receptor internalization and endosomal signaling mediate the pituitary adenylate cyclase activating polypeptide-induced increase in guinea pig cardiac neuron excitability. *J Neurosci* 33**,** 4614-4622.

Mock, E.J., and Niswender, G.D. (1983). Differences in the rates of internalization of 125I-labeled human chorionic gonadotropin, luteinizing hormone, and epidermal growth factor by ovine luteal cells. *Endocrinology* 113**,** 259-264.

Mock, E.J., Papkoff, H., and Niswender, G.D. (1983). Internalization of ovine luteinizing hormone/human chorionic gonadotropin recombinants: differential effects of the alpha- and beta-subunits. *Endocrinology* 113**,** 265-269.

Müller, T., Gromoll, J., and Simoni, M. (2003). Absence of exon 10 of the human luteinizing hormone (LH) receptor impairs LH, but not human chorionic gonadotropin action. *J Clin Endocrinol Metab* 88**,** 2242-2249.

Müllershausen, F., Zecri, F., Cetin, C., Billich, A., Guerini, D., and Seuwen, K. (2009). Persistent signaling induced by FTY720-phosphate is mediated by internalized S1P1 receptors. *Nat Chem Biol* 5**,** 428-434.

Munro, S., and Nichols, B.J. (1999). The GRIP domain - a novel Golgi-targeting domain found in several coiled-coil proteins. *Curr Biol* 9**,** 377-380.

Muslin, A.J., Tanner, J.W., Allen, P.M., and Shaw, A.S. (1996). Interaction of 14-3-3 with signaling proteins is mediated by the recognition of phosphoserine. *Cell* 84**,** 889-897.

Neumann, S., Geras-Raaka, E., Marcus-Samuels, B., and Gershengorn, M.C. (2010). Persistent cAMP signaling by thyrotropin (TSH) receptors is not dependent on internalization. *FASEB J* 24**,** 3992-3999.

Nikolaev, V.O., Bünemann, M., Hein, L., Hannawacker, A., and Lohse, M.J. (2004). Novel Single Chain cAMP Sensors for Receptor-induced Signal Propagation. *Journal of Biological Chemistry* 279**,** 37215-37218.

Nikolaev, V.O., and Lohse, M.J. (2006). Monitoring of cAMP synthesis and degradation in living cells. *Physiology (Bethesda)* 21**,** 86-92.

Niswender, G.D., Roess, D.A., Sawyer, H.R., Silvia, W.J., and Barisas, B.G. (1985). Differences in the lateral mobility of receptors for luteinizing hormone (LH) in the luteal cell plasma membrane when occupied by ovine LH versus human chorionic gonadotropin. *Endocrinology* 116**,** 164-169.

Norris, R.P., Freudzon, M., Mehlmann, L.M., Cowan, A.E., Simon, A.M., Paul, D.L., Lampe, P.D., and Jaffe, L.A. (2008). Luteinizing hormone causes MAP kinase-dependent phosphorylation and closure of connexin 43 gap junctions in mouse ovarian follicles: one of two paths to meiotic resumption. *Development* 135**,** 3229-3238.

Norris, R.P., Freudzon, M., Nikolaev, V.O., and Jaffe, L.A. (2010). Epidermal growth factor receptor kinase activity is required for gap junction closure and for part of the decrease in ovarian follicle cGMP in response to LH. *Reproduction* 140**,** 655-662.

Norris, R.P., Ratzan, W.J., Freudzon, M., Mehlmann, L.M., Krall, J., Movsesian, M.A., Wang, H., Ke, H., Nikolaev, V.O., and Jaffe, L.A. (2009). Cyclic GMP from the surrounding somatic cells regulates cyclic AMP and meiosis in the mouse oocyte. *Development* 136**,** 1869-1878.

Ock, S., Ahn, J., Lee, S.H., Kang, H., Offermanns, S., Ahn, H.Y., Jo, Y.S., Shong, M., Cho, B.Y., Jo, D., Abel, E.D., Lee, T.J., Park, W.J., Lee, I.K., and Kim, J. (2013). IGF-1 receptor deficiency in thyrocytes impairs thyroid hormone secretion and completely inhibits TSH-stimulated goiter. *FASEB J* 27**,** 4899-4908.

Ozment, T.R., Goldman, M.P., Kalbfleisch, J.H., and Williams, D.L. (2012). Soluble Glucan Is Internalized and Trafficked to the Golgi Apparatus in Macrophages via a Clathrin-Mediated, Lipid Raft-Regulated Mechanism. *Journal of Pharmacology and Experimental Therapeutics* 342**,** 808-815.

Palczewski, K., Kumasaka, T., Hori, T., Behnke, C.A., Motoshima, H., Fox, B.A., Le Trong, I., Teller, D.C., Okada, T., Stenkamp, R.E., Yamamoto, M., and Miyano, M. (2000). Crystal structure of rhodopsin: A G protein-coupled receptor. *Science* 289**,** 739-745.

Pannekoek, W.J., Kooistra, M.R., Zwartkruis, F.J., and Bos, J.L. (2009). Cell-cell junction formation: the role of Rap1 and Rap1 guanine nucleotide exchange factors. *Biochim Biophys Acta* 1788**,** 790-796.

Park, J.-Y., Su, Y.-Q., Ariga, M., Law, E., Jin, S.L.C., and Conti, M. (2004). EGF-Like Growth Factors As Mediators of LH Action in the Ovulatory Follicle. *Science* 303**,** 682-684.

Patel, T.B. (2004). Single Transmembrane Spanning Heterotrimeric G Protein-Coupled Receptors and Their Signaling Cascades. *Pharmacological Reviews* 56**,** 371-385.

Peng, X.R., Hsueh, A.J.W., Lapolt, P.S., Bjersing, L., and Ny, T. (1991). Localization of Luteinizing-Hormone Receptor Messenger-Ribonucleic-Acid Expression in Ovarian Cell-Types during Follicle Development and Ovulation. *Endocrinology* 129**,** 3200-3207.

Philips, M.R. (2005). Compartmentalized signalling of Ras. *Biochem Soc Trans* 33**,** 657-661.

Pierce, K.L., Premont, R.T., and Lefkowitz, R.J. (2002). Seven-transmembrane receptors. *Nat Rev Mol Cell Biol* 3**,** 639-650.

Pincus, G., and Enzmann, E.V. (1935). The Comparative Behavior of Mammalian Eggs in Vivo and in Vitro : I. The Activation of Ovarian Eggs. *J Exp Med* 62**,** 665-675.

Pinschewer, D.D., Ochsenbein, A.F., Odermatt, B., Brinkmann, V., Hengartner, H., and Zinkernagel, R.M. (2000). FTY720 immunosuppression impairs effector T cell peripheral homing without affecting induction, expansion, and memory. *J Immunol* 164**,** 5761-5770.

Piston, D.W., and Kremers, G.J. (2007). Fluorescent protein FRET: the good, the bad and the ugly. *Trends Biochem Sci* 32**,** 407-414.

Ponsioen, B., Zhao, J., Riedl, J., Zwartkruis, F., Van Der Krogt, G., Zaccolo, M., Moolenaar, W.H., Bos, J.L., and Jalink, K. (2004). Detecting cAMP-induced Epac activation by fluorescence resonance energy transfer: Epac as a novel cAMP indicator. *EMBO Rep* 5**,** 1176-1180.

Porcellini, A., Messina, S., De Gregorio, G., Feliciello, A., Carlucci, A., Barone, M., Picascia, A., De Blasi, A., and Avvedimento, E.V. (2003). The expression of the thyroid-stimulating hormone (TSH) receptor and the cAMP-dependent protein kinase RII beta regulatory subunit confers TSH-cAMP-dependent growth to mouse fibroblasts. *J Biol Chem* 278**,** 40621-40630.

Pyne, S., and Pyne, N. (2000). Sphingosine 1-phosphate signalling via the endothelial differentiation gene family of G-protein-coupled receptors. *Pharmacol Ther* 88**,** 115-131.

Rajagopalan-Gupta, R.M., Lamm, M.L., Mukherjee, S., Rasenick, M.M., and Hunzicker-Dunn, M. (1998). Luteinizing hormone/choriogonadotropin receptor-mediated activation of heterotrimeric guanine nucleotide binding proteins in ovarian follicular membranes. *Endocrinology* 139**,** 4547-4555.

Richards, J.S. (1994). Hormonal control of gene expression in the ovary. *Endocr Rev* 15**,** 725-751.

Richards, J.S. (2001). Perspective: the ovarian follicle--a perspective in 2001. *Endocrinology* 142**,** 2184-2193.

Richards, J.S., Russell, D.L., Ochsner, S., Hsieh, M., Doyle, K.H., Falender, A.E., Lo, Y.K., and Sharma, S.C. (2002). Novel signaling pathways that control ovarian follicular development, ovulation, and luteinization. *Recent Prog Horm Res* 57**,** 195-220.

Riedel, C., Levy, O., and Carrasco, N. (2001). Post-transcriptional regulation of the sodium/iodide symporter by thyrotropin. *J Biol Chem* 276**,** 21458-21463.

Rios, R.M., Celati, C., Lohmann, S.M., Bornens, M., and Keryer, G. (1992). Identification of a high affinity binding protein for the regulatory subunit RII beta of cAMP-dependent protein kinase in Golgi enriched membranes of human lymphoblasts. *EMBO J* 11**,** 1723-1731.

Rivas, M., and Santisteban, P. (2003). TSH-activated signaling pathways in thyroid tumorigenesis. *Molecular and Cellular Endocrinology* 213**,** 31-45.

Robinson-Steiner, A.M., and Corbin, J.D. (1983). Probable involvement of both intrachain cAMP binding sites in activation of protein kinase. *J Biol Chem* 258**,** 1032-1040.

Robinson, J.W., Zhang, M., Shuhaibar, L.C., Norris, R.P., Geerts, A., Wunder, F., Eppig, J.J., Potter, L.R., and Jaffe, L.A. (2012). Luteinizing hormone reduces the activity of the NPR2 guanylyl cyclase in mouse ovarian follicles, contributing to the cyclic GMP decrease that promotes resumption of meiosis in oocytes. *Dev Biol* 366**,** 308-316.

Roess, D.A., Brady, C.J., and Barisas, B.G. (2000). Biological function of the LH receptor is associated with slow receptor rotational diffusion. *Biochim Biophys Acta* 1464**,** 242-250.

Rousset, B., and Mornex, R. (1991). The thyroid hormone secretory pathway--current dogmas and alternative hypotheses. *Mol Cell Endocrinol* 78**,** C89-93.

Rubin, C.S. (1994). A kinase anchor proteins and the intracellular targeting of signals carried by cyclic AMP. *Biochim Biophys Acta* 1224**,** 467-479.

Russell, D.L., and Robker, R.L. (2007). Molecular mechanisms of ovulation: co-ordination through the cumulus complex. *Hum Reprod Update* 13**,** 289-312.

Saiki, R.K., Gelfand, D.H., Stoffel, S., Scharf, S.J., Higuchi, R., Horn, G.T., Mullis, K.B., and Erlich, H.A. (1988). Primer-directed enzymatic amplification of DNA with a thermostable DNA polymerase. *Science* 239**,** 487-491.

Salvador, L.M., Maizels, E., Hales, D.B., Miyamoto, E., Yamamoto, H., and Hunzicker-Dunn, M. (2002). Acute signaling by the LH receptor is independent of protein kinase C activation. *Endocrinology* 143**,** 2986-2994.

Sample, V., Dipilato, L.M., Yang, J.H., Ni, Q., Saucerman, J.J., and Zhang, J. (2012). Regulation of nuclear PKA revealed by spatiotemporal manipulation of cyclic AMP. *Nat Chem Biol* 8**,** 375-382.

Santisteban, P., Kohn, L.D., and Di Lauro, R. (1987). Thyroglobulin gene expression is regulated by insulin and insulin-like growth factor I, as well as thyrotropin, in FRTL-5 thyroid cells. *J Biol Chem* 262**,** 4048-4052.

Schwede, F., Christensen, A., Liauw, S., Hippe, T., Kopperud, R., Jastorff, B., and Doskeland, S.O. (2000a). 8-Substituted cAMP analogues reveal marked differences in adaptability, hydrogen bonding, and charge accommodation between homologous binding sites (AI/AII and BI/BII) in cAMP kinase I and II. *Biochemistry* 39**,** 8803-8812.

Schwede, F., Maronde, E., Genieser, H., and Jastorff, B. (2000b). Cyclic nucleotide analogs as biochemical tools and prospective drugs. *Pharmacol Ther* 87**,** 199-226.

Seger, R., Hanoch, T., Rosenberg, R., Dantes, A., Merz, W.E., Strauss, J.F., 3rd, and Amsterdam, A. (2001). The ERK signaling cascade inhibits gonadotropin-stimulated steroidogenesis. *J Biol Chem* 276**,** 13957-13964.

Sela-Abramovich, S., Chorev, E., Galiani, D., and Dekel, N. (2005). Mitogen-activated protein kinase mediates luteinizing hormone-induced breakdown of communication and oocyte maturation in rat ovarian follicles. *Endocrinology* 146**,** 1236-1244.

Sela-Abramovich, S., Edry, I., Galiani, D., Nevo, N., and Dekel, N. (2006). Disruption of gap junctional communication within the ovarian follicle induces oocyte maturation. *Endocrinology* 147**,** 2280-2286.

Shi, Y.F., Zou, M.J., Ahring, P., Alsedairy, S.T., and Farid, N.R. (1995). Thyrotropin Internalization Is Directed by a Highly Conserved Motif in the 7th Transmembrane Region of Its Receptor. *Endocrine* 3**,** 409-414.

Shimada, M., Nishibori, M., Isobe, N., Kawano, N., and Terada, T. (2003). Luteinizing hormone receptor formation in cumulus cells surrounding porcine oocytes and its role during meiotic maturation of porcine oocytes. *Biology of Reproduction* 68**,** 1142-1149.

Shuhaibar, L.C., Egbert, J.R., Norris, R.P., Lampe, P.D., Nikolaev, V.O., Thunemann, M., Wen, L., Feil, R., and Jaffe, L.A. (2015). Intercellular signaling via cyclic GMP diffusion through gap junctions restarts meiosis in mouse ovarian follicles. *Proc Natl Acad Sci U S A* 112**,** 5527-5532.

Simoni, M., Gromoll, J., and Nieschlag, E. (1997). The follicle-stimulating hormone receptor: biochemistry, molecular biology, physiology, and pathophysiology. *Endocr Rev* 18**,** 739-773.

Skalhegg, B.S., Landmark, B., Foss, K.B., Lohmann, S.M., Hansson, V., Lea, T., and Jahnsen, T. (1992). Identification, purification, and characterization of subunits of cAMP-dependent protein kinase in human testis. Reverse mobilities of human RII alpha and RII beta on sodium dodecyl sulfate-polyacrylamide gel electrophoresis compared with rat and bovine RIIs. *J Biol Chem* 267**,** 5374-5379.

Skalhegg, B.S., and Tasken, K. (2000). Specificity in the cAMP/PKA signaling pathway. Differential expression,regulation, and subcellular localization of subunits of PKA. *Front Biosci* 5**,** D678-693.

Smith, P.K., Krohn, R.I., Hermanson, G.T., Mallia, A.K., Gartner, F.H., Provenzano, M.D., Fujimoto, E.K., Goeke, N.M., Olson, B.J., and Klenk, D.C. (1985). Measurement of protein using bicinchoninic acid. *Anal Biochem* 150**,** 76-85.

Solc, P., Schultz, R.M., and Motlik, J. (2010). Prophase I arrest and progression to metaphase I in mouse oocytes: comparison of resumption of meiosis and recovery from G2-arrest in somatic cells. *Mol Hum Reprod* 16**,** 654-664.

Sorkin, A., and Von Zastrow, M. (2009). Endocytosis and signalling: intertwining molecular networks. *Nat Rev Mol Cell Biol* 10**,** 609-622.

Stryer, L. (1978). Fluorescence energy transfer as a spectroscopic ruler. *Annu Rev Biochem* 47**,** 819-846.

Su, Y.Q., Sugiura, K., and Eppig, J.J. (2009). Mouse oocyte control of granulosa cell development and function: paracrine regulation of cumulus cell metabolism. *Semin Reprod Med* 27**,** 32-42.

Szkudlinski, M.W., Fremont, V., Ronin, C., and Weintraub, B.D. (2002). Thyroid-stimulating hormone and thyroid-stimulating hormone receptor structure-function relationships. *Physiol Rev* 82**,** 473-502.

Bibliography

Takahashi, S., Conti, M., and Van Wyk, J.J. (1990). Thyrotropin potentiation of insulin-like growth factor-I dependent deoxribonucleic acid synthesis in FRTL-5 cells: mediation by an autocrine amplification factor(s). *Endocrinology* 126**,** 736-745.

Törnell, J., Billig, H., and Hillensjo, T. (1991). Regulation of oocyte maturation by changes in ovarian levels of cyclic nucleotides. *Hum Reprod* 6**,** 411-422.

Tortora, G., Pepe, S., Cirafici, A.M., Ciardiello, F., Porcellini, A., Clair, T., Colletta, G., Yoon, S.C.C., and Bianco, A.R. (1993). Thyroid-Stimulating Hormone-Regulated Growth and Cell-Cycle Distribution of Thyroid-Cells Involve Type-I Isozyme of Cyclic Amp-Dependent Protein-Kinase. *Cell Growth & Differentiation* 4**,** 359-365.

Tramontano, D., Cushing, G.W., Moses, A.C., and Ingbar, S.H. (1986). Insulin-like growth factor-I stimulates the growth of rat thyroid cells in culture and synergizes the stimulation of DNA synthesis induced by TSH and Graves'-IgG. *Endocrinology* 119**,** 940-942.

Traub, L.M. (2003). Sorting it out: AP-2 and alternate clathrin adaptors in endocytic cargo selection. *J Cell Biol* 163**,** 203-208.

Tsafriri, A., Chun, S.Y., Zhang, R., Hsueh, A.J., and Conti, M. (1996). Oocyte maturation involves compartmentalization and opposing changes of cAMP levels in follicular somatic and germ cells: studies using selective phosphodiesterase inhibitors. *Dev Biol* 178**,** 393-402.

Tsafriri, A., and Reich, R. (1999). Molecular aspects of mammalian ovulation. *Exp Clin Endocrinol Diabetes* 107**,** 1-11.

Tsao, P., Cao, T., and Von Zastrow, M. (2001). Role of endocytosis in mediating downregulation of G-protein-coupled receptors. *Trends Pharmacol Sci* 22**,** 91-96.

Tsvetanova, N.G., Irannejad, R., and Von Zastrow, M. (2015). G protein-coupled receptor (GPCR) signaling via heterotrimeric G proteins from endosomes. *J Biol Chem* 290**,** 6689-6696.

Tsvetanova, N.G., and Von Zastrow, M. (2014). Spatial encoding of cyclic AMP signaling specificity by GPCR endocytosis. *Nat Chem Biol* 10**,** 1061-1065.

Vaccari, S., Weeks, J.L., Hsieh, M., Menniti, F.S., and Conti, M. (2009). Cyclic GMP Signaling Is Involved in the Luteinizing Hormone-Dependent Meiotic Maturation of Mouse Oocytes. *Biology of Reproduction* 81**,** 595-604.

Van Staveren, W.C., Beeckman, S., Tomas, G., Dom, G., Hebrant, A., Delys, L., Vliem, M.J., Tresallet, C., Andry, G., Franc, B., Libert, F., Dumont, J.E., and Maenhaut, C. (2012). Role of Epac and protein kinase A in thyrotropin-induced gene expression in primary thyrocytes. *Exp Cell Res* 318**,** 444-452.

Vansande, J., Lefort, A., Beebe, S., Roger, P., Perret, J., Corbin, J., and Dumont, J.E. (1989). Pairs of Cyclic-Amp Analogs, That Are Specifically Synergistic for Type-I and Type-Ii Camp-Dependent Protein-Kinases, Mimic Thyrotropin Effects on the Function, Differentiation Expression and Mitogenesis of Dog Thyroid-Cells. *European Journal of Biochemistry* 183**,** 699-708.

Vassart, G., and Dumont, J.E. (1992). The thyrotropin receptor and the regulation of thyrocyte function and growth. *Endocr Rev* 13**,** 596-611.

Vassart, G., Pardo, L., and Costagliola, S. (2004). A molecular dissection of the glycoprotein hormone receptors. *Trends Biochem Sci* 29**,** 119-126.

Veldhuis, J.D. (1996). Gender differences in secretory activity of the human somatotropic (growth hormone) axis. *Eur J Endocrinol* 134**,** 287-295.

Verveer, P.J., Squire, A., and Bastiaens, P.I. (2000). Global analysis of fluorescence lifetime imaging microscopy data. *Biophys J* 78**,** 2127-2137.

Vieira, A.V., Lamaze, C., and Schmid, S.L. (1996). Control of EGF receptor signaling by clathrin-mediated endocytosis. *Science* 274**,** 2086-2089.

Vilardaga, J.P., Bunemann, M., Krasel, C., Castro, M., and Lohse, M.J. (2003). Measurement of the millisecond activation switch of G protein-coupled receptors in living cells. *Nat Biotechnol* 21**,** 807-812.
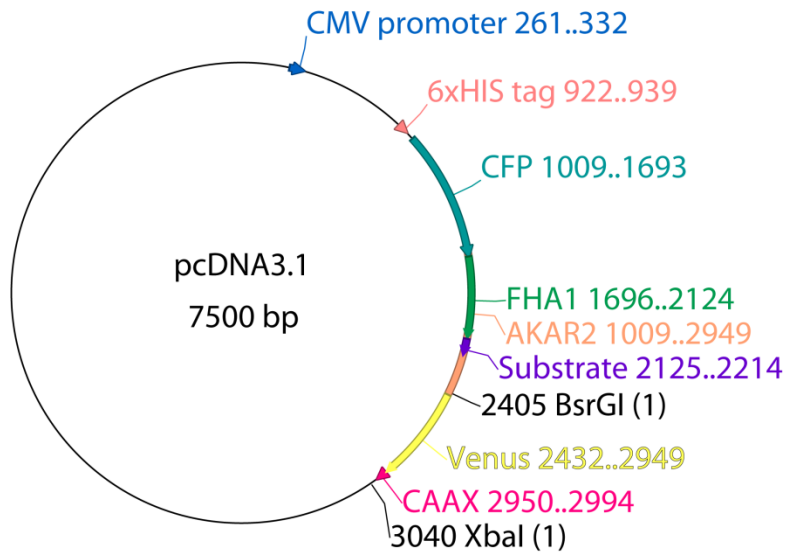
Vilardaga, J.P., Jean-Alphonse, F.G., and Gardella, T.J. (2014). Endosomal generation of cAMP in GPCR signaling. *Nat Chem Biol* 10**,** 700-706.

Vivarelli, E., Conti, M., De Felici, M., and Siracusa, G. (1983). Meiotic resumption and intracellular cAMP levels in mouse oocytes treated with compounds which act on cAMP metabolism. *Cell Differ* 12**,** 271-276.

Weetman, A.P. (2000). Graves' disease. *N Engl J Med* 343**,** 1236-1248.

Werthmann, R.C., Volpe, S., Lohse, M.J., and Calebiro, D. (2012). Persistent cAMP signaling by internalized TSH receptors occurs in thyroid but not in HEK293 cells. *FASEB J* 26**,** 2043-2048.

Yoon, C.M., Hong, B.S., Moon, H.G., Lim, S., Suh, P.G., Kim, Y.K., Chae, C.B., and Gho, Y.S. (2008). Sphingosine-1-phosphate promotes lymphangiogenesis by stimulating S1P1/Gi/PLC/Ca2+ signaling pathways. *Blood* 112**,** 1129-1138.

Yu, S.S., Lefkowitz, R.J., and Hausdorff, W.P. (1993). Beta-adrenergic receptor sequestration. A potential mechanism of receptor resensitization. *J Biol Chem* 268**,** 337-341.

Zaballos, M.A., Garcia, B., and Santisteban, P. (2008). Gbetagamma dimers released in response to thyrotropin activate phosphoinositide 3-kinase and regulate gene expression in thyroid cells. *Mol Endocrinol* 22**,** 1183-1199.

Zaccolo, M., De Giorgi, F., Cho, C.Y., Feng, L., Knapp, T., Negulescu, P.A., Taylor, S.S., Tsien, R.Y., and Pozzan, T. (2000). A genetically encoded, fluorescent indicator for cyclic AMP in living cells. *Nat Cell Biol* 2**,** 25-29.

Zagotta, W.N., Olivier, N.B., Black, K.D., Young, E.C., Olson, R., and Gouaux, E. (2003). Structural basis for modulation and agonist specificity of HCN pacemaker channels. *Nature* 425**,** 200-205.

Zarrilli, R., Formisano, S., and Di Jeso, B. (1990). Hormonal regulation of thyroid peroxidase in normal and transformed rat thyroid cells. *Mol Endocrinol* 4**,** 39-45.

Zhang, J., Campbell, R.E., Ting, A.Y., and Tsien, R.Y. (2002). Creating new fluorescent probes for cell biology. *Nat Rev Mol Cell Biol* 3**,** 906-918.

Zhang, J., Hupfeld, C.J., Taylor, S.S., Olefsky, J.M., and Tsien, R.Y. (2005). Insulin disrupts beta-adrenergic signalling to protein kinase A in adipocytes. *Nature* 437**,** 569-573.

Zhang, J., Ma, Y.L., Taylor, S.S., and Tsien, R.Y. (2001). Genetically encoded reporters of protein kinase A activity reveal impact of substrate tethering. *Proceedings of the National Academy of Sciences of the United States of America* 98**,** 14997-15002.

Zhang, M., Su, Y.Q., Sugiura, K., Xia, G., and Eppig, J.J. (2010). Granulosa cell ligand NPPC and its receptor NPR2 maintain meiotic arrest in mouse oocytes. *Science* 330**,** 366-369.

Zhou, X., Herbst-Robinson, K.J., and Zhang, J. (2012). "Chapter sixteen - Visualizing Dynamic Activities of Signaling Enzymes Using Genetically Encodable Fret-Based Biosensors: From Designs to Applications," in *Methods in Enzymology,* ed. P.M. Conn. Academic Press), 317-340.
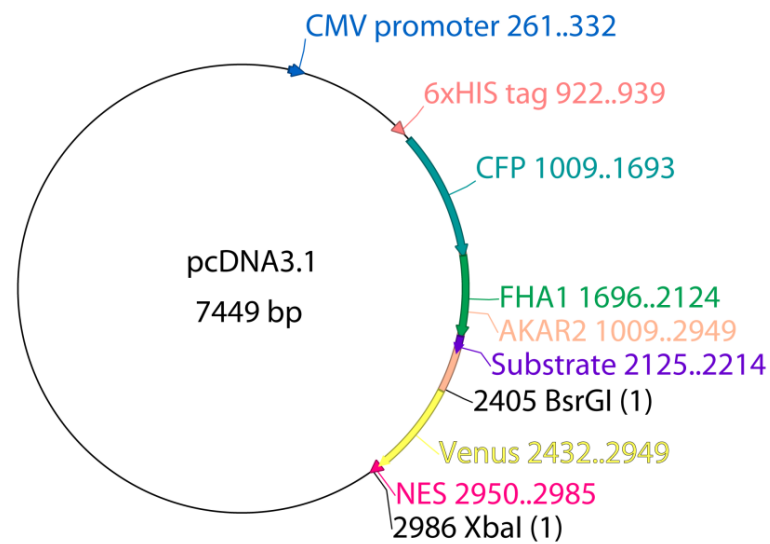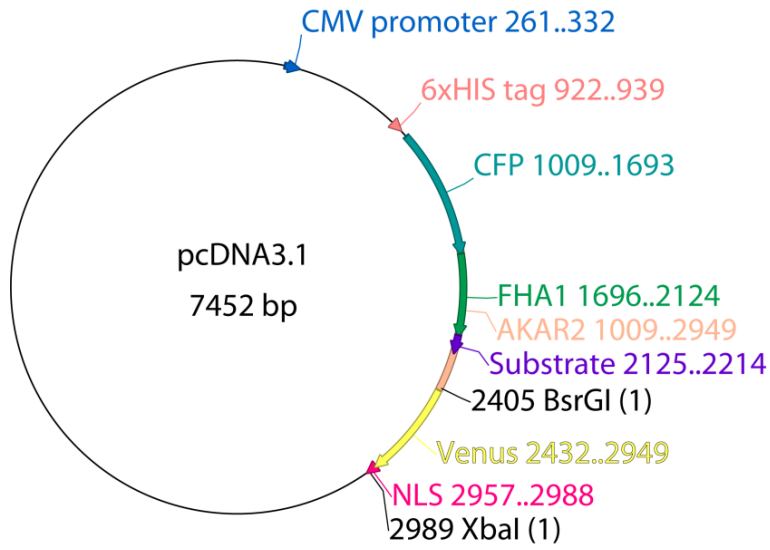
8. Appendix

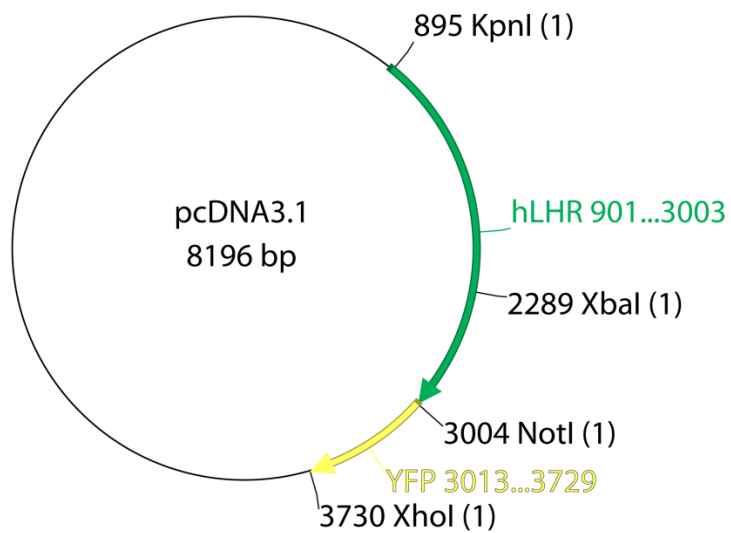## 8.1. PLASMID MAPS

PCDNA3.1 AKAR2-CAAX

CMV promoter 261..332

6xHIS tag 922..939

CFP 1009..1693

pcDNA3.1
7500 bp

FHA1 1696..2124
AKAR2 1009..2949
Substrate 2125..2214
2405 BsrGI (1)
Venus 2432..2949
CAAX 2950..2994
3040 XbaI (1)

PCDNA3.1 AKAR2-NES

CMV promoter 261..332

6xHIS tag 922..939

CFP 1009..1693

pcDNA3.1
7449 bp

FHA1 1696..2124
AKAR2 1009..2949
Substrate 2125..2214
2405 BsrGI (1)
Venus 2432..2949
NES 2950..2985
2986 XbaI (1)

PCDNA3.1 AKAR2-NLS

CMV promoter 261..332
6xHIS tag 922..939
CFP 1009..1693
pcDNA3.1
7452 bp
FHA1 1696..2124
AKAR2 1009..2949
Substrate 2125..2214
2405 BsrGI (1)
Venus 2432..2949
NLS 2957..2988
2989 XbaI (1)

PCDNA3.1 HLHR-YFP

895 KpnI (1)
pcDNA3.1
8196 bp
hLHR 901...3003
2289 XbaI (1)
3004 NotI (1)
YFP 3013...3729
3730 XhoI (1)

8.2. CURRICULUM VITAE

CONTACT INFORMATION

Name   Lyga Sandra

PERSONAL INFORMATION

Date of Birth   15/04/1986
Place of Birth   Falkenberg, Poland
Nationality   German
Sex   female

EMPLOYMENT HISTORY

08/2006-10/2006   Trainee, Trifolio-M GmbH, Lahnau

07/2007-08/2007   Trainee, Hirsch-Apotheke, Giessen

10/2009-02/2010   Trainee, Lead Discovery Center GmbH, Dortmund
                        Assay Development & Screening

05/2010-12/2010   Diplom student, Merck KGaA, Darmstadt
                        Lead Discovery Technology

09/2011-present   PhD student, Department of Pharmacology and Toxicology and
                        Rudolf Virchow Center for Experimental Biomedicine, University of
                        Würzburg
                        Supervisor: Dr. Davide Calebiro

UNIVERSITY

10/2005-07/2006   Fachhochschule Giessen-Friedberg, Giessen

Degree program: Environment, hygiene- and control engineering (Dipl.-Ing.)

07/2008-12/2008   Victoria University in Melbourne, Australian

10/2006-01/2011   Fachhochschule Giessen-Friedberg, Giessen

Degree program: Bio pharmaceutical technology (Dipl.-Ing.)

EDUCATION

09/2002-06/2005   Ricarda-Huch-Schule, Giessen

Graduation: A-level

ADDITIONAL INFORMATION

Language skills: -English (fluent in conversation and writing)

-French

Software skills: Microsoft Office, GraphPad Prism, ImageJ, Adobe Illustrator

ACTIVITY AND INTERESTS

Travelling, climbing, music

8.3. PUBLICATION LIST AND CONFERENCE CONTRIBUTIONS

RESEARCH ARTICLES

Calebiro D, Hannawacker A, **Lyga S**, Bathon K, Zabel U, Ronchi C, Beuschlein F, Reincke M, Lorenz K, Allolio B, Kisker C, Fassnacht M, Lohse MJ.(2014) PKA catalytic subunit mutations in adrenocortical Cushing's adenoma impair association with the regulatory subunit.
Nat Commun.; 5:5680

Calebiro D, Godbole A, **Lyga S**, Lohse MJ.(2015) Trafficking and function of GPCRs in the endosomal compartment. Methods Mol Biol.;1234:197-211.

Lyga S, Volpe S, Werthmann RC, Götz K, Sungkaworn T, Lohse MJ, Calebiro D. (2016) Persistent cAMP signaling by internalized LH receptors in ovarian follicles.
Endocrinology; en.20151945

Lyga S[*], Godbole A[*], Lohse MJ, Calebiro D. (2016) A new paradigm of TSH receptor signaling in the trans-Golgi network (in preparation)

[*]equal contribution

ORAL PRESENTATIONS

Date	Organizer	Presentation Title
July 2012	Annual retreat of the Department of pharmacology	'Live cell imaging of TSH receptor signaling in the endosomal compartment'
July 2013	Annual retreat of the Department of pharmacology	'Live cell imaging of TSH receptor signaling in the endosomal compartment'
October 2013	Annual retreat of the Rudolf-Virchow-Center	'Live cell imaging of G-protein-coupled receptor signaling in the endosomal compartment'
July 2014	Annual retreat of the Department of pharmacology	'Live cell imaging of G-protein-coupled receptor signaling in the endosomal compartment'

POSTER PRESENTATIONS

Date	Organizer	Presentation Title
October 2012	Annual retreat of the Rudolf-Virchow-Center	'Live cell imaging of TSHR-cAMP signaling in the endosomal compartment'
October 2012	5. Würzburger GPCR Symposium	'Live cell imaging of TSHR-cAMP signaling in the endosomal compartment'
March 2013	79. DGPT Congress Halle	'Effects of TSHR internalization on PKA activation and nuclear signaling in intact thyroid cells'
October 2013	Annual retreat of the Rudolf-Virchow-Center	'Effects of TSHR internalization on PKA signaling in intact thyroid cells'
April 2014	80. DGPT Congress Hannover	'A second wave of protein kinase A signaling after internalization of the thyroid stimulating hormone receptor'
February 2016	GPCR Keystone Symposium	'Persistent cAMP signaling by internalized LH receptors promotes meiosis resumption in mouse ovarian follicles'

8.4. AFFIDAVIT

I hereby declare that my thesis entitled

'Glycoprotein hormone receptor signaling in the endosomal compartment'

is the result of my own work. I did not receive any help or support from commercial consultants. All sources and / or materials applied are listed and specified in the thesis.

Furthermore, I confirm that this thesis has not yet been submitted as part of another examination process neither in identical nor similar form.

Eidesstattliche Erklärung

Hiermit erkläre ich an Eides statt, die Dissertation

„Glykoproteinhormon-Rezeptor Signaltransduktion im endosomalen Kompartiment"

eigenständig, d.h. insbesondere selbständig und ohne Hilfe eines kommerziellen Promotionsberaters, angefertigt und keine anderen als die von mir angegebenen Quellen und Hilfsmittel verwendet zu haben.

Ich erkläre außerdem, dass die Dissertation weder in gleicher noch in ähnlicher Form bereits in einem anderen Prüfungsverfahren vorgelegen hat.

Würzburg…………………………………………………………………………………………

            Date   Signature

8.5. ACKNOWLEDGMENT